University of Kentucky
UKnowledge

University of Kentucky Master's Theses | Graduate School

2010

ORIGIN OF BLUE RIDGE BASEMENT ROCKS, DELLWOOD QUAD, WESTERN NC: NEW EVIDENCE FROM U-PB ZIRCON GEOCHRONOLOGY AND WHOLE ROCK GEOCHEMISTRY

Donald Franklin Loughry Jr.
University of Kentucky, thedonald@uky.edu

Right click to open a feedback form in a new tab to let us know how this document benefits you.

Recommended Citation

Loughry, Donald Franklin Jr., "ORIGIN OF BLUE RIDGE BASEMENT ROCKS, DELLWOOD QUAD, WESTERN NC: NEW EVIDENCE FROM U-PB ZIRCON GEOCHRONOLOGY AND WHOLE ROCK GEOCHEMISTRY" (2010). *University of Kentucky Master's Theses*. 11.
https://uknowledge.uky.edu/gradschool_theses/11

This Thesis is brought to you for free and open access by the Graduate School at UKnowledge. It has been accepted for inclusion in University of Kentucky Master's Theses by an authorized administrator of UKnowledge. For more information, please contact UKnowledge@lsv.uky.edu.

ABSTRACT OF THESIS

ORIGIN OF BLUE RIDGE BASEMENT ROCKS, DELLWOOD QUAD, WESTERN NC: NEW EVIDENCE FROM U-PB ZIRCON GEOCHRONOLOGY AND WHOLE ROCK GEOCHEMISTRY

Terrane discrimination in polycyclic continental basement rocks is challenging due to high-grade metamorphism and intense deformation. Based on early USGS mapping the Blue Ridge basement in the Dellwood quadrangle of the eastern Great Smoky Mountains was proposed to consist of augen orthogneisses of Laurentian (Grenvillian) affinity interfolded with migmatitic hornblende and biotite paragneisses ("Carolina Gneiss") and amphibolites of uncertain affinity. However, detailed study reveals that the hornblende gneiss of Hadley and Goldsmith (1963) is a heterogeneous map unit consisting of (1) metaplutonic rocks; (2) variably foliated and folded felsic orthogneisses; (3) strongly migmatitic, folded Hbl+Bt-bearing gneisses; (4) foliated and lineated garnet amphibolites. Field relations, petrology, and geochemistry demonstrate that felsic orthogneisses are related to metaplutonic rocks via (post-Taconian) progressive deformation and reconstitution. Whole rock XRF geochemistry reveals likely protoliths of Hbl gneiss and Bt gneiss are geochemically similar and have common sources. U-Pb zircon geochronology and field relationships suggest felsic orthogneisses (1050 Ma, 1150-1190 Ma, 1250-1300 Ma) are components of the Mesoproterozoic Grenville basement, and not part of a metamorphosed Neoproterozoic syn-rift Laurentian margin cover sequence. A previously unknown age mode for Mesoproterozoic plutonism in the southern Appalachians was discovered (~1250-1300 Ma) suggesting the presence of a component exotic to pre-Grenvillian Laurentia (Amazonia?).

KEYWORDS: Grenville basement, geochronology, geochemistry, Blue Ridge, petrogenesis

Donald F. Loughry, Jr.

May 11, 2010

ORIGIN OF BLUE RIDGE BASEMENT ROCKS, DELLWOOD QUAD, WESTERN NC: NEW EVIDENCE FROM U-PB ZIRCON GEOCHRONOLOGY AND WHOLE ROCK GEOCHEMISTRY

By

Donald F. Loughry, Jr.

David P. Moecher
Director of Thesis

Alan Fryar
Director of Graduate Studies

May 11, 2010
Date

RULES FOR THE USE OF THESES

Unpublished theses submitted for the Master's degree and deposited in the University of Kentucky Library are as a rule open for inspection, but are to be used only with due regard to the rights of the authors. Bibliographical references may be noted, but quotations or summaries of parts may be published only with the permission of the author, and with the usual scholarly acknowledgments.

Extensive copying or publication of the thesis in whole or in part also requires the consent of the Dean of the Graduate School of the University of Kentucky.

A library that borrows this thesis for use by its patrons is expected to secure the signature of each user.

Name	Date

THESIS

Donald Franklin Loughry, Jr.

The Graduate School

University of Kentucky

2010

ORIGIN OF BLUE RIDGE BASEMENT ROCKS, DELLWOOD QUAD, WESTERN NC: NEW EVIDENCE FROM U-PB ZIRCON GEOCHRONOLOGY AND WHOLE ROCK GEOCHEMISTRY

THESIS

A thesis submitted in partial fulfillment of the
requirements for the degree of Master of Science in the
College of Arts and Sciences
at the University of Kentucky

By

Donald Franklin Loughry, Jr.

Lexington, Kentucky

Director: Dr. David P. Moecher, Professor of Geology

Lexington, Kentucky

2010

Copyright © Donald Franklin Loughry, Jr. 2010

This thesis is dedicated to my beautiful and loving wife, Jamie,

and to my wonderful children, Olivia and Boston

ACKNOWLEDGEMENTS

The following thesis, while an individual work, benefited from the insights and direction of several people. First, my Thesis Advisor, Dr. David P. Moecher, who exemplifies the high quality scholarship to which I aspire, provided timely and instructive comments and evaluation at every stage of the thesis process, allowing me to complete this project on schedule. Next, I wish to thank my Thesis Committee: Dr. David P. Moecher, Dr. Dhananjay Ravat, and Dr. Kent Ratajeski. Each provided insights that guided and challenged my thinking, substantially improving the finished product.

In addition to the technical and instrumental assistance above, I received equally important assistance from my family and friends. My wife, Jamie, and my children, Olivia and Boston, provided on-going support (in the form of hugs and smiles) throughout the thesis process. My friend and colleague, Suvankar Chakraborty, was selflessly available to help in any way possible, from troubleshooting software problems to guiding sample preparations. Finally, I wish to thank the Department of Earth and Environmental Sciences for offering the opportunity and providing the support needed to complete this project.

TABLE OF CONTENTS

LIST OF FIGURES

SECTION I. INTRODUCTION

Terrane discrimination in polycyclic continental basement rocks is challenging due to the high grade of metamorphism and intense deformation. Protolith characteristics (mineralogy, fabrics) are obscured by processes such as prograde metamorphic reactions and migmatization. Hybridization alters protolith compositions at lithologic contacts so that contacts are compositionally gradational and difficult to identify for mapping or sampling purposes. Lithologic contacts may also exhibit contrasts so that strain may be partitioned into the weaker unit resulting in differences in foliation intensity or fold style and history. Subsequent periods of tectonometamorphism, either prograde or retrograde, amplify difficulties in discrimination.

Southern Appalachian Blue Ridge basement, a terrane of Amazonian provenance accreted ~ 1.15 Ga during the Grenville orogeny (Tohver et al., 2004), has experienced multiple tectonometamorphic events in its *ca*. 1 Ga history (Grenvillian: 1.3 to 0.9 Ga; Taconian: 450 Ma; Neo-Acadian to Alleghanian: 360-300 Ma) (Hatcher, 1987; Rankin, 1975; Thomas, 1991). In the vicinity of the Great Smoky Mountains, the basement is proposed to contain numerous pre-metamorphic terrane boundaries that are manifested as lithologic contacts between predominantly single lithologies. For example, the Ashe Metamorphic Suite-basement contact and the Great Smoky Group-basement contact are proposed to be the Chattahoochee-Holland Mountain (Merschat et al., 2006) and Greenbrier faults (Clemons and Moecher, 2008; Hadley and Goldsmith, 1963), respectively. Packages of lithologies may also define a terrane. The Hayesville fault has been identified as the Western Blue Ridge (Laurentian continental margin)-Eastern Blue Ridge (Iapetan oceanic assemblage) contact (Hatcher, 1978; Massey and Moecher, 2005).

Within the Mesoproterozoic (Grenville) basement terranes of western North Carolina and eastern Tennessee, Berquist et al. (2005) identified the Mars Hill terrane based primarily on relatively old Nd model ages (T_{DM} = ~ 1.8 Ga) and zircon U-Pb ion probe ages (1.77 – 1.38 Ga). The Mars Hill terrane is cryptic in the sense that it is lithologically similar to other Grenville basement rocks (gneisses, relict granulites) but was recognized solely from geochemistry.

Within the Dellwood area the basement rocks include those of likely Laurentian affinity interfolded with migmatitic rocks of uncertain affinity. The latter were first designated as part of the Carolina gneiss (Grenvillian?) (Hadley and Goldsmith, 1963), then assigned to the Eastern Blue Ridge basement, then proposed to be Cartoogechaye terrane (Hatcher et al., 2004), a highly deformed and metamorphosed post-Grenvillian sequence. Clearly, detailed petrologic, structural, and geochemical work is needed to provide additional constraints on the petrogenesis of the basement rocks within the quadrangle.

Previous Work

Since Hadley and Goldsmith's (1963) description of the basement complex and mapping of the Dellwood quad, little work has been done in the quadrangle. Massey and Moecher (2005) confirmed Hadley and Goldsmith's (1963) assessment of the basement rocks in the region as polymetamorphic, and further correlated deformational events with metamorphic events along the Eastern Blue Ridge-Western Blue Ridge terrane boundary, showing how each phase of metamorphism is recognized in the rocks. Moecher et al. (2004) provided precise time constraints for peak Taconian metamorphism (granulite facies) in the southern Blue Ridge, using zircons in migmatitic gneiss. Montes (1997)

concluded that both the Greenbrier and Hayesville thrust sheets were emplaced before the peak metamorphic event. Montes and Hatcher (1999) correlated the Great Smoky Group-Snowbird Group contact in the easternmost Western Blue Ridge with the premetamorphic Greenbrier fault, confining the entire Snowbird Group to the footwall of the Greenbrier fault. Merschat and Cattanach (2008) completed mapping of the Asheville quadrangle at 1:100,000 scale, illustrating the most recent interpretation of structural relations among the basement rocks in the region. Tohver et al. (2004) traced the transfer of the southern Appalachian Blue Ridge/Mars Hill terrane during Grenville orogenesis using Pb and Nd isotope geochemistry. They concluded that isotopic signatures of basement gneisses in this terrane are distinct from those of the rest of the Grenville belt, but are similar to basement rocks of the southwest Amazon craton. New age data (zircon U-Pb ion microprobe geochronology, E. Anderson, unpublished data) and field relationships (Anderson and Moecher, 2009) suggest that the hornblende gneisses may be an intensely deformed and metamorphosed component of the Mesoproterozoic Grenville basement, and not part of a Neoproterozoic cover sequence deposited on the rifted margin of Laurentia and subsequently metamorphosed during the Taconian orogeny (Hatcher et al., 2005). Anderson and Moecher (2009) suggest that westward subduction of Laurentian (Grenvillian) continental crust beneath the Laurentian margin during the Taconian orogeny, which was later displaced cratonward during late Paleozoic deformation, may be responsible for the presence of Grenville-age hornblende gneisses in the Dellwood quadrangle as well as high-pressure metabasites and eclogites throughout the region. Ryan et al. (2005) analyzed amphibolites and ultramafic rocks 5-32 km to the southwest along strike of the Hayesville fault from Dellwood quadrangle

and concluded that the bulk chemical and trace element signatures of the amphibolites were consistent with igneous rocks of calc-alkaline composition. They inferred that these rocks along with the enveloping metasedimentary rocks represent the block and matrix of an ancient accretionary sequence related to subduction. They did not provide age constraints for these rocks.

Purpose of Study

Due to lack of exposure, the high grade of metamorphism, and structural complexity, the relationship between and origins of the biotite gneiss and hornblende gneiss are uncertain. Detailed field work, structural analysis (comparison of foliation and fold histories), geochemistry, and geochronology have never been carried out on the basement units. Preliminary geochronology (Anderson and Moecher, 2008; Anderson and Moecher, 2009) indicates some units initially mapped as hornblende gneiss (pЄch) (Hadley and Goldsmith, 1963) are Mesoproterozoic (1.25 Ga), and protoliths of biotite gneiss (pЄc) are post-Mesoproterozoic (Neoproterozoic sediments?) (Bream et al., 2004). Preliminary field work and petrology suggest that some rock bodies mapped as hornblende gneisses are related via progressive deformation and reconstitution to Mesoproterozoic orthogneisses. This study is a detailed petrologic, structural, geochronological, and geochemical study of the hornblende gneisses and enclosing biotite gneisses intended to test the hypothesis that the hornblende gneisses are not components of the Neoproterozoic Laurentian margin sequence (i.e., a separate terrane), and to determine the age and likely protoliths of the gneisses.

SECTION II. GEOLOGIC SETTING AND STUDY AREA

The Dellwood quadrangle, positioned on the eastern flank of the Great Smoky Mountains region (Figure 2.1), was one of the first quadrangles to be mapped in the Blue Ridge of western North Carolina (Hadley and Goldsmith, 1963). The basement rocks in the Dellwood quadrangle initially served as a frame of reference for understanding the Precambrian evolution of eastern Laurentia in the southern Appalachians. These rocks, designated collectively as the Carolina Gneiss (Hadley and Goldsmith, 1963), consist of foliated to migmatitic biotite paragneisses originally inferred to have a sedimentary origin, foliated to migmatitic hornblende orthogneisses, which appear to have mafic to intermediate igneous protoliths based on mineralogy (hornblende + plagioclase ± biotite), and small amphibolite bodies (> 50 modal % hornblende + plagioclase). The basement rocks are interpreted (Hadley and Goldsmith, 1963) to be nonconformably overlain by the Wading Branch and Longarm Formations of the Snowbird Group and the Thunderhead/Copperhill Formation of the Great Smoky Group, a thick sequence of metamorphosed siliciclastic rocks deposited in the late Precambrian (Hadley and Goldsmith, 1963; Hatcher et al., 2005; Merschat and Wiener, 1990; Montes, 1997). The Ocoee, the stratigraphic equivalent of protoliths of the Ashe Metamorphic Suite (Rankin, 1975), has been interpreted as eastern Laurentian syn-rift turbidite and fluvial to shallow marine deposits (King, 1964; Rast and Kohles, 1986) accompanying the break-up of Rodinia and the opening of the Iapetus Ocean (proto-Atlantic).

Both the basement rocks and the metasedimentary cover sequence in the Dellwood quadrangle are enveloped within a larger belt (at least 35 miles wide) of rocks

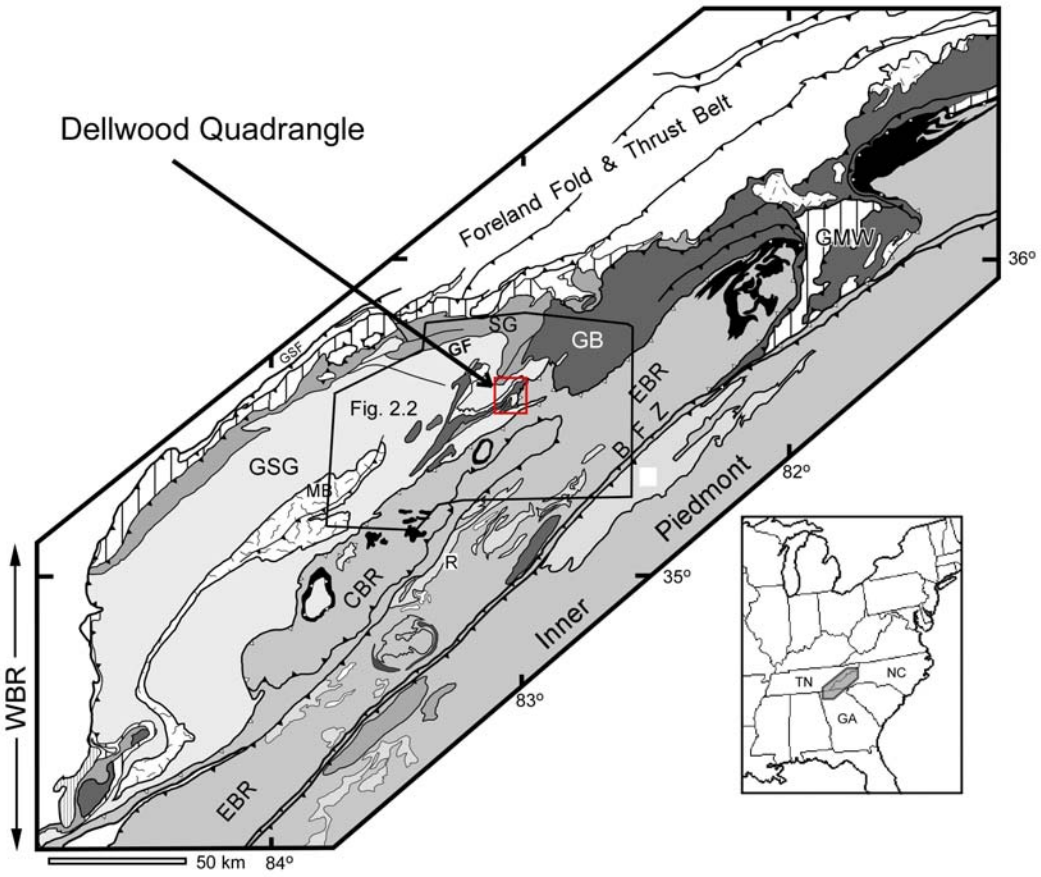

Figure 2.1. Regional map of the Western Blue Ridge (WBR) and Eastern Blue Ridge (EBR) in the vicinity of the Great Smoky Mountains, TN and NC showing location (inset) and geologic setting of study area (after Rankin et al., 1990). Red rectangle shows the location of Dellwood quadrangle; black polygon shows extent of Fig. 2.2; GSG=Great Smoky Group, MB=Murphy Belt, CBR=Central Blue Ridge, BFZ=Brevard Fault Zone, GSF=Great Smoky Fault, GF=Greenbrier Fault, SG=Snowbird Group, GMW=Grandfather Mountain Window, GB=Grenville Basement.

experiencing regional metamorphism during the early Paleozoic (Taconian) that increases in intensity to the southeast (Hadley and Goldsmith, 1963; M_{2A} and M_{2B} of Massey and Moecher, 2005) represented by isograds marking the initial occurrence of metamorphic index minerals (Hadley and Goldsmith, 1963). A subsequent period of metamorphism and deformation produced the anticlinal uplifts of the basement and synclinal exposures of the Ocoee that dominate the structure within the quad (Hadley and Goldsmith, 1963; M_3 and D_3 of Massey and Moecher, 2005).

Basement Rocks of Grenvillian Affinity

The eastern Great Smoky Mountains region is located in a transitional area between rocks of known Grenville affinity (Mesoproterozoic: Merschat et al., 2006; (Mars Hill terrane: Gulley, 1985; Miller et al., 2000) to the north and northeast with rocks of inferred post-Grenvillian affinity (Neoproterozoic) (Cartoogechaye terrane: Hatcher et al., 2004) that extend farther to the south and southeast (Figure 2.2). The Hayesville fault, inferred to be a premetamorphic fault separating the metasedimentary rocks of the Western Blue Ridge (Ocoee) from the high grade gneisses of the Central Blue Ridge (Hatcher, 1978), strikes northeast and purportedly enters the Dellwood quadrangle in its southeast corner (Montes, 1997). Generally, the rocks to the northwest of the fault are proposed to be autochthonous and the rocks to the southeast of the fault are interpreted as allochthonous. Gulley (1985) dated the ~ 1.8 Ga Early Proterozoic rocks of the Mars Hill terrane that crop out along strike of the Hayesville fault to the northeast of Dellwood quadrangle (Merschat and Cattanach, 2008). The basement rocks in the Mars Hill terrane, accreted during the Grenville orogeny (Gulley, 1985; Ownby et al., 2004), are

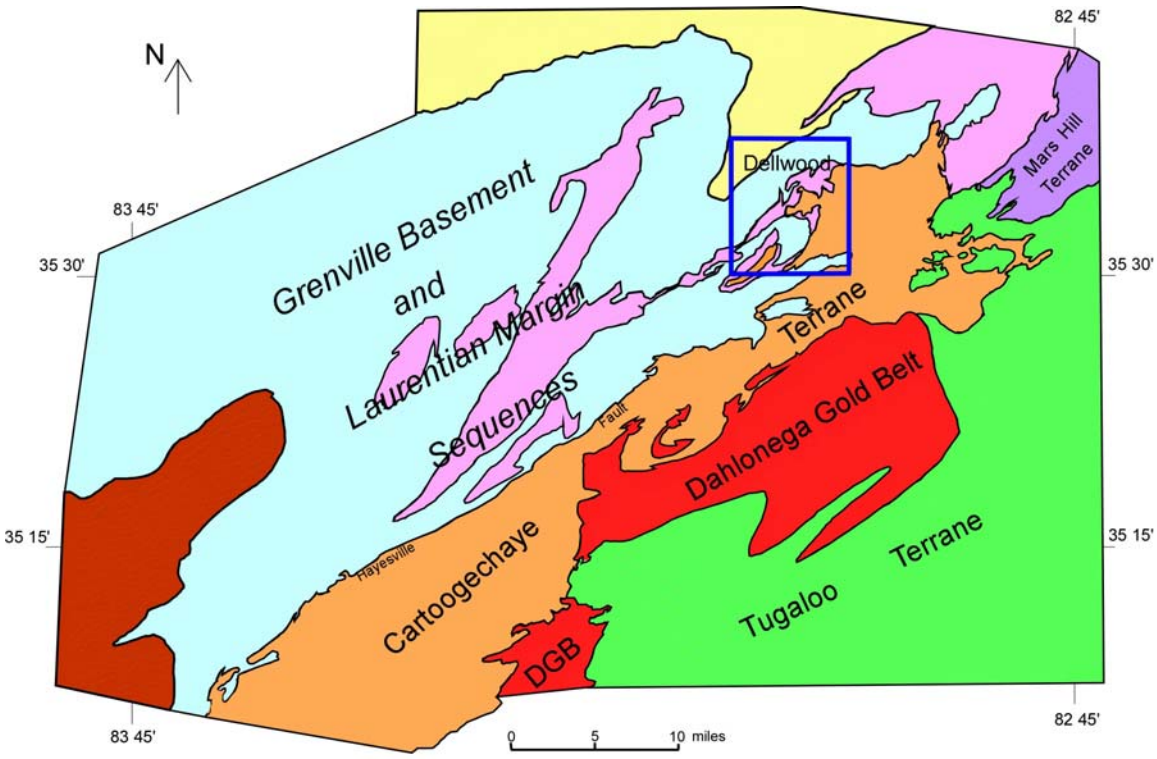

Figure 2.2. Terrane map of the western, central, and eastern Blue Ridge, western NC showing the position of the Dellwood quadrangle (blue rectangle). Geology after Hatcher et al. (2005).

- 1.8 Ga Mars Hill terrane gneisses
- 1.15 Ga granitic gneiss
- Snowbird Group (meta)sandstone and shale
- Great Smoky Group (meta)sandstone and shale
- Murphy Belt
- Cartoogechaye terrane metasedimentary and volcanic rocks
- Dahlonega Gold Belt metasandstone and schist
- Ash-Tallulah Falls Fm. metasandstone, schist, and metavolcanic rocks

footwall components of the Hayesville thrust sheet (see Hatcher, 2005, figure 2a). Additionally, small Grenville age basement massifs such as those of the Tallulah Falls dome, Toxaway dome, and the Trimont Ridge complex likely represent continental fragments rifted from Laurentia during the Neoproterozoic that were later accreted to the margin during Ordovician subduction and arc accretion (Hatcher et al., 2004).

Rocks of Inferred post-Grenvillian Affinity

Hatcher et al. (2004) identified two tectonostratigraphic terranes in the Hayesville thrust sheet. The Cowrock terrane (not shown on Figure 2.2), on the leading edge of the thrust sheet in northern Georgia extending northeastward into southern North Carolina, is the southernmost of these terranes. This terrane is composed of schists, metamafic rocks, metaultramafic rocks, biotite-plagioclase gneisses and "metasandstones," the latter containing Grenville-age detrital zircons (Bream et al., 2004) indicating that these rocks are not basement, but likely a distal Laurentian margin sequence derived from erosion of Grenville gneisses (Hatcher et al., 2005). The Cartoogechaye terrane (Hatcher et al., 2004) structurally overlies the Cowrock terrane and is exposed to the northeast of it along the Hayesville fault. Rocks composing this terrane include pelitic schist, metasandstone, metamafic and metaultramafic rocks, and some Grenville basement (Hatcher et al., 2004). Migmatitic fabrics are present as these rocks reached granulite facies metamorphism, experiencing peak temperature conditions at 458±1.0 Ma (Taconian) (Moecher et al., 2004). Dating of detrital zircons from the metasandstones produced Grenville and older ages (Miller et al., 2000). Farther east are the post-Grenvillian terranes of the Dahlonega Gold Belt, whose mafic and ultramafic complexes have

produced Ordovician U-Pb zircon ages (Bream, 2003; Thomas, 2001) and the Tugaloo terrane, consisting predominantly of Tallulah Falls-Ashe Formation metasandstone, pelitic schist, and amphibolite (Hatcher et al., 2005).

SECTION III. LITHOLOGIC DESCRIPTIONS

Rocks of the basement complex comprise more than two-thirds of the area of the Dellwood quadrangle. Lithologies designated as the Carolina Gneiss by Hadley and Goldsmith (1963), specifically biotite gneiss (pЄc), hornblende gneiss (pЄch), and amphibolite (pЄca) (Figure 3.1) are the main focus of the current study. Due to the high grade of metamorphism and migmatization in the area, distinguishing among the lithologies can be problematic upon first inspection. However, the biotite gneiss is easily distinguished in outcrop from hornblende gneiss by the lack of hornblende in the former, a higher abundance of coarse-grained muscovite, and, in migmatitic varieties, thicker leucosomes that locally exhibit a characteristic purple-gray hue. Amphibolite is easily recognized in outcrop by its dark gray to black color, medium- to coarse-grained hornblende crystals, and the general presence of garnet. The other common basement units in the map area are the granitoid and augen gneisses (pЄg and pЄga, respectively), which are generally considered to be Grenville-aged metaplutonic orthogneisses (E. Anderson, unpublished data; Hadley and Goldsmith, 1963; Montes, 1997).

Biotite Gneiss

Biotite gneiss, the major constituent of the Carolina Gneiss suite, is exposed in the southeastern two-thirds of the quadrangle. Large exposures are found at road cuts along Spy Rock Road in the Trinity Cove housing development (location 2, Figure 3.2); The Preserve housing development on Tanner Trail (location 12); just north of Garrett Cemetery along Wheat Grass Loop (location 13); and along Coleman Mtn. Road

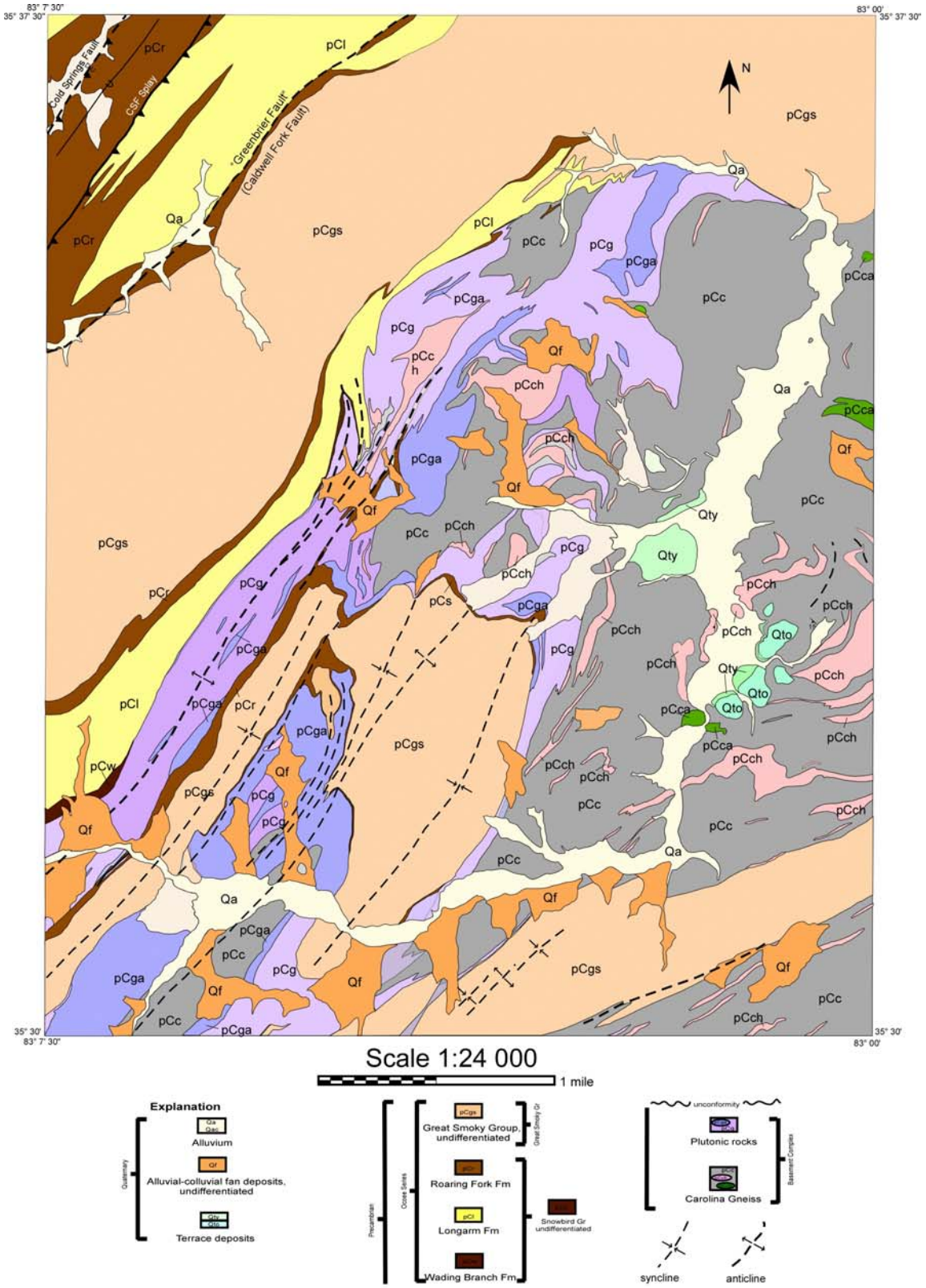

Figure 3.1. Geologic map of the Dellwood 7.5 minute quadrangle, eastern Great Smoky Mountains, after Hadley and Goldsmith (1963). pCc-biotite gneiss, pCch-hornblende gneiss, pCca-amphibolite, pCg-granitoid gneiss, pCga-augen gneiss.

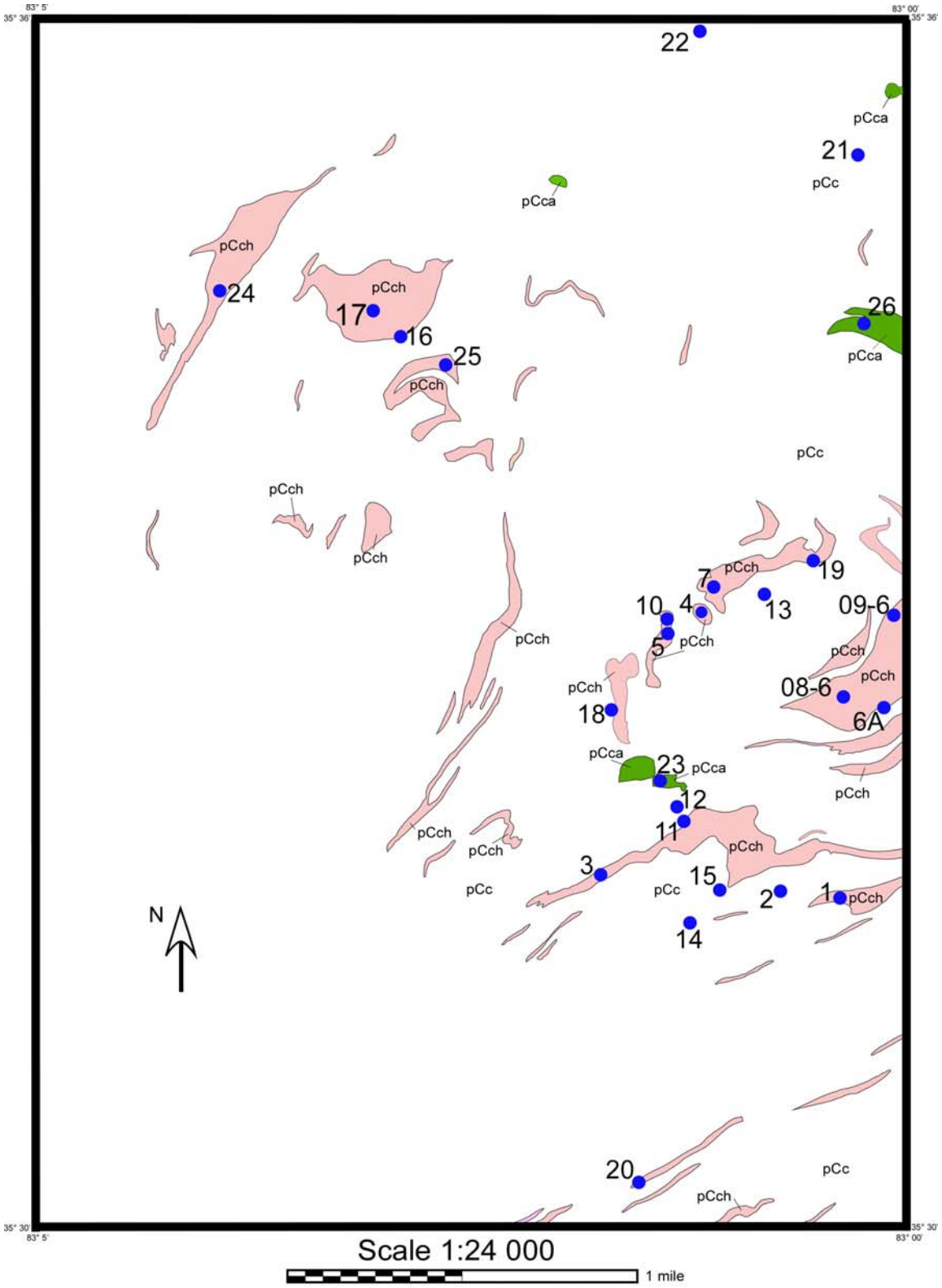

Figure 3.2. Sample locations in the Dellwood Quadrangle, eastern Great Smoky Mountains, showing only hornblende gneisses (pink) and amphibolites (green) after Hadley and Goldsmith (1963).

approximately 0.5 km from the junction of U.S. Rt. 276 in the northeastern part of the quad (location 21).

Biotite gneiss (Figure 3.3) is banded to migmatitic, light to medium gray in color, medium to coarse grained, consisting primarily of plagioclase, varying proportions of alkali feldspar, biotite, muscovite, and quartz. Garnet is generally absent, but may be present locally. Foliation is defined by the alignment of medium to coarse-grained biotite ± muscovite. Multiple foliations are present owing to the polymetamorphic history of the region. Some varieties exhibit compositional layering (Figure 3.4) cross-cut by later fabrics defined by the fold hinges of chevron shaped similar folds (Figure 3.5). Migmatitic varieties exhibit highly deformed fabrics recognized by alternating leucosome/melanosome domains (Figure 3.6) that may exhibit syn- to post- peak metamorphic ptygmatic folding. Thicknesses of quartzofeldspathic leucosomes, possibly resulting from dehydration melting of muscovite ± biotite (Le Breton and Thompson, 1988), range from 0.5 cm to 5 cm; melanosome selvages are < 1 cm thick.

Hornblende Gneiss

Bodies mapped collectively as "hornblende gneiss" are scattered throughout the central and eastern portions of the Dellwood quadrangle and are enveloped by the biotite gneiss. Large exposures occur at several outcrops within The Preserve housing development along Tanner Trail near Utah Mountain (locations 11 and 12), east on Utah Mountain Road (SR 1311) along Countryside Drive (locations 6, 6A, and 6B), along Boyd Farm Road near Roundhill Cemetery (locations 5 and 10), at the Messer Farm

Figure 3.3. Hand sample of migmatitic biotite gneiss at Trinity Cove. White bar is 5 cm.

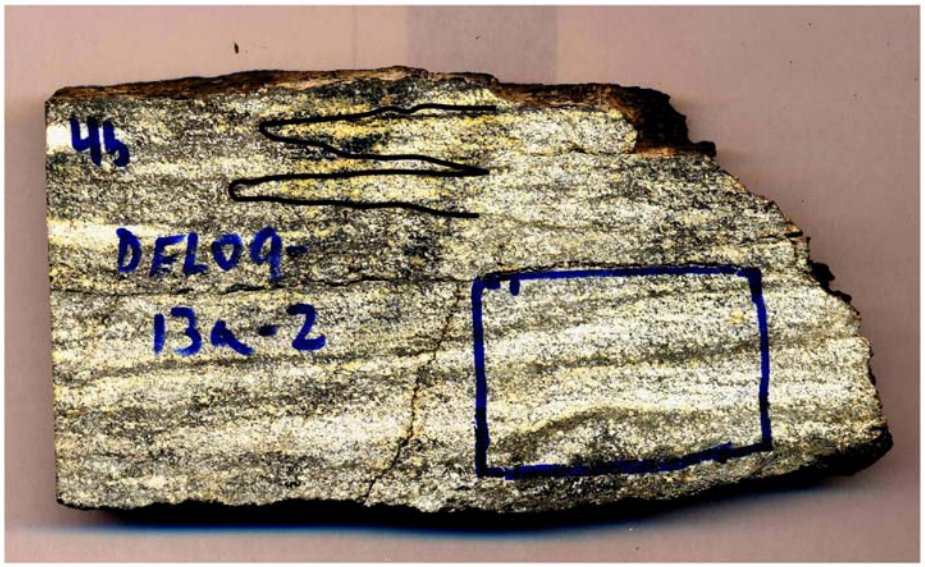

Figure 3.4. Sawn slab (DEL09-13a) from location 13 showing compositional layering and fold cross-sections at top (outlined in black).

Figure 3.5. Migmatitic Bt-gneiss (location 13) showing presence of late tight similar folds. Note the folded leucosome domain to the right of the rock hammer.

Figure 3.6. Outcrop of migmatitic biotite gneiss at Trinity Cove showing strong foliation defined by the alignment of biotite and muscovite and thick leucosomes possibly resulting from dehydration melting of muscovite.

along U.S Rt. 276 ~300 m north of the Utah Mountain Road junction (locations 4 and 7), along Erwin Lane near Goatrock Ridge (location 19), and along Abbey Cove Road (location 16) on the southern margin of a large body on the southeast ridge of Purchase Knob.

In contrast to the enclosing biotite gneiss, hornblende gneiss exhibits a greater heterogeneity in appearance. This study resolved three separate lithologic types within the hornblende gneiss suite of Hadley and Goldsmith (1963): (1) unfoliated to foliated metaplutonic orthogneiss, (2) strongly foliated and deformed orthogneiss equivalents, and (3) hornblende-bearing migmatites. There is a gradation in texture of the hornblende gneisses from massive orthogneiss, usually found within cores of the larger mapped bodies, to strongly foliated and deformed gneisses generally found within the smaller hornblende gneiss bodies or in large bodies near inferred contacts with biotite gneiss (ie., the contact between a more competent (pЄch) and less competent (pЄc) lithology).

Some varieties of hornblende gneiss are texturally homogeneous (Figure 3.7). Others contain mafic enclaves (m- to cm-scale) of sub-round to extremely deformed, flattened pods or lenses of garnet amphibolite (Figure 3.8). In several localities, migmatitic hornblende gneiss exhibits conspicuous hornblende-speckled leucosomes (Figure 3.9). In varieties with minimal migmatization, rocks exhibit weak to well-defined foliations defined by both compositional banding and late stage open to tight parallel folds whose hinges may represent axial plane crenulations of larger folds. Some weakly deformed varieties preserve igneous textures (Figure 3.10) and appear to be related to the intensely deformed varieties via progressive deformation (Figure 3.11).

Figure 3.7. Migmatitic Hbl gneiss outcrop at Holiday Drive in The Preserve development showing a generally homogeneous distribution of mafic minerals.

Figure 3.8. Migmatitic Hbl gneiss outcrop at The Preserve showing heterogeneous distribution of mafic minerals. Hbl-rich domains (H; outlined) are partitioned from Hbl-poor domains.

Figure 3.9. Hornblende-speckled leucosomes in Hbl-gneiss from a) The Preserve (location 2) and b) Coleman Gap (location CG09-1-1). Pen for scale.

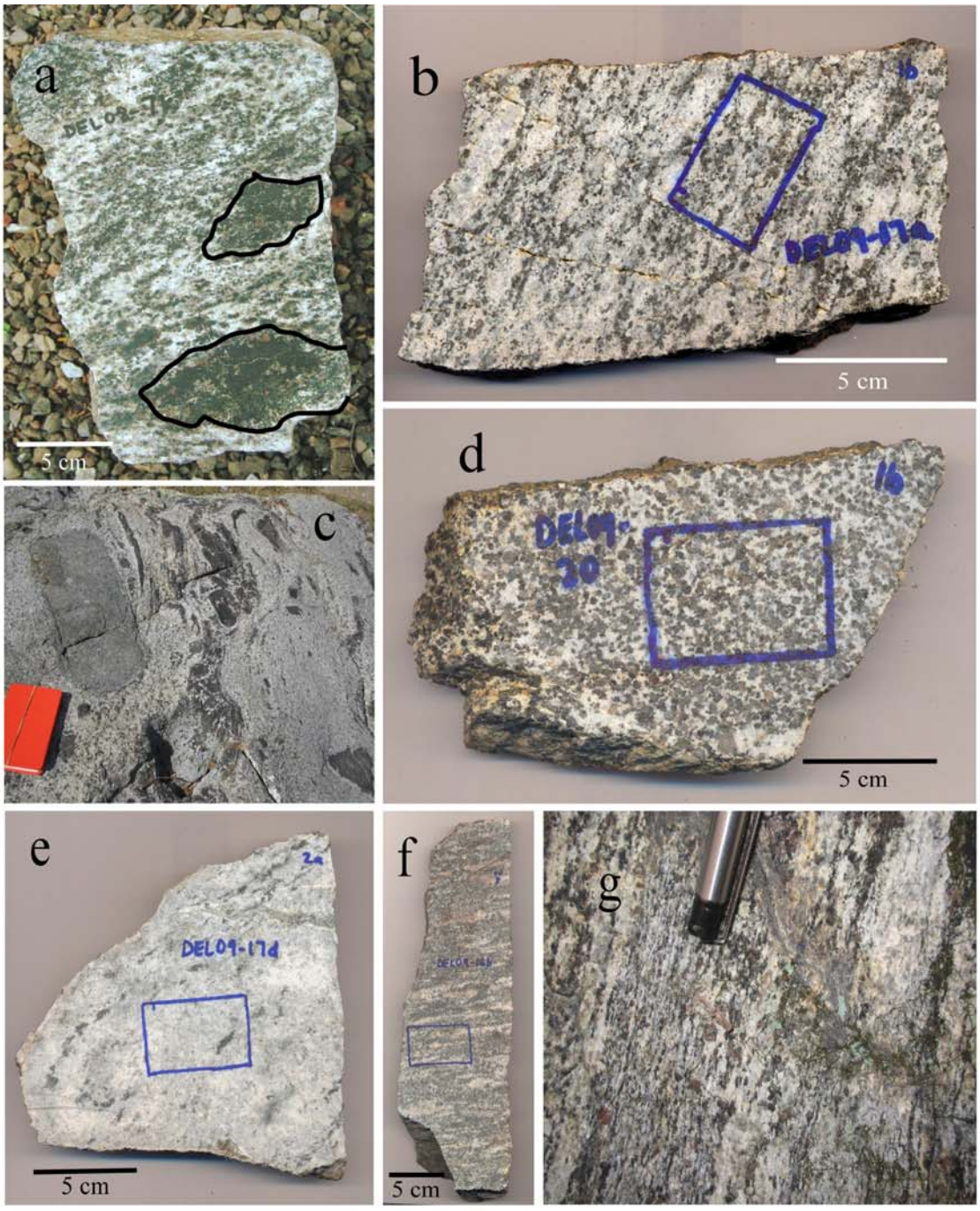

Figure 3.10. Hbl-gneisses exhibiting various forms of metaplutonic orthogneissic texture. a) hand sample exhibiting weakly foliated granoblastic texture with included amphibolite xenoliths (outlined) b) sawn slab showing moderate foliation and elongated feldspar augen c) outcrop at Messer Farm showing igneous texture with included amphibolite and diorite xenoliths d) sawn slab from Gaddis Branch outcrop showing granoblastic igneous texture e) sawn slab from location 17 showing granoblastic igneous texture f) sawn slab from location 16 exhibiting moderately deformed granoblastic igneous texture g) outcrop showing granoblastic texture, unfolded foliation, and elongated feldspar augen (top right).

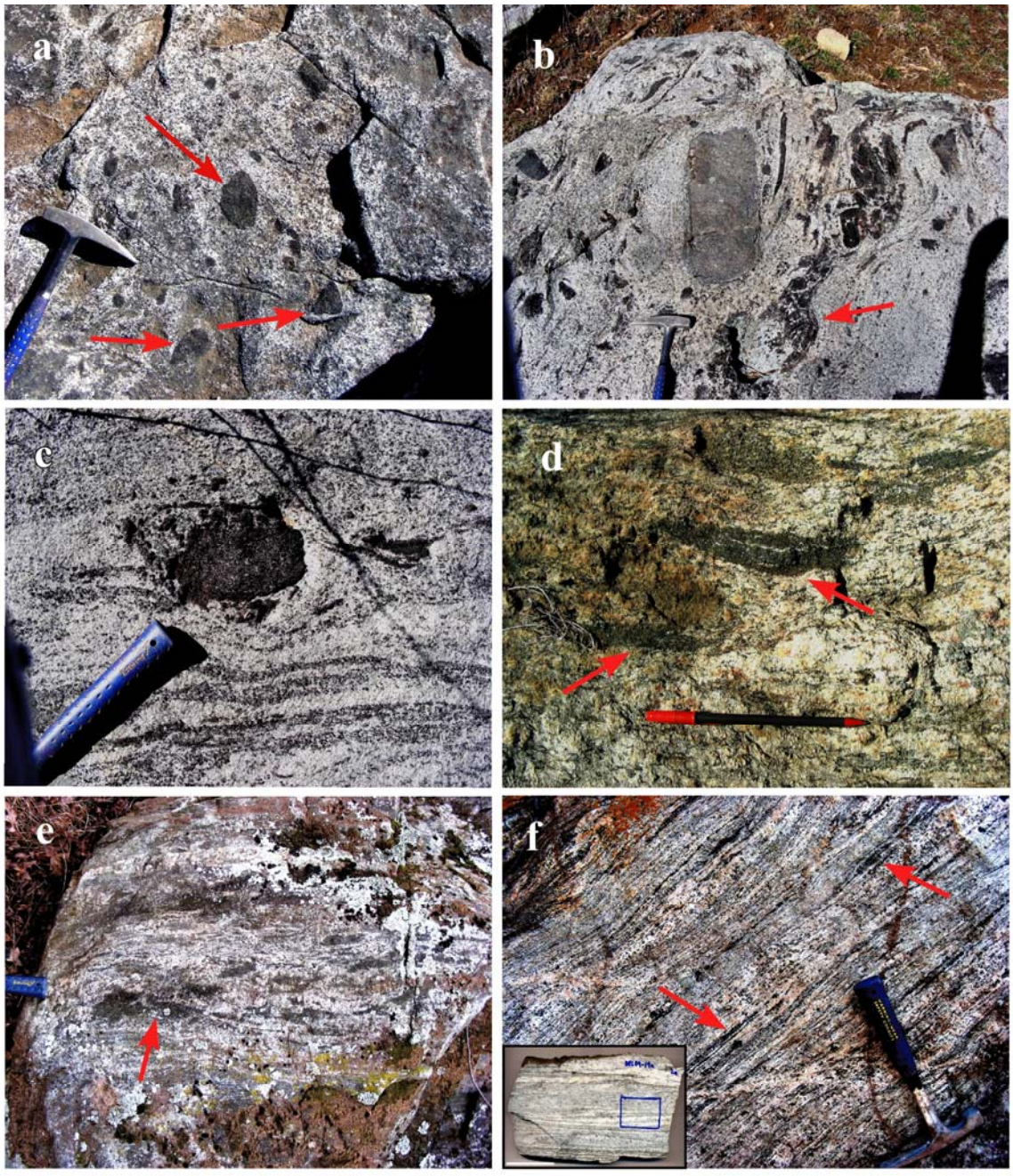

Figure 3.11. Progressive deformation of metaplutonic orthogneiss with included amphibolite xenoliths (red arrows) beginning at Messer Farm (location 7) and ending at Erwin Ln. outcrop (location 19). a) metaplutonic orthogneiss at Messer Farm with sub-round to sub-angular xenoliths b) and c) amphibolite xenoliths become deformed and disaggregated d) flattening of amphibolite xenoliths farther away from Messer Farm e) flattened xenoliths become sheared and disaggregated f) amphibolite xenoliths are intensely flattened at Erwin Ln. (location 19). Sawn slab (inset) shows flattening fabric. White bar is 5 cm.

The hornblende gneisses are generally darker in color than the biotite gneisses, but all gradations exist owing to the varying proportions of mafic minerals present. The common mineral assemblage is plagioclase + hornblende >>quartz ± biotite, though potassium feldspar and quartz are present in moderate quantities in the more leucocratic varieties. Accessory minerals include garnet, titanite, and epidote. Evidence of biotite replacing hornblende exists which may indicate a gradational relationship between the two rock types. However, the relationship (age, petrogenesis) between biotite gneiss and hornblende gneiss is inconclusive based on outcrop scale observations alone.

Granitoid and Augen Gneiss

Large bodies of granitoid and augen gneiss are found in the central portion of the quadrangle. These rocks are massive coarse-textured, inequigranular gneisses often containing elongated, lenticular, alkali feldspar augen that are variably recrystallized and set in a matrix of biotite + quartz folia (Figure 3.12). Previous workers have concluded that these rocks are Grenville-age and plutonic in origin (E. Anderson, unpublished data; Hadley and Goldsmith, 1963; Montes, 1997) and, therefore, are not the focus of this study.

Amphibolite

Rare amphibolite bodies ranging from centimeter-scale pods and xenoliths within orthogneiss (Figure 3.10 a and c, Figure 3.11) to meter-scale pods (Figure 3.13) or lenses

Figure 3.12. Outcrops of augen gneiss in the Dellwood area. a) moderately foliated gniess with elongated and recrystallized alkali feldspar augen (arrows) b) weakly foliated gneiss with alkali feldspar augen (arrows) from large body south of location 16.

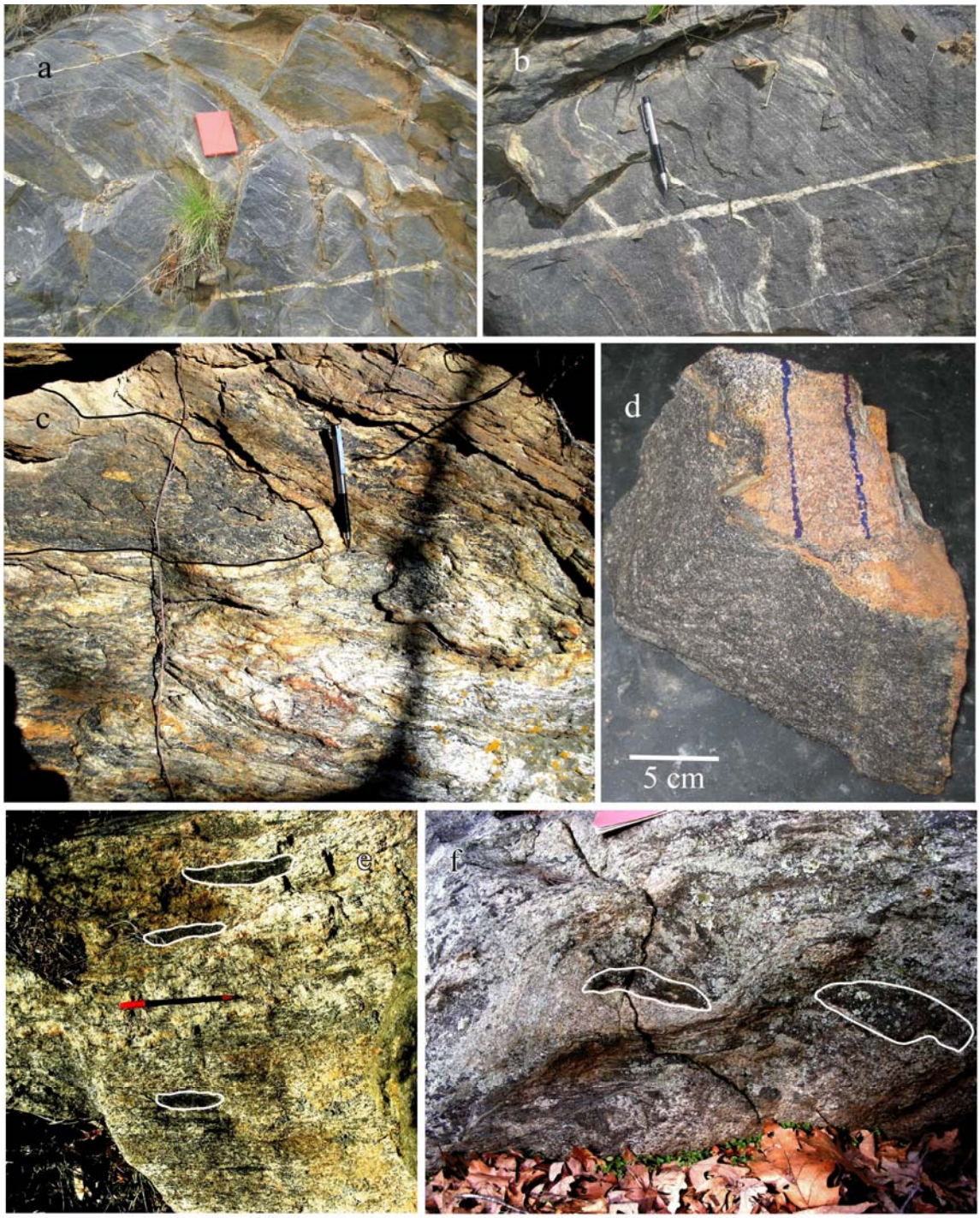

Figure 3.13. Dellwood amphibolites. a) outcrop of foliated amphibolite from location 23 with late hydrothermally filled fractures. b) closer view of same outcrop showing foliation (top left to bottom right) c) outcrop of Hbl-gneiss along inferred contact with biotite gneiss at location 6 containing a deformed amphibolite pod (outlined to left of pen). d) hand sample from large body along Qualla Dr. (location 26). Notice dark gray color of fresh surface. e) and f) flattened amphibolite xenoliths (outlined: white) at Messer Farm (location 7).

to mappable bodies several hundreds of meters in all dimensions are present within the southern and east-central portions of the quadrangle. Hadley and Goldsmith (1963) defined the amphibolite in this region as rocks containing 50% or more hornblende. The largest exposure can be found at the entrance of the Ridge Crest housing development (location 23) along U.S. Rt. 276 and directly across the highway. A smaller body with less exposure was found on private property (location 26) along Qualla Drive (Rt. 1324). A large (~2 m x 2 m x 2 m) float boulder was found near the top of the Trinity Cove housing development.

The rocks are black to dark green/gray in hand sample, contain abundant hornblende and subordinate amounts of plagioclase, garnet, clinopyroxene, biotite, and quartz. Accessory minerals include epidote, titanite, ilmenite, and apatite. Meter-scale amphibolite bodies are found intercalated with biotite and/or hornblende gneiss and may represent deformed dikes, xenoliths, or a partitioning of mafic minerals during metamorphism (Figure 3.8). The larger amphibolite bodies are generally granoblastic, medium- to coarse-grained, relatively homogenous, and weakly foliated. The circular to sub-circular map pattern of large bodies appears consistent with Hadley and Goldsmith's (1963) assumption that these bodies may be intrusive in origin. Most are isolated and appear to have previously been relatively equidimensional and later folded and/or flattened along with the enclosing biotite and hornblende gneisses. However, the presence of foliations in the amphibolite body at the entrance to the Ridge Crest development (location 23) led Anderson and Moecher (2009) to interpret the contacts between amphibolite and the enclosing gneisses to be tectonic in origin.

SECTION IV. PETROGRAPHY

Petrology was based on examination of forty thin sections obtained from representative samples of biotite gneiss, three hornblende-bearing gneiss varieties, and amphibolite. Petrographic analysis primarily focused on resolving relict igneous textures in orthogneisses, understanding the petrologic relationship between these rocks and their intensely deformed equivalents, and determining the relationship (if any) between the hornblende gneisses and the enveloping biotite gneisses. Point counts were performed on three samples of metaplutonic orthogneiss, two samples of deformed orthogneiss, and one sample of biotite gneiss using a Swift Model F electronic counting stage. Selected thin sections were deemed visually representative of the rocks from which they were taken. For each sample, 1500 points were counted using a horizontal spacing of 2 mm and a vertical spacing of 1 mm. Modes were recalculated on the basis of volumetric percentage of quartz, alkali feldspar, and plagioclase.

Biotite Gneiss

The common mineral assemblage in the biotite gneiss is plagioclase + quartz + biotite in varying proportions. Alkali feldspar, usually microcline, is present and subordinate to plagioclase in all samples and is locally perthitic. Quartz ranges in modal abundance from 25 to 45 percent. Muscovite, when present, amounts to as much as 5 modal percent. Biotite comprises as much as 30 modal percent. Accessory minerals include titanite, epidote, apatite, garnet, spinel, ilmenite, and rarely zircon. Garnet is poikiloblastic and fractured.

Biotite gneiss exhibits an overall inequigranular texture consisting of coarse grains of porphyroclastic biotite and feldspar and finer grains of recrystallized quartz. The prevalent gneissic banding has diffuse margins, is compositional in nature, and appears to be the result of incomplete mineralogic partitioning of quartz + feldspar from biotite ± muscovite during migmatization. A small percentage (< 5%) of mica is present within quartzofeldspathic leucosomes. A moderate to strong, spaced schistosity (Figure 4.1) is present and is defined by the alignment of micas within microlithons and, additionally, recrystallization of quartz within parallel micro-shear bands. The margins of biotite crystals are commonly found adjacent to and parallel with the long axes of feldspar grains, both aligned parallel to the foliation, in a manner which suggests dissolution of feldspar along the margin and possible replacement with biotite, further defining the foliation. Epidote and titanite are commonly clustered within biotite-rich layers. Within microlithons, strain appears to be accommodated in quartz mostly through sub-grain rotation, as quartz most often exhibits undulose extinction. Recrystallization of quartz within these zones is less prevalent. Deformation-induced myrmekite (Figure 4.2) commonly occurs along grain boundaries between microcline and plagioclase.

Replacement textures in biotite gneiss are generally limited to garnet with thin reaction rims of biotite (Figure 4.3) or replacement of garnet by biotite along fractures (Figure 4.4).

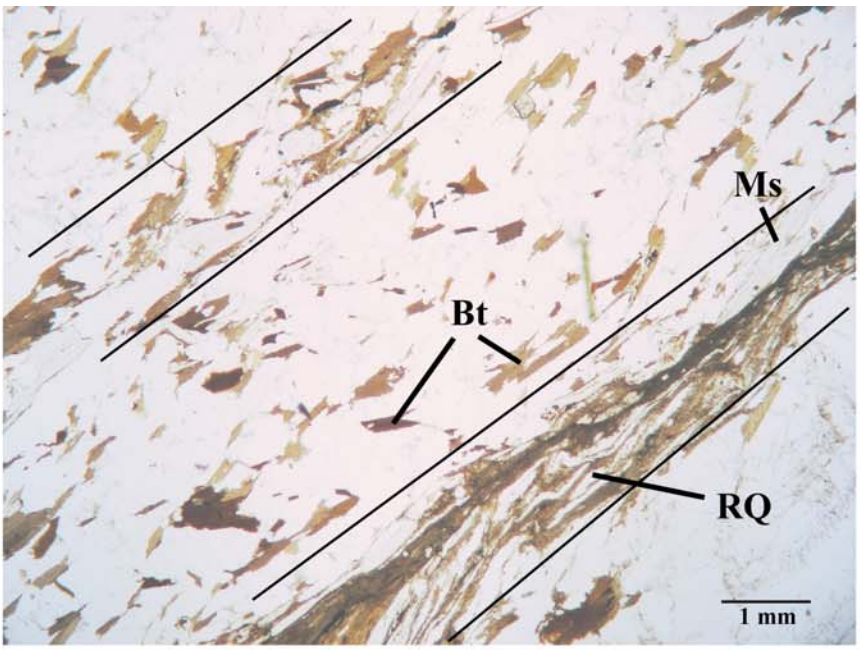

Figure 4.1. Photomicrograph of biotite gneiss showing spaced parallel schistosity defined by recrystallization of quartz (RQ) and alignment of biotite (Bt) and muscovite (Ms). Plane light. (DEL08-2d).

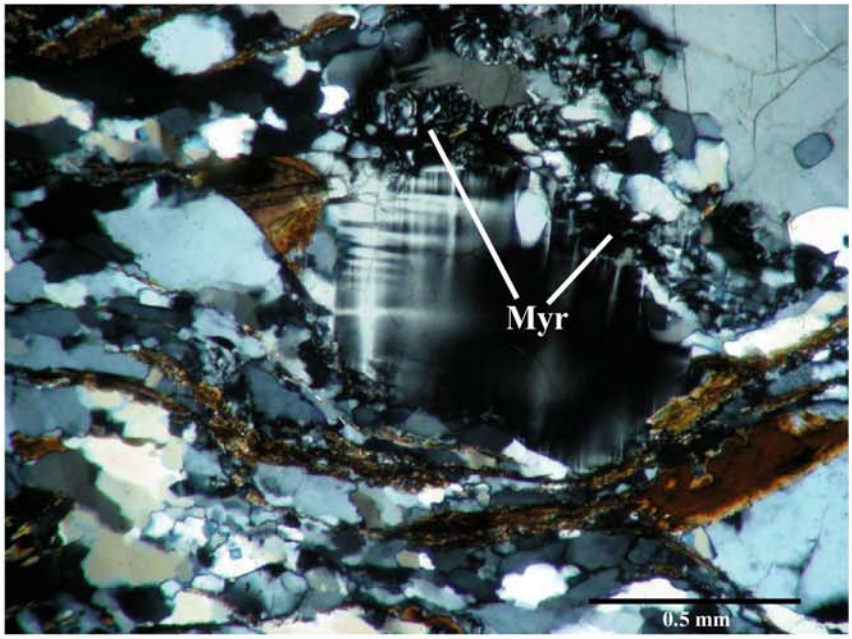

Figure 4.2. Deformation induced myrmekite (Myr) on microcline porphyroclast grain margins in mylonitic Bt gneiss. Cross polars. (DEL09-14a-1).

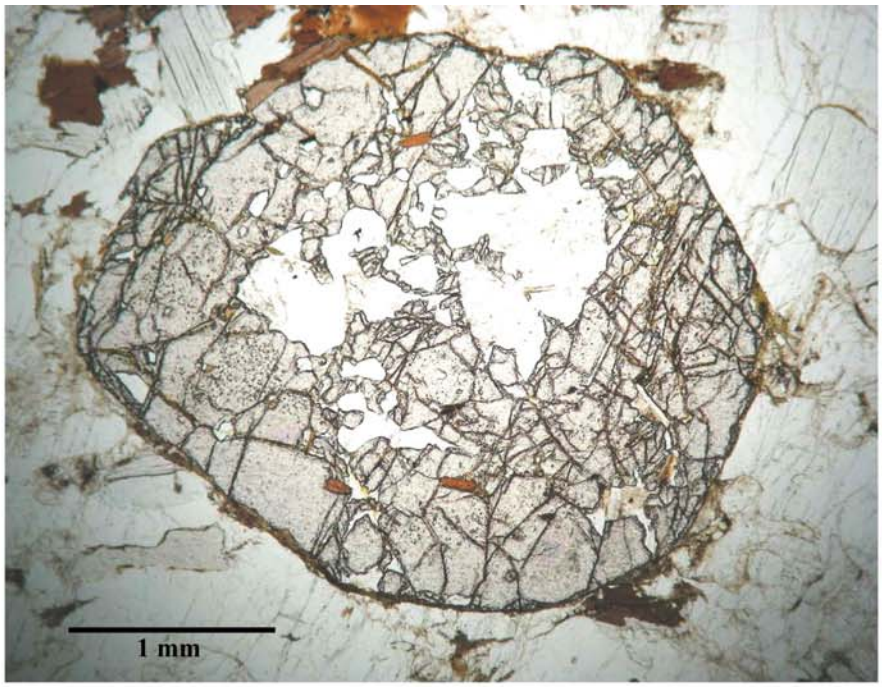

Figure 4.3. Poikiloblastic garnet with thin reaction rim of biotite. Plane light. (DEL09-15a).

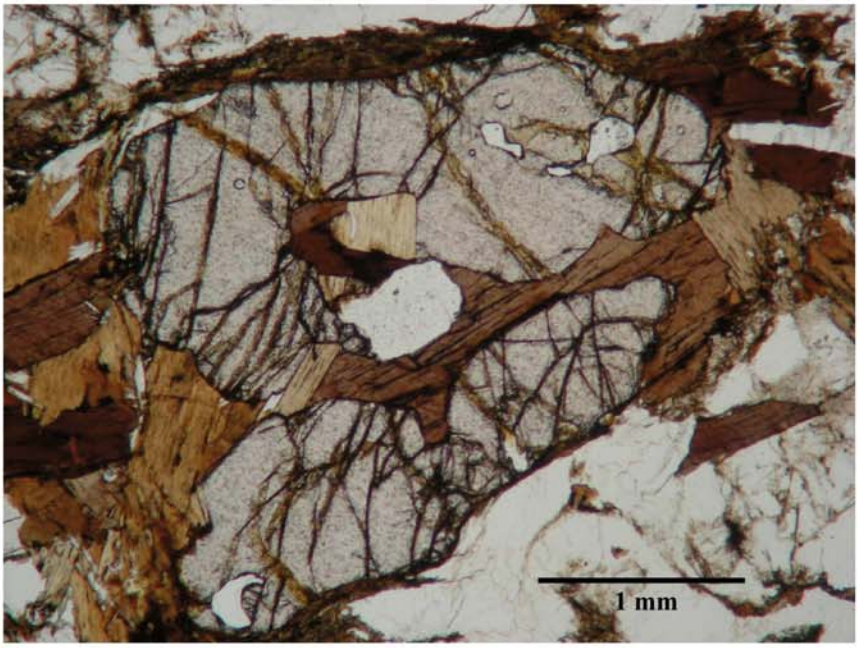

Figure 4.4. Retrograde biotite replacing garnet along fractures. Plane light. (DEL09-15a).

Hornblende Gneiss

The common mineral assemblage in the three hornblende gneiss varieties is alkali feldspar (commonly microcline) + quartz + hornblende + biotite + plagioclase. Plagioclase varies from trace to as much as 25 modal percent and is greatly exceeded by alkali feldspar in all samples. Quartz ranges in amount from 25 to 45 percent. Accessory minerals include anhedral to euhedral titanite and epidote, apatite, poikiloblastic and fractured garnet, ilmenite, spinel, and rarely zircon.

Metaplutonic Orthogneiss

Metaplutonic rocks at several locations exhibit an overall inequigranular and granoblastic to hypidiomorphic igneous texture (Figure 4.5). Fine-grained recrystallization on margins of relict feldspar phenocrysts is common. At one locality (location 7, Figure 3.2) metaplutonic rocks contain coarse-grained clinopyroxene phenocrysts (Figure 4.6) amounting to as much as 20 percent of the rock. Medium-grained interlocking hornblende phenocrysts are common and include prismatic allanite crystals (Figure 4.7).

Conspicuous replacement textures are present within the metaplutonic hornblende gneisses and are chiefly hydration reactions resulting from late Paleozoic uplift of the basement in this region. Hornblende reaction rims encapsulating clinopyroxene phenocrysts (Figure 4.6) and biotite partially or completely replacing hornblende phenocrysts (Figure 4.8) may represent progressive hydration-replacement reactions. Biotite after garnet pseudomorphs (Figure 4.9) and hornblende + quartz symplectites after clinopyroxene (Figure 4.10) are present as well.

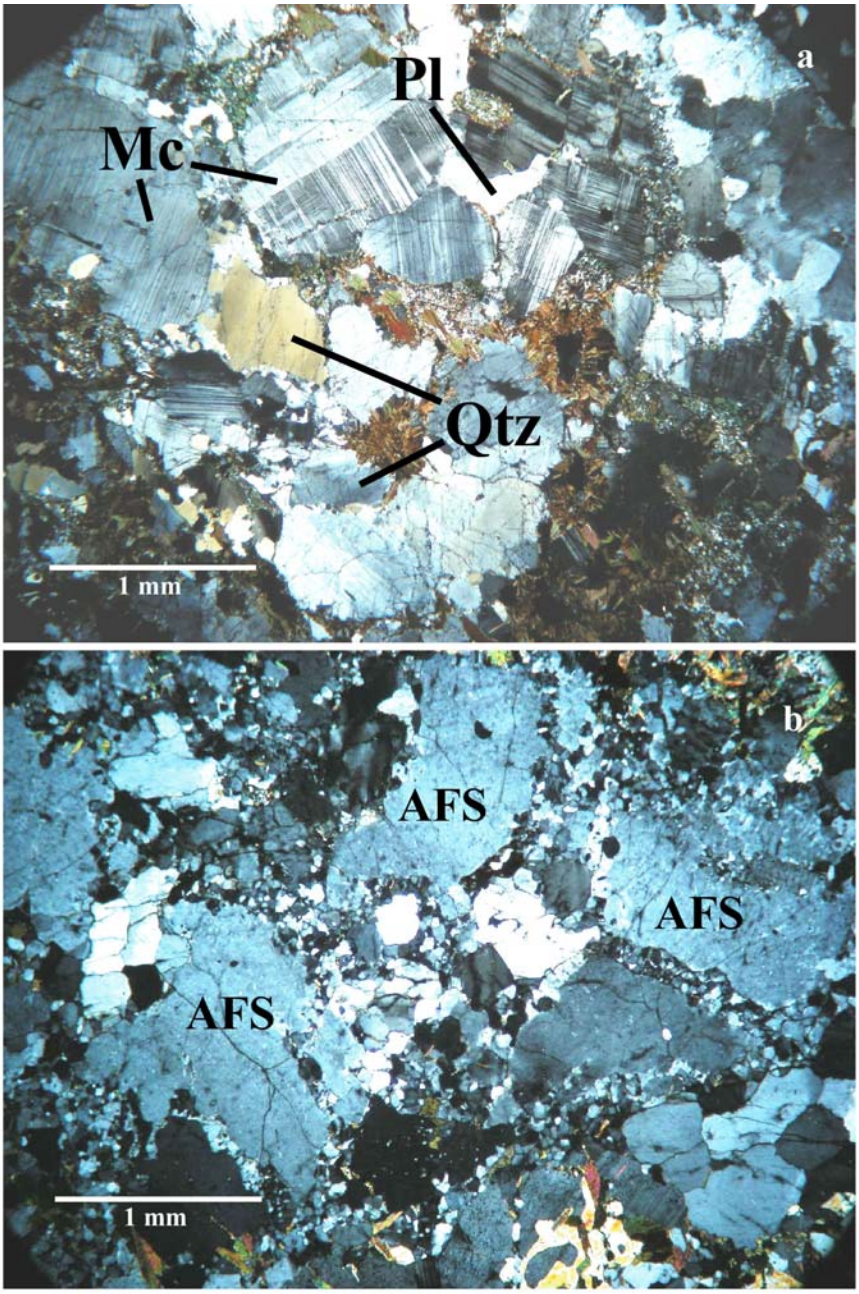

Figure 4.5. Igneous textures in metaplutonic rocks. a) interlocking texture of metaplutonic hornblende-biotite orthogneiss. (DEL09-17a). Mc=microcline, Pl=plagioclase, Qtz=quartz. Cross polars. b) relict interlocking igneous texture of alkali feldspar (AFS) with fine-grained recrystallized alkali feldspar on grain margins. Cross polars. (DEL09-16b).

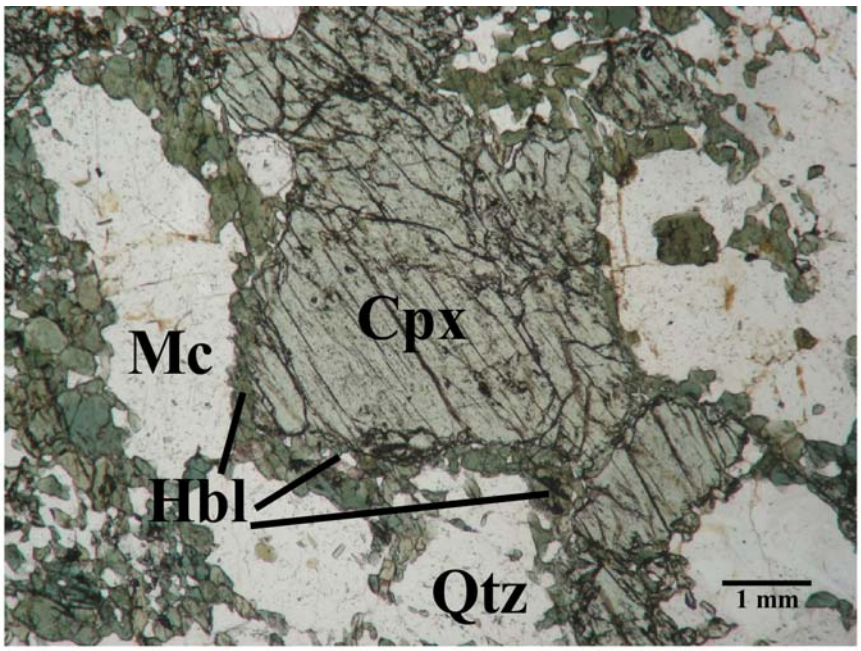

Figure 4.6. Relict clinopyroxene (Cpx) phenocryst in metaplutonic orthogneiss retrograding to hornblende (Hbl) along grain margins (DEL08-7c-2). Mc=microcline, Qtz=quartz. Plane light.

Figure 4.7. Prismatic allanite (Aln) with pleochroic halo included in hornblende. (DEL09-20). Plane light.

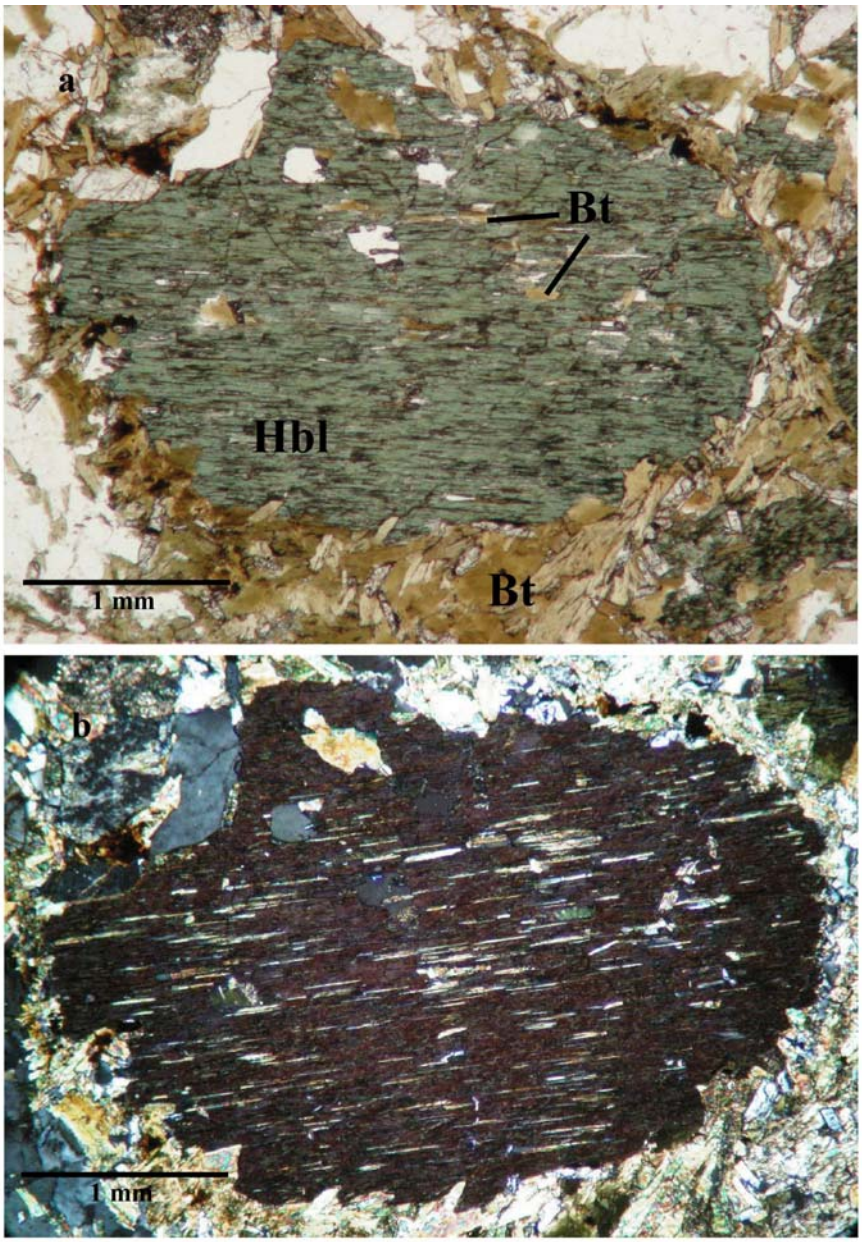

Figure 4.8. Hornblende (Hbl) phenocryst in metaplutonic orthogneiss exhibiting replacement with biotite (Bt) (DEL09-16b). a) Plane light and b) cross polars. Extensive replacement along cleavage planes is evident under cross polars.

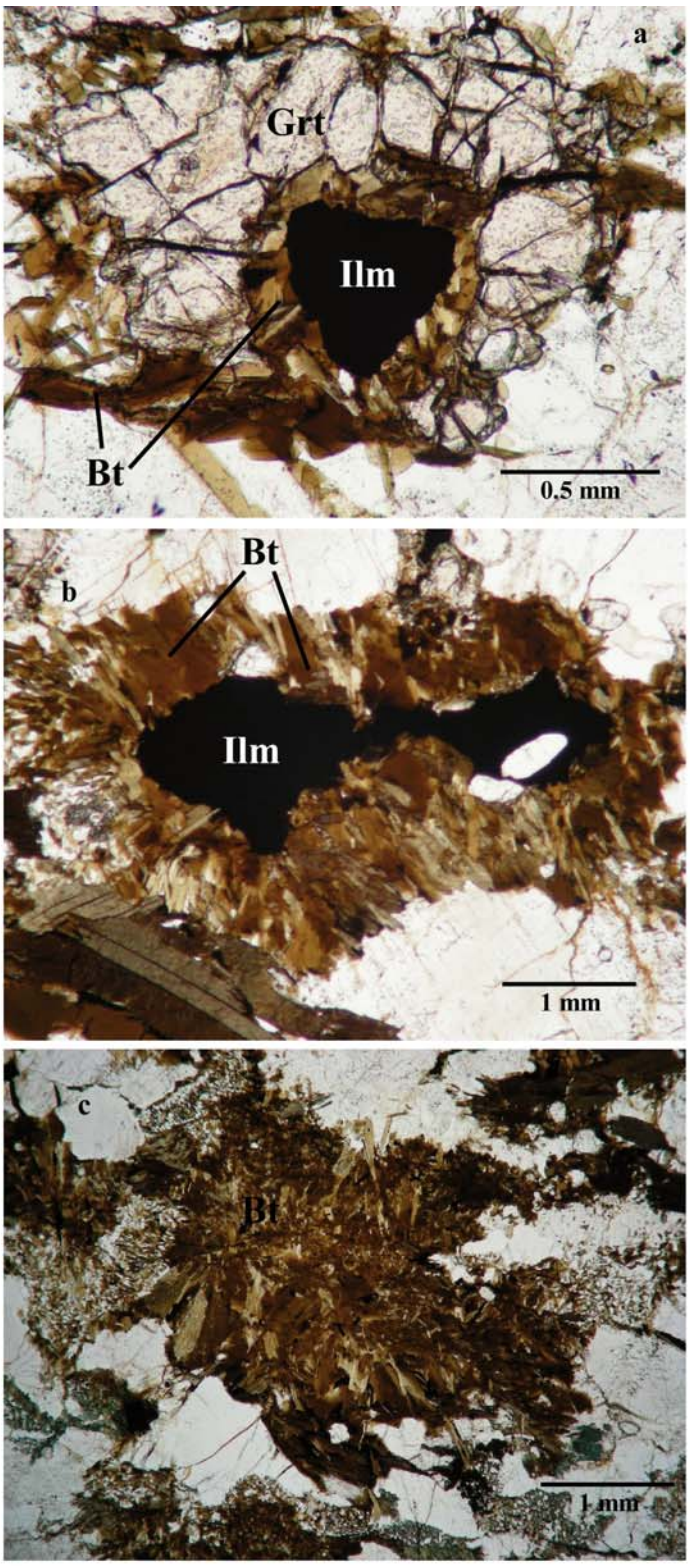

Figure 4.9. Progressive replacement of garnet (Grt) with biotite (Bt). a) Highly fractured Grt containing ilmenite (Ilm) inclusion is replaced by Bt along brittle fractures and at margins. b) and c) Fully developed Bt after Grt pseudomorphs exhibiting intergrown Bt crystals. All figures are shown in plane light. (DEL09-17a).

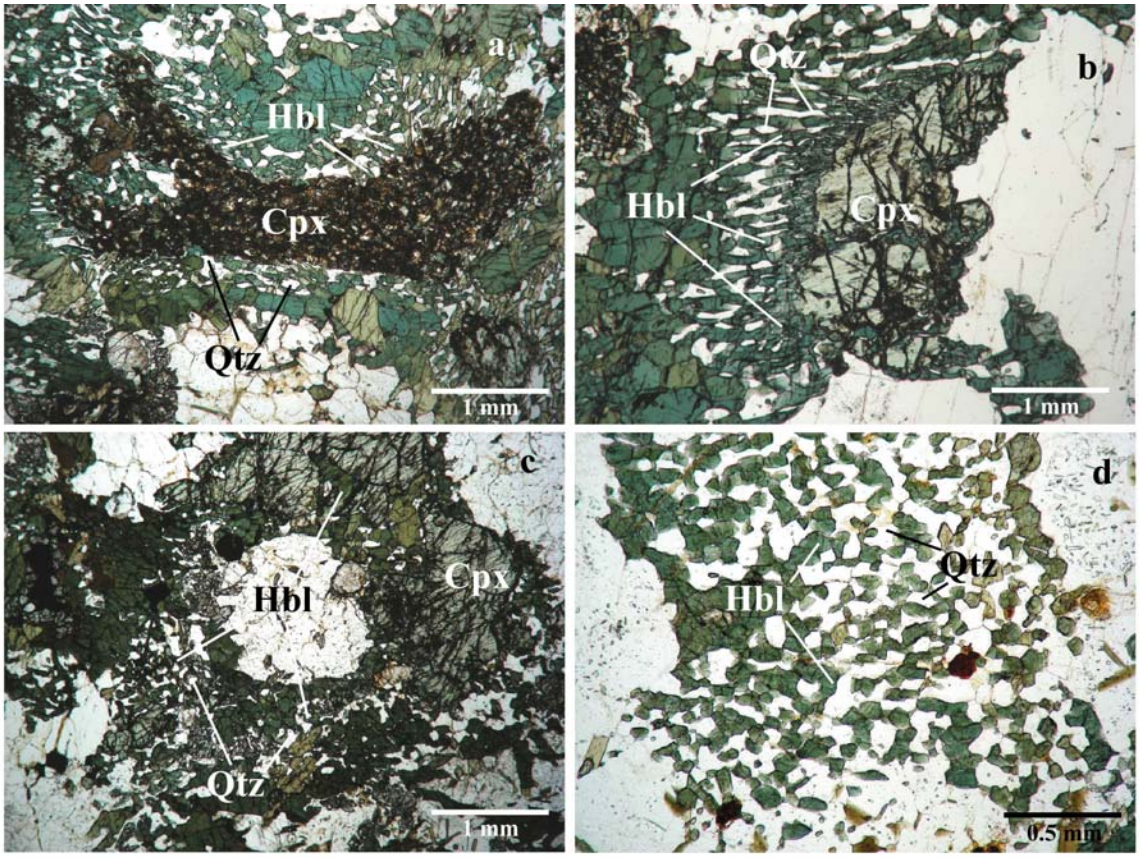

Figure 4.10. Clinopyroxene (Cpx) in metaplutonic orthogneiss exhibiting various stages of retrogression to hornblende (Hbl). Distinct reaction rims of Hbl + quartz (Qtz) envelop Cpx (a,b, and c). c) Cpx is an optically continuous grain (in crossed polars, not shown) d) fully developed hornblende + quartz symplectite after Cpx. Plane light.

Deformed Orthogneiss

Aside from textural differences, the main petrologic difference between the metaplutonic orthogneiss and their intensely deformed equivalents is the occurrence of titanite and epidote (Figure 4.11). Epidote is much more abundant in the deformed varieties due to deformation-induced retrograde metamorphic reactions involving the breakdown of hornblende to biotite + epidote. Epidote has a much lower abundance in the less deformed orthogneisses. Replacement of hornblende with biotite along cleavage planes and on rims is common (Figure 4.12).

Textural and mineralogical similarities exist between the metaplutonic rocks and their intensely deformed equivalents. The highly foliated varieties retain the inequigranular and granoblastic interlocking igneous texture, though often more deformed as indicated by a higher occurrence of recrystallized quartz and feldspar (Figure 4.13). Deformed and amalgamated hornblende + quartz symplectites after clinopyroxene are present that show further progressive replacement of hornblende by biotite (Figure 4.14). Modal percentages of quartz, alkali feldspar, and plagioclase are similar between the two lithologies and are distinct from that of biotite gneiss (Figure 4.15).

Migmatitic Hornblende Gneiss

Hornblende-bearing migmatites do not exhibit primary igneous textures, although they are mineralogically similar to and may be genetically related to the orthogneisses. They are distinctive in that these rocks exhibit obvious mesoscopic leucosomes (Figures 3.7 and 3.8) that display igneous textures (Figure 4.16) possibly due to dehydration melting during peak thermal conditions. Alternating with the leucosomes are

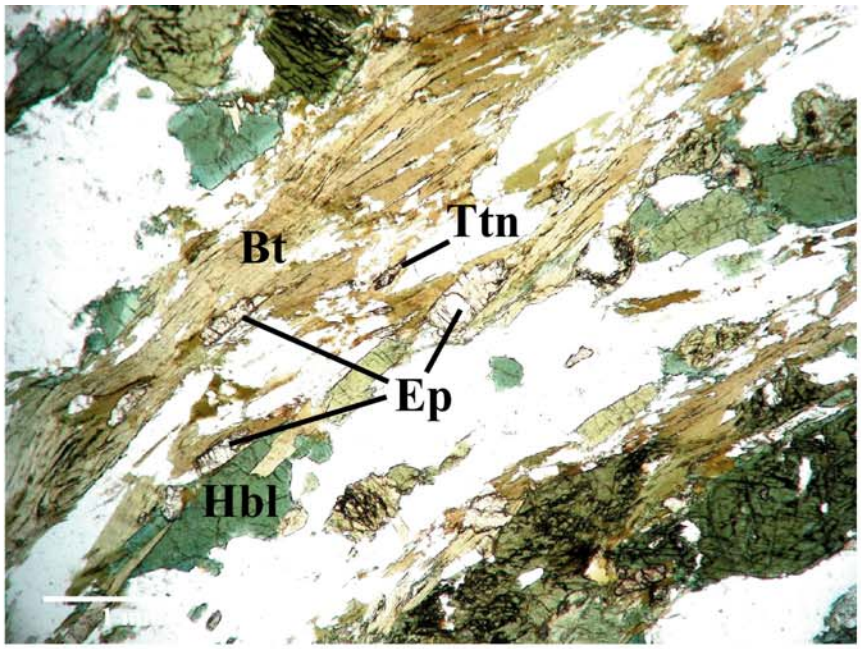

Figure 4.11. Photomicrograph of deformed orthogneiss (DEL08-11c) showing occurrence of hornblende (Hbl), biotite (Bt), epidote (Ep), and titanite (Ttn). Bt penetrates Hbl along cleavage planes (lower left) and Ep is present between Hbl and Bt. Plane light.

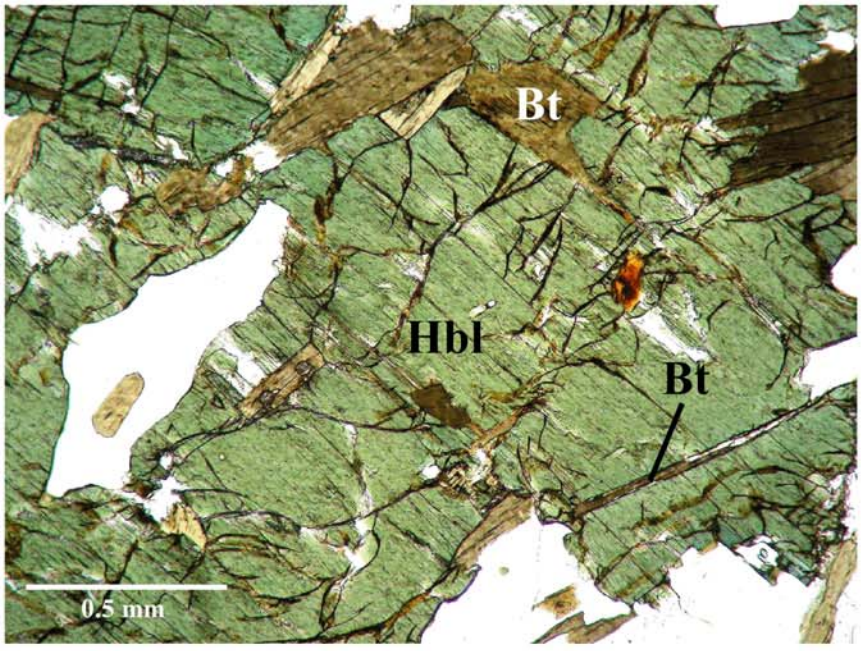

Figure 4.12. Replacement texture in deformed orthogneiss. Penetration of biotite (Bt) along cleavage planes and fractures suggests replacement of hornblende (Hbl). Width of view is 2 mm. Plane light. (DEL09-6A-1).

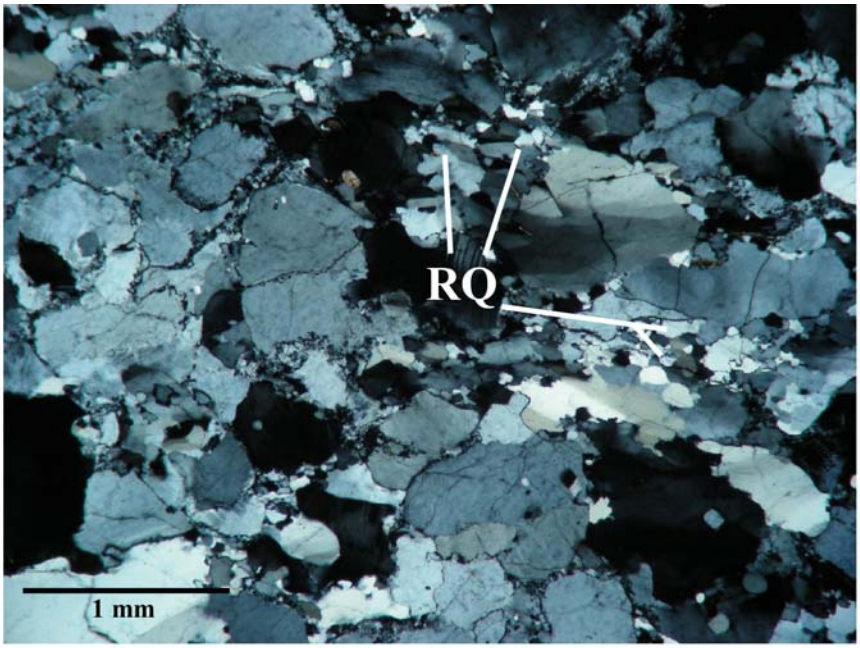

Figure 4.13. Deformed orthogneiss texture. Deformed interlocking igneous texture showing larger occurrence of recrystallized quartz (RQ) and feldspar than in meta-plutonic rocks. Cross polars. (DEL08-6c).

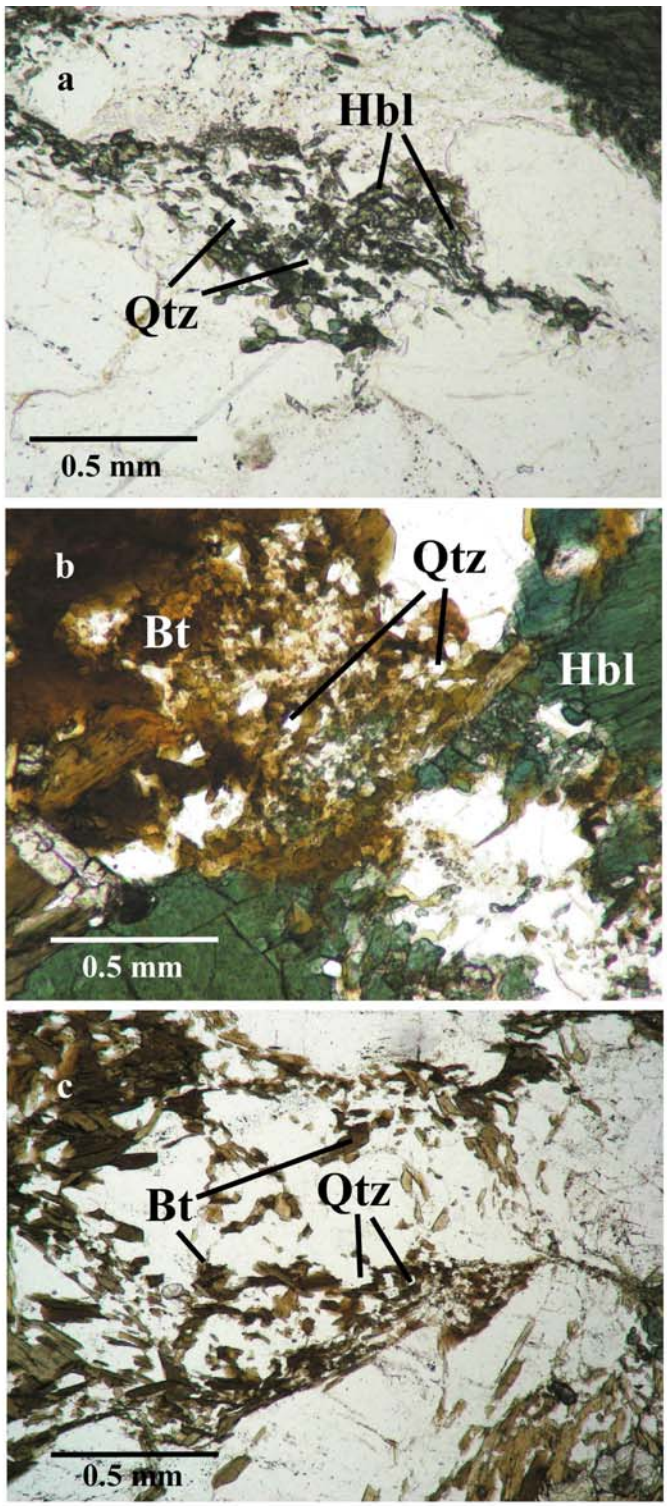

Figure 4.14. Progressive replacement of hornblende (Hbl) + quartz (Qtz) symplectites after clinopyroxene by biotite (Bt) in deformed orthogneiss. a) deformed Hbl + Qtz symplectite after clinopyroxene b) Bt replacing Hbl in symplectite c) fully developed replacement of Hbl by Bt in symplectite. Notice preserved skeletal texture in all figures. Plane light.

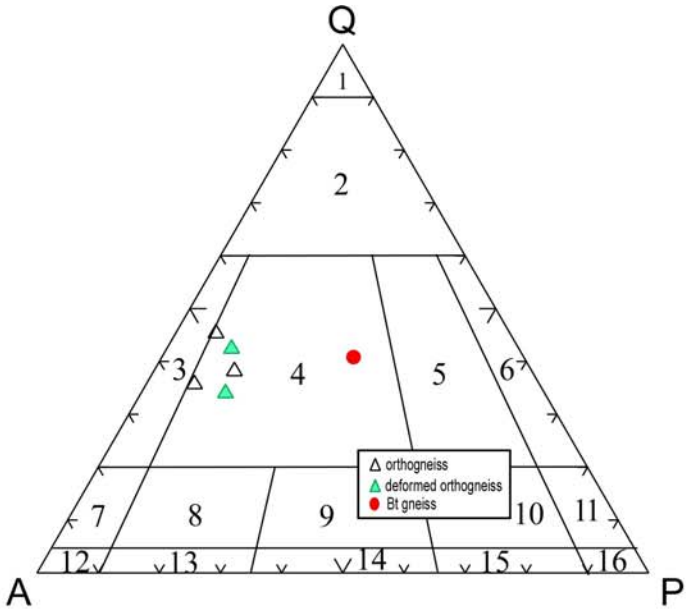

Figure 4.15. Quartz (Q)-alkali feldspar (A)-plagioclase (P) diagram of representative samples of three lithologies recalculated on the basis of volumetric percentage of quartz, alkali feldspar, and plagioclase. Note the mineralogical distinction between Bt gneiss and orthogneiss. 1-quartzolite, 2-quartz-rich granitoid, 3-alkali feldspar granite, 4-granite, 5-granodiorite, 6-tonalite, 7-alkali feldspar quartz seyenite, 8-quartz seyenite, 9-quartz monzonite, 10-quartz monzodiorite, 11-quartz diorite, 12-alkali feldspar seyenite, 13-seyenite, 14-monzonite, 15-monzodiorite, 16-diorite. Classification after Streckeisen (1976).

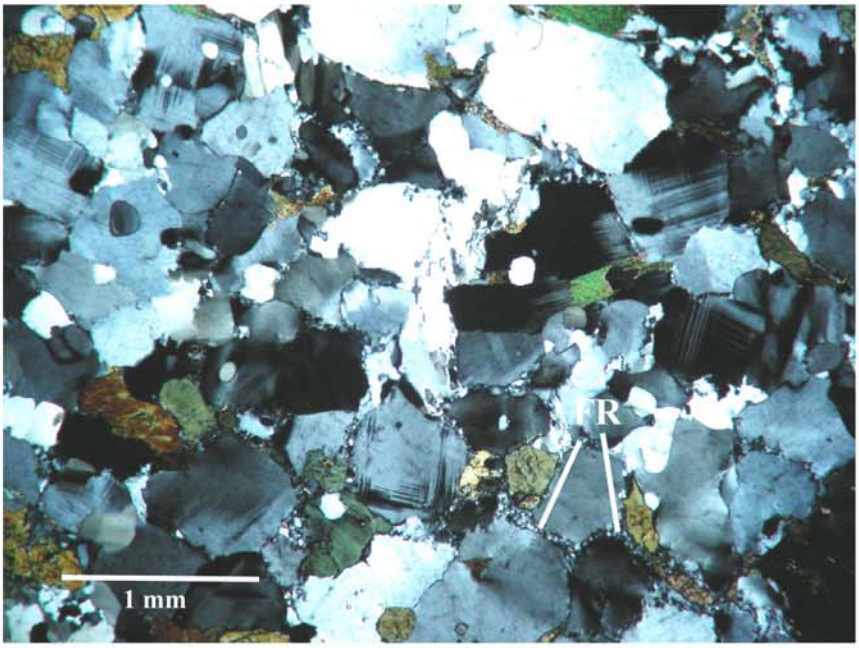

Figure 4.16. Minimally deformed leucosome in migmatitic hornblende gneiss with fine grained recrystallization of feldspars (FR) on grain margins. Cross polars. (DEL08-10a).

melanosomes containing mafic minerals that appear preferentially aligned (Figure 4.17), either through a previous foliation-producing event or reorientation to make space for crystallizing leucosome melt. Field relationships indicate the former, as most migmatitic bodies contain similar foliation orientations.

Although most migmatitic hornblende gneiss in the study area displays medium-grained, minimally deformed leucosomes, one locality (CG09-1-1) contains narrow late-stage mylonite zones (Figure 4.18) that deform the leucosomatic texture in areas between hornblende porphyroclasts that have apparently impinged upon one another during deformation. Poikiloblastic garnets containing two stages of inclusion trails (Figure 4.19) are also present at this location.

Conspicuous brittle fractures within melanosomes (Figure 4.20) occur at the mesoscopic scale at several locations resulting from late deformation occurring at high strain rates and/or low confining pressures. Alignment of platy minerals (ie. biotite, hornblende) within melanosomes offer weak zones conducive to slip.

Amphibolite

Rare amphibolite bodies in the study area exhibit inequigranular to equigranular unfoliated granoblastic texture and are interpreted as meta-igneous bodies, though one locality (location 23) exhibits moderate foliation. The common mineral assemblage is hornblende + quartz + plagioclase ± garnet ± clinopyroxene ± titanite ± ilmenite (Figure 4.21). Hornblende comprises more than 50 percent of the rock volume, greatly exceeding both quartz and plagioclase. Garnet exhibits resorbed margins and includes titanite. At one locality (location 7) amphibolite xenoliths contain clinopyroxene, amounting to approximately 20 percent of the rock.

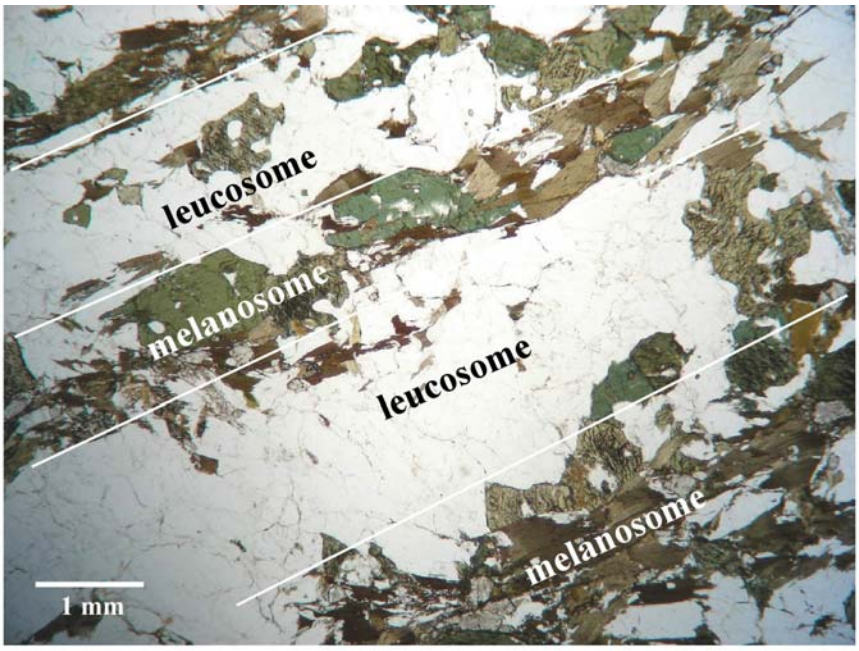

Figure 4.17. Thin alternating melanosomes and leucosomes (bounded by white lines) in migmatitic hornblende gneiss. Mafic minerals in melanosomes exhibit a preferred orientation parallel to compositional banding. Plane light. (DEL09-10a).

Figure 4.18. Late mylonite zone in migmatite (CG09-1-1a). Leucosomatic material is recrystallized within high strain areas between hornblende porphyroclasts. a) Plane light and b) cross polars.

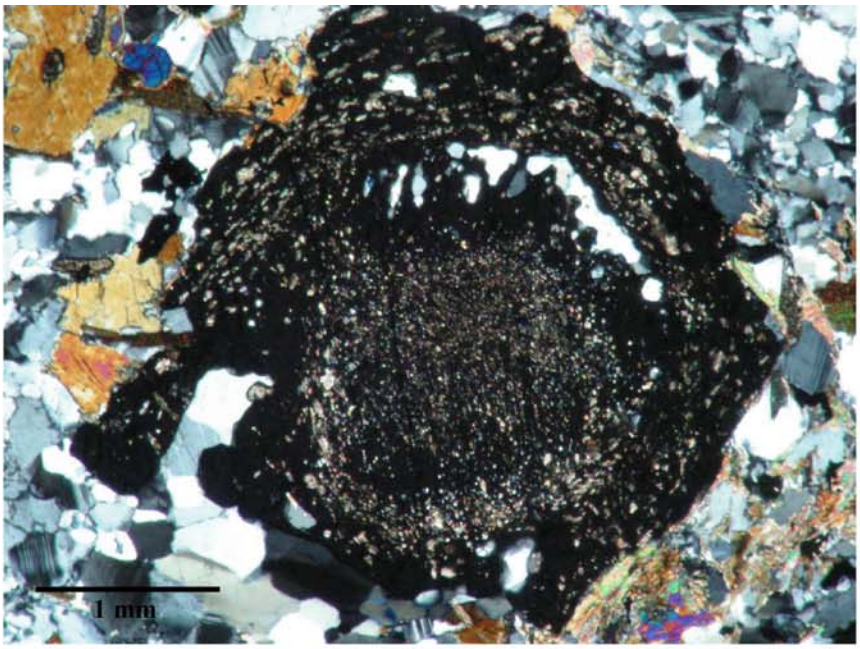

Figure 4.19. Poikiloblastic garnet within hornblende migmatite. Note two sets of inclusion trails. Vertical orientation within core preserves relict foliation and suggests pre-kinematic growth. Spiral trails near rim suggest syn-kinematic overgrowth. Inclusions are fine-grained titanite and coarser-grained quartz. Cross polars. (CG09-1-1a).

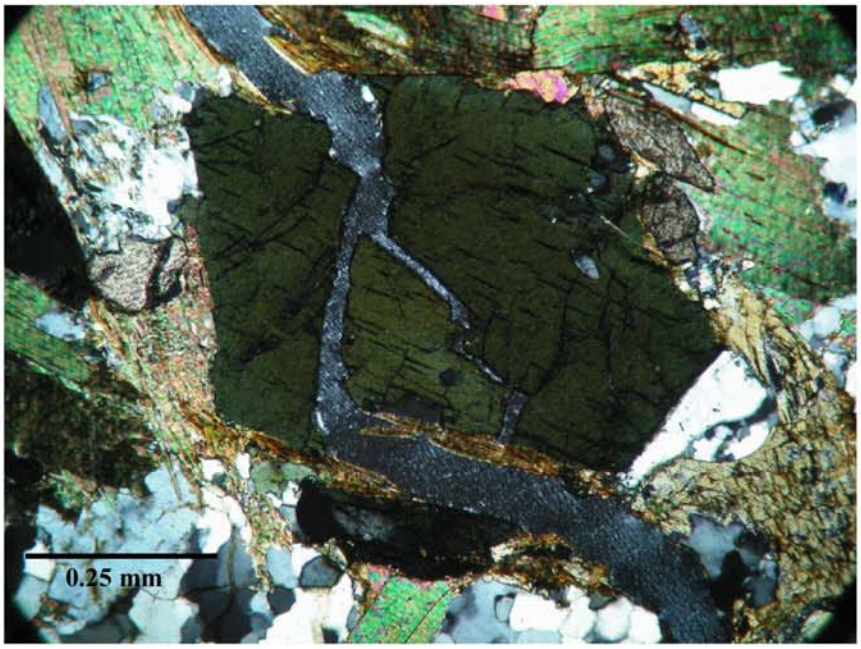

Figure 4.20. Brittle deformation in hornblende migmatite. Fracture through hornblende crystal evident at scale of hand sample continuing along melanosome. Aligned platy minerals allow slip parallel to melanosome. Cross polars. (DEL09-18a).

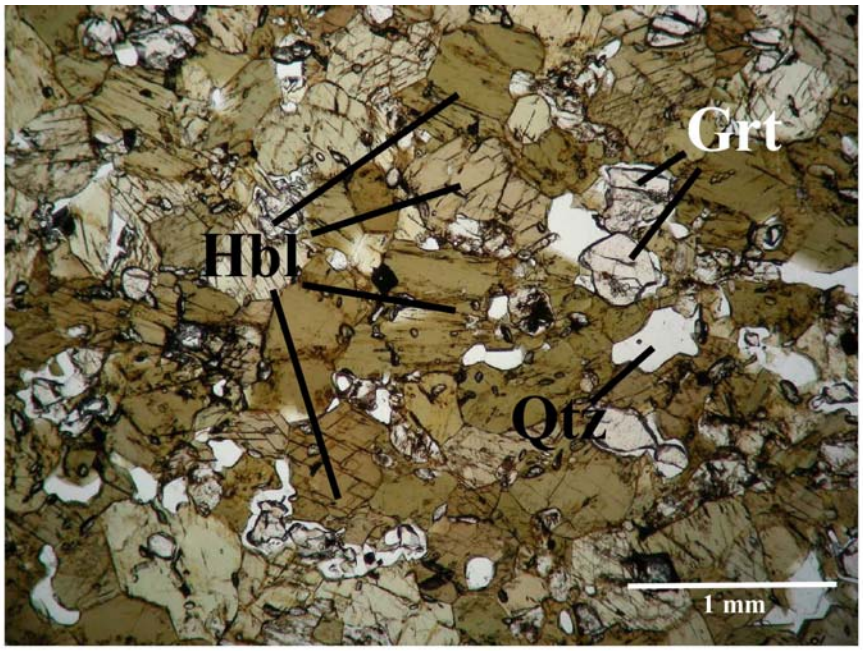

Figure 4.21. Typical hornblende-rich amphibolite assemblage. Plane light. (DEL09-26a).

SECTION V. STRUCTURAL GEOLOGY

Structural observations were performed on the macro-, meso-, and microscopic scale for each sample location within the study area. Measurement and description of structural elements focused on resolving the fold history and associated planar and linear petrofabrics in the area in order to characterize the deformation history of the basement rocks. Thin sections from 16 oriented hand samples were analyzed to resolve microstructures associated with hand sample and outcrop-scale structural elements.

Structural measurements were taken at every accessible basement outcrop within the quadrangle. Where possible, multiple foliation and fold axis orientation measurements were acquired to account for outcrop-scale heterogeneity. Complete structural data can be found in Appendix A.

Structural Elements

Foliations

Although one NE-SW striking foliation (Figure 5.1) dominates the study area, an additional foliation associated with hand sample-scale to map-scale folds in the region is resolved in this study. The dominant foliation (Figure 5.2) is compositional in nature resulting in the banded and layered appearance of the basement gneisses and is assumed to be the result of peak thermal conditions during regional metamorphism (Taconian), as dated by Anderson and Moecher (2009). Although bedding (S_0) and an early schistosity (S_1) parallel to bedding is recognized in some metapsammitic rocks and metapelites in

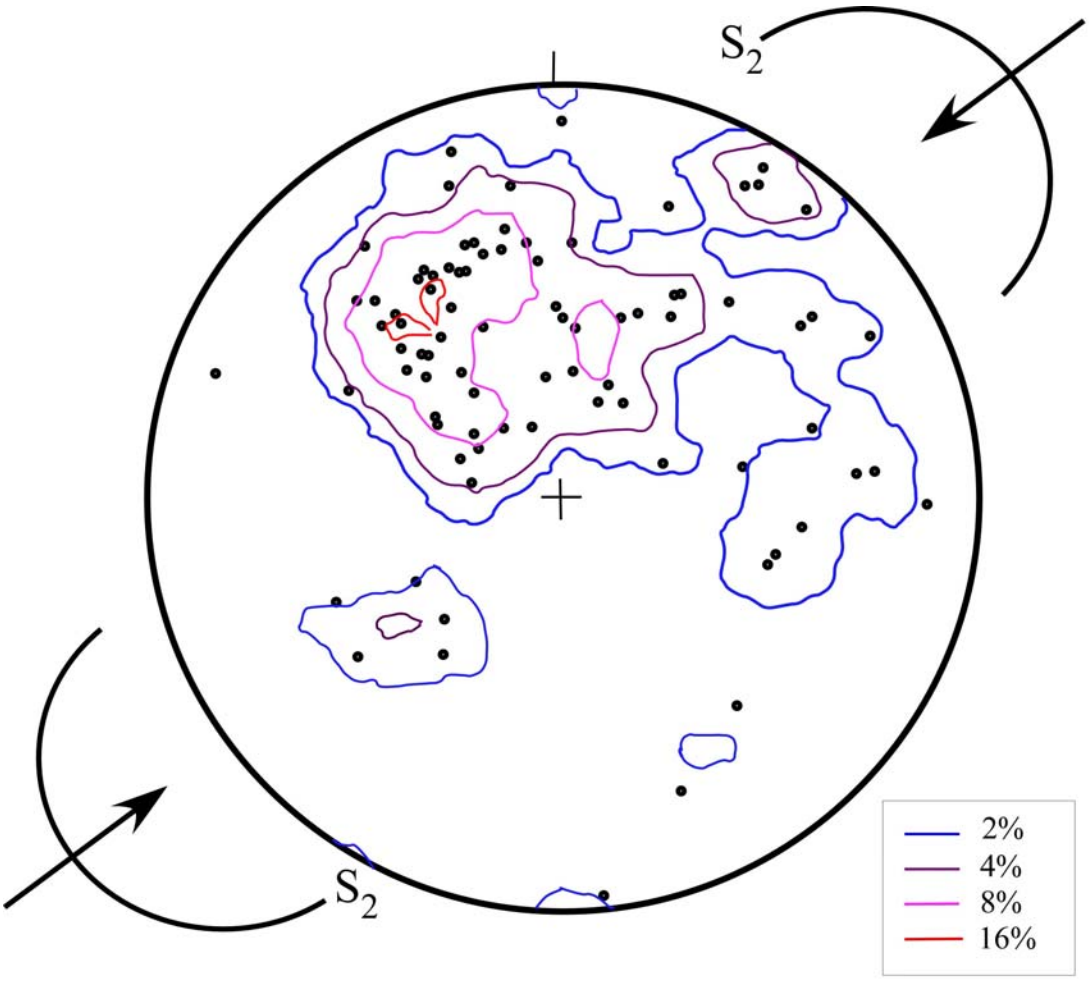

Figure 5.1. Contoured equal area net of poles to foliations throughout study area. Folded dominant foliation (S_2; arrows) strikes NE-SW. Semicircles show approximate range of S_2 orientation. Georient used with permission (Holcombe, 2009).

Figure 5.2. Compositional foliation (S_2) in biotite gneiss at Trinity Cove (location 2). a) Outcrop showing leucosome development parallel to S_2. b) Hand sample from same outcrop in (a) showing banded appearance of S_2.

the region (Massey, 2003; Massey and Moecher, 2005), S_0 and S_1 are not preserved in the basement gneisses. Foliation nomenclature will hereafter follow that of Massey and Moecher (2005), where S_0 (bedding) and S_1 are not resolved in Dellwood quadrangle gneisses due to the high grade of metamorphism, S_2 is the regional compositional foliation, and S_3 is the late fabric associated with the dominant folding event. S_0, S_1, and S_2 relationships are consistent with previous work in the area (Eckert, 1984; Massey, 2003; Massey and Moecher, 2005; Montes, 1997; Quinn, 1991). A late non-penetrative S_3 fabric deforms S_2, is manifested locally as an axial plane crenulation (Figure 5.3), and is associated with macroscopic to microscopic, open to tight, chevron-shaped flexural slip and flexural flow folds (Figure 5.4) whose axial planes are at a moderate to high angle to S_2.

Folds

Polyphase folding is readily apparent at the outcrop scale throughout the study area. The earliest generation of folds is manifested as tight to isoclinal, intrafolial, passive flow folds whose axial planes parallel S_2 (Figure 5.5) and whose isoclines contribute to the banded appearance of the dominant foliation (Figure 5.6). This generation of folds appears identical to the F_2 folds of Massey (2003) and Massey and Moecher (2005) who described the fold history of the Eastern Blue Ridge-Western Blue Ridge boundary in the Sylva North quadrangle immediately to the southwest of Dellwood quad. F_1 folds, if preserved at all in the basement gneisses, were not differentiable from the aforementioned folds. Thus, the earliest fold generation in the study area is hereafter regarded as F_2.

Figure 5.3. S_3 axial plane crenulation in Bt gneiss (location 21).

Figure 5.4. Development of S_3 fabric related to axial planes of F_3 folds. a) Mesoscopic open folds deform migmatitic S_2 foliation at location 13. b) close up view of same outcrop showing fold cross-sections. Note S_3 is not penetrative. c) S_3 planar fabric in Bt gneiss at location 15.

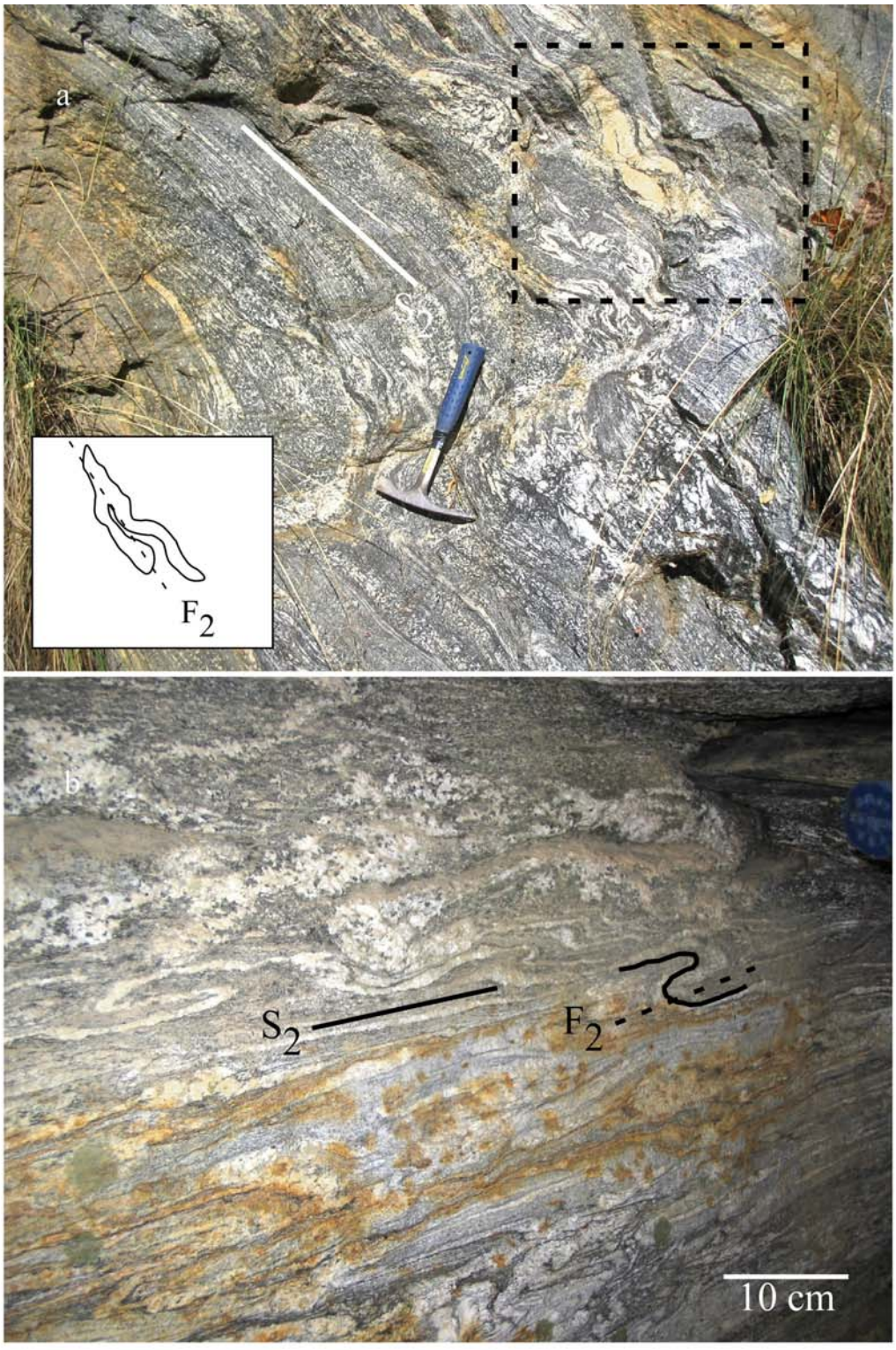

Figure 5.5. F_2 folds in Hbl gneiss at a) The Preserve housing development at location 11 showing isoclinally folded leucosome (inset is interpretation) and b) Erwin Ln. outcrop at location 19. Note that fold axial planes parallel S_2 foliation.

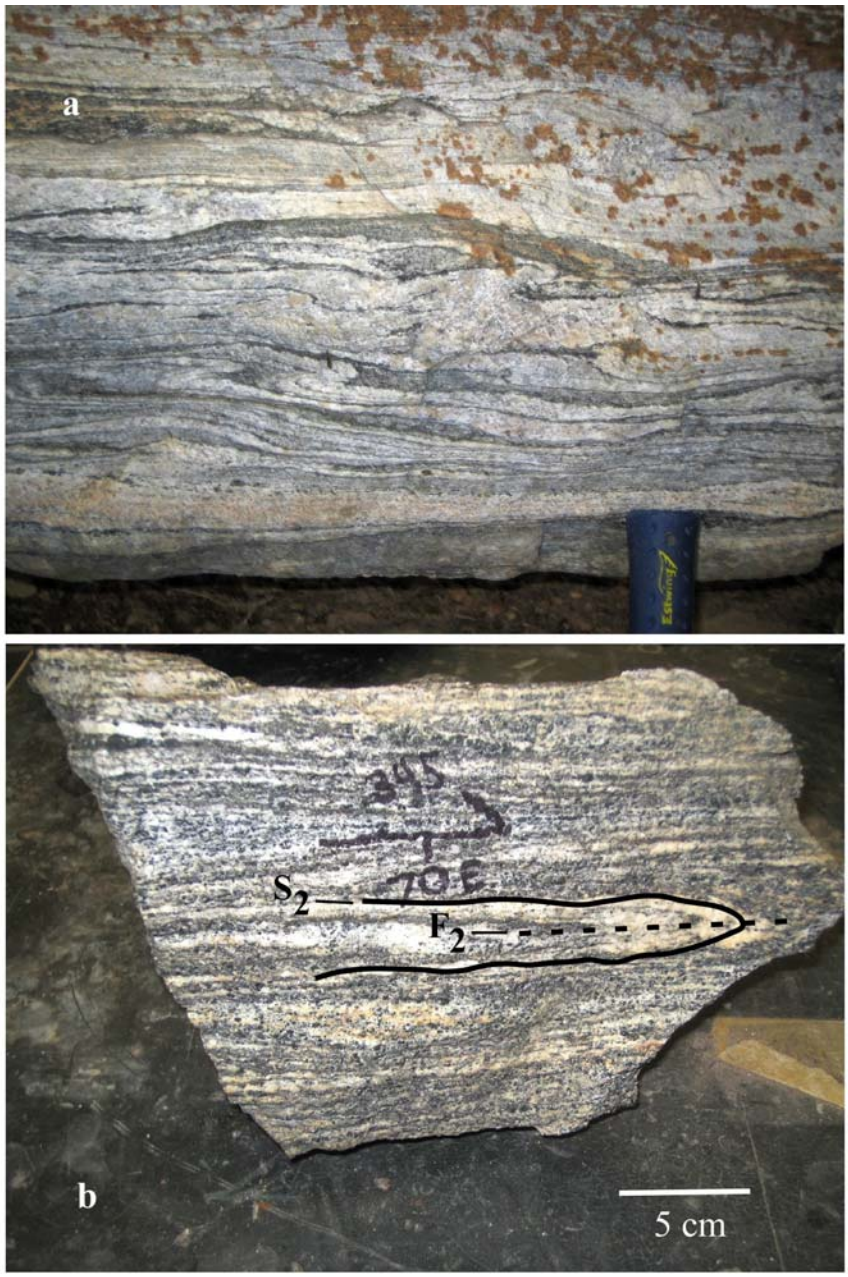

Figure 5.6. F_2 fold isoclines contributing to banded appearance of Hbl gneiss. a) Outcrop at Erwin Ln., location 19 (hammer for scale) b) Hand sample from eastern flank of Trit Knob (location 10). Fold axial planes parallel S_2.

The dominant folding event in the study area (F_3), characterized by open to tight chevron-shaped flexural folding as well as open to tight ptygmatic folding in migmatites, locally folds S_2 and transposes the dominant foliation into a non-penetrative axial plane cleavage. F_3 folds commonly refold isoclinal F_2 folds within S_2 (Figure 5.7). F_3 folds have shallow to moderately plunging fold axes that plunge in a direction parallel to dip of S_3. Two dominant trends (Figure 5.8) occur in the F_3 folds within the study area. One set of mesoscopic F_3 folds trend in a NE-SW direction consistent with macroscopic folding in the quadrangle. Another set of F_3 folds trend in a NW-SE direction. This set is parallel to those with Grenvillian orogenesis (Cattanach and Merschat, 2005; Merschat and Wiener, 1990), but geochronology (Taconian metamorphism and migmatization) require it to result from transposition of F_3 fold axial planes during late Paleozoic deformation associated with formation of high strain zones as there is no discernable difference in fold appearance between the sets.

The axial planes of F_3 folds produce the S_3 planar fabric in all basement lithologies, with the exception of the meta-plutonic hornblende orthogneiss found in the interiors of large hornblende gneiss bodies. The non-penetrative S_3 foliation produced by the F_3 folding event is possibly absent in these rocks due to contrasting competencies between the orthogneisses and the enveloping metasedimentary-derived biotite gneisses. Thus, the interiors of these bodies appear to have been shielded from the deformation associated with the F_3 event.

High Strain Zones

Retrograde high strain zones are found throughout the basement rocks within the quadrangle. Most notable are thin (< 1 cm), relatively straight ultramylonite bands within

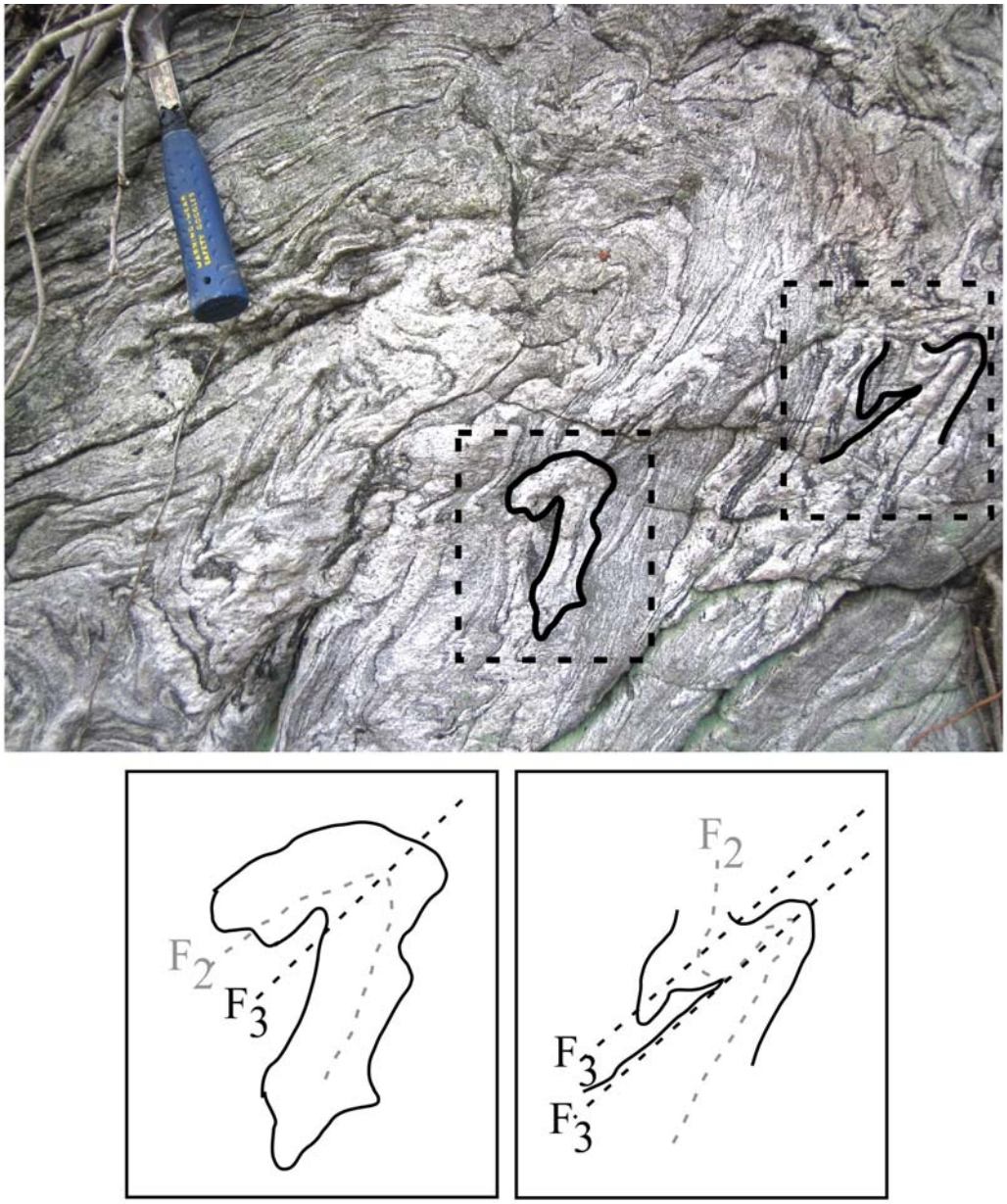

Figure 5.7. F_2 isoclinal folds refolded by F_3 in Bt gneiss, location 19. Interpretation below photograph.

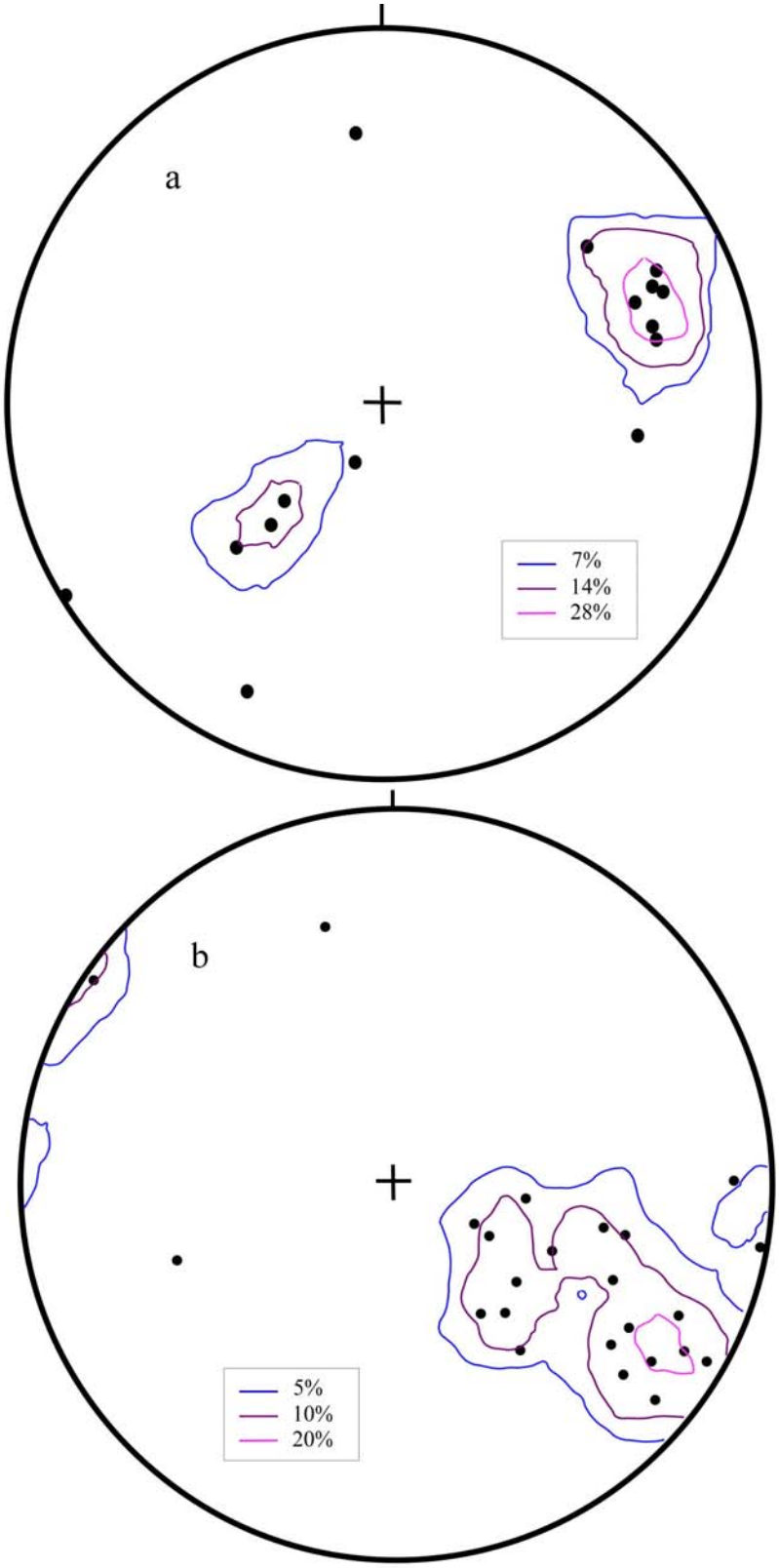

Figure 5.8. Equal area stereonets of F_3 fold axes. Note two modes of axis trends. a) NE and SW trending folds and b) NW and SE trending folds. Georient used with permission (Holcombe, 2009).

granitoid augen gneiss (Figure 5.9) that cross-cut the dominate foliation at moderate to high angles, thus post-dating S_2 formation. Similar ultramylonite bands (Figure 5.10) are found within Eastern Blue Ridge hornblende gneiss assemblages along the Blue Ridge Parkway at the Mt. Lynn Lowry overlook in Sylva North quad, at Coleman Gap along Coleman Mountain Road in Clyde quad, and in Great Smoky Group kyanite-garnet-staurolite schists throughout the Dellwood quadrangle. These bands also appear late relative to S_2 as they dismember earlier F_2 isoclinal folds. Similar localized high strain zones were described by Massey (2003) and are characterized microscopically by dynamic recrystallization of quartz and fracture of feldspar (Massey and Moecher, 2005).

A high temperature, high strain zone (Figure 5.11) ~ 2 m wide was discovered at a roadcut within The Preserve housing development near the Holiday Drive-Tanner Trail junction. This zone exhibits a flattening fabric parallel to S_2 resulting in boudinage of amphibolite pods and void-filling leucosome and, therefore, may be interpreted to be syn-deformational relative to S_2. However, the same structure could also result from intensification of foliation around a more competent inclusion (boudin) during S_3 formation. Outcrop-scale brittle faulting is not apparent within the basement suite in the field area.

Microstructures

Microstructures associated with S_2 foliation (Figure 5.12) consist primarily of the preferred orientation of porphyroclastic coarse-grained biotite ± muscovite ± hornblende and recrystallization of quartz to accommodate flattening perpendicular to foliation.

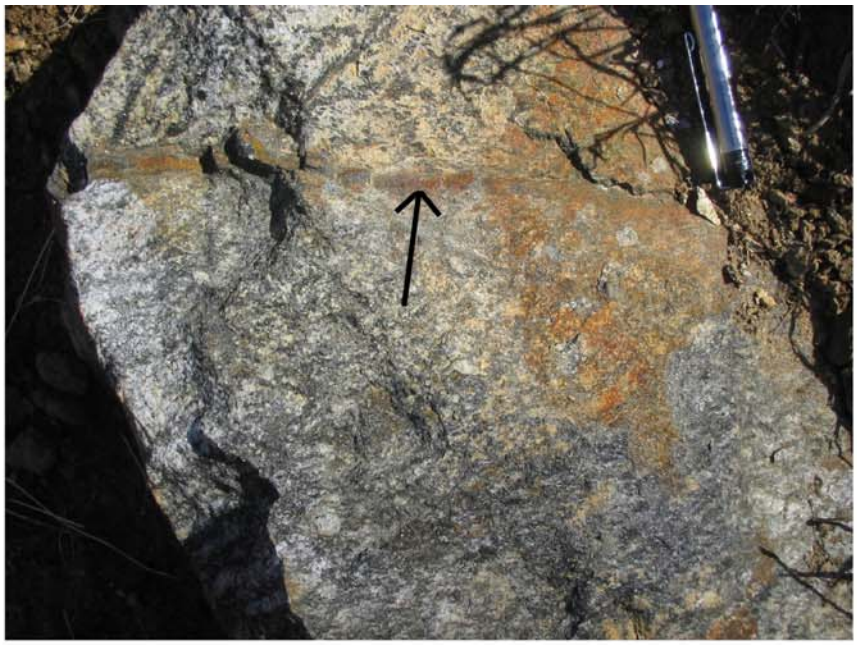

Figure 5.9. Ultramylonite zone (arrow) in granitoid gneiss (pCg) near location 16.

Figure 5.10. Thin ultramylonite zones (black lines) along the Blue Ridge Parkway (Mt. Lynn Lowry overlook) dismember isoclinal fold limbs from hinges, causing folds to exhibit a wispy appearance. Leucosomes become thinned and attenuated (white arrow).

Figure 5.11. Amphibolite boudin in high strain zone in hornblende gneiss outcrop within The Preserve housing development.

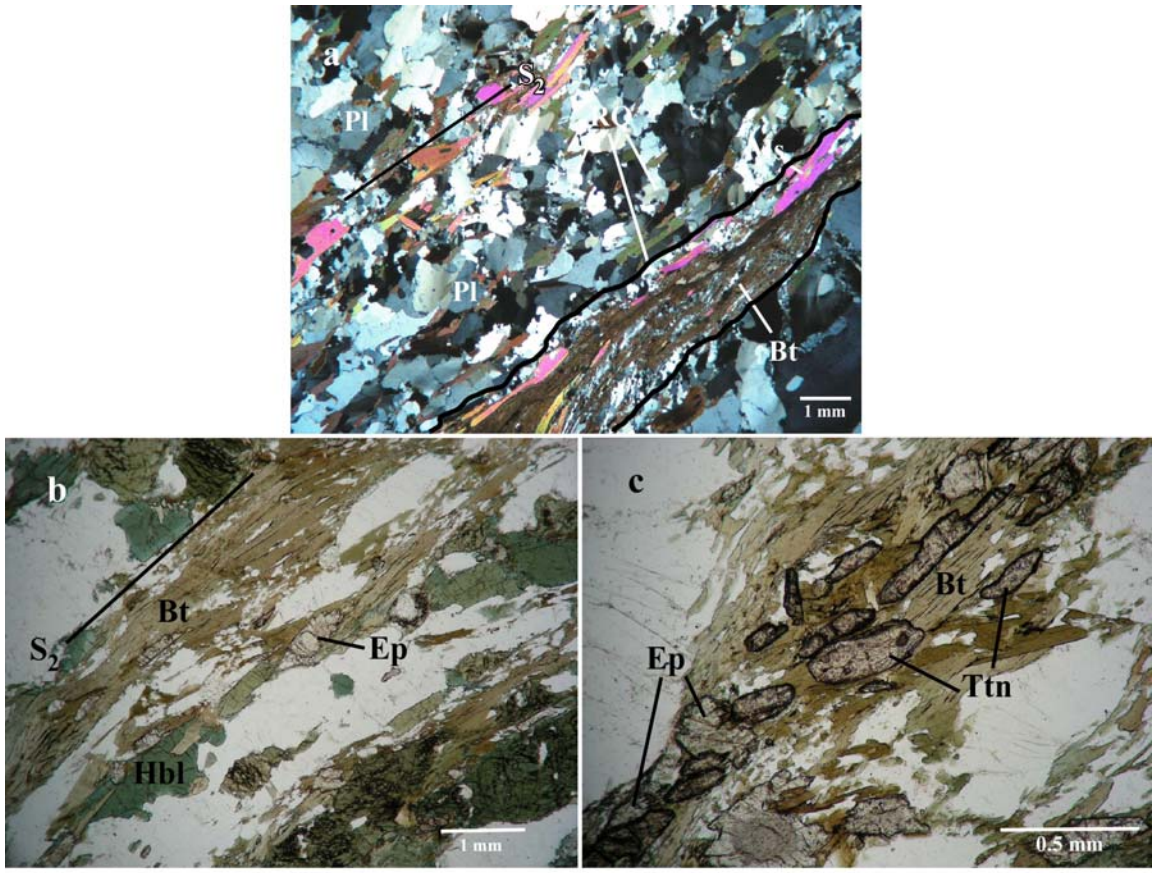

Figure 5.12. Microstructures associated with S_2 foliation. a) Photomicrograph of biotite gneiss (DEL08-2d) showing compositional foliation (S_2) defined by recrystallization of quartz (RQ) and alignment of biotite (Bt) and muscovite (Ms). Note fine-grained recrystallization of Bt + quartz within spaced micro-shear bands (outlined). Cross polars. b) Prekinematic (relative to S_2) Bt+hornblende (Hbl)+Ep aligned to define S_2. Plane light. (DEL08-11c). c) Titanite (Ttn) and Epidote (Ep) strung out along S_2 within biotite-rich zone. Planelight. (DEL08-11c).

Clasts of titanite and epidote, mostly within biotite-rich zones, are commonly strung out parallel to S_2 and help to define the foliation. The compositional nature of S_2 is a result of alternating compositionally distinct zones of biotite, hornblende, titanite and epidote with zones primarily consisting of quartz and feldspars formed during migmatization. Spaced micro-shear bands consisting of finely recrystallized biotite and quartz parallel the foliation, contribute to its compositional nature, and contain cataclasized titanite grains (Figure 5.13), locally. Mylonitic textures were observed at one locality (location 14) in a float boulder of biotite gneiss. The mylonitic foliation (Figure 5.14) is defined by complete recrystallization of quartz into fine, irregularly shaped crystals exhibiting sutured grain boundaries and is deflected by feldspar porphyroclasts. Rare quartz ribbons are present. Quartz and feldspar behavior within mylonite zones require lower temperatures relative to peak metamorphic conditions in the region. Thus, mylonitic foliation must have occurred later than S_2.

The incipient, non-penetrative nature of S_3 results in more obscure microstructures. Where present, S_3 is manifested as a disjunctive, anastomosing axial planar foliation (Figure 5.15) that wraps feldspar porphyroclasts, is defined by the reorientation and neocrystallization of mica paralleling F_3 fold axial planes, and is more clearly resolved in the hinges of folds rather than the limbs.

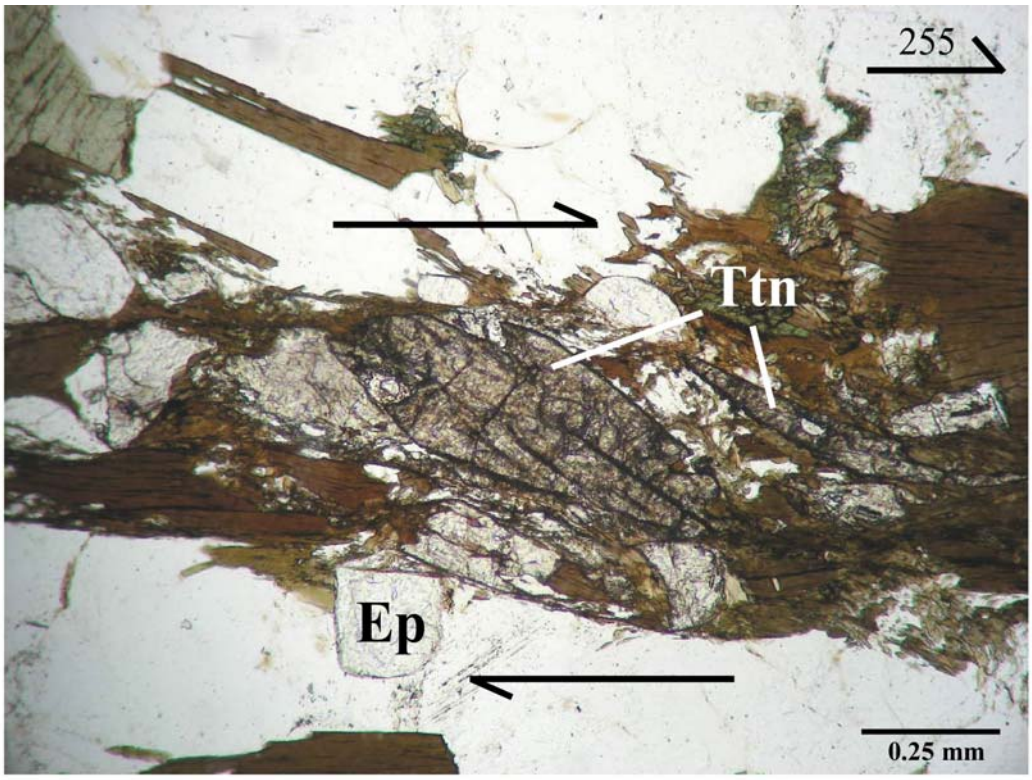

Figure 5.13. Brittle micro-faulting of titanite (Ttn) parallel to S_2 showing dextral shear sense. Note fragment of Ttn has been completely removed from the rest of the crystal. Epidote (Ep) crystals outside of high strain zone remain undeformed. Section cut perpendicular to foliation strike and parallel to dip direction (orientation top right). Plane light. (DEL08-10a).

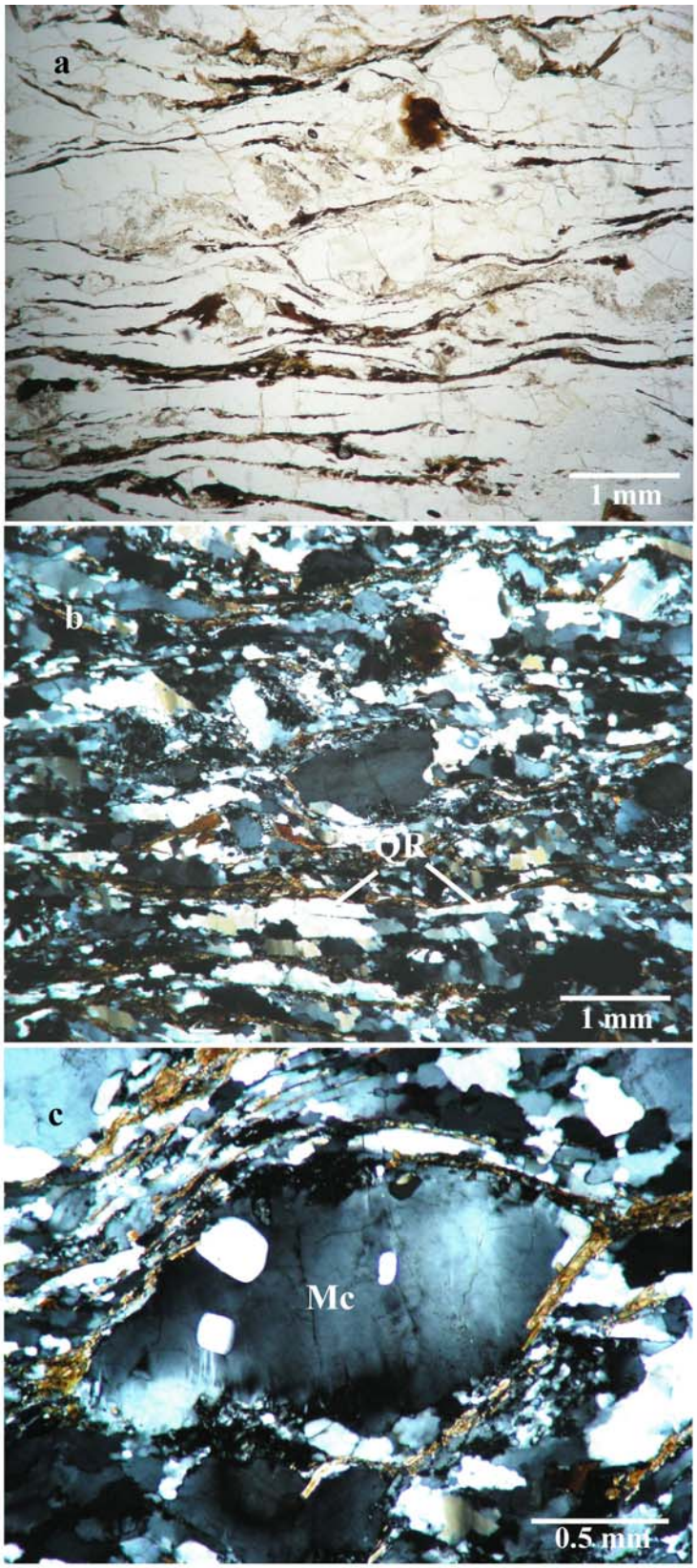

Figure 5.14. S_3 mylonitic texture. a) plane light and b) cross polars. c) foliation wraps microcline (Mc) porphyoclast. cross polars. QR=quartz ribbon.

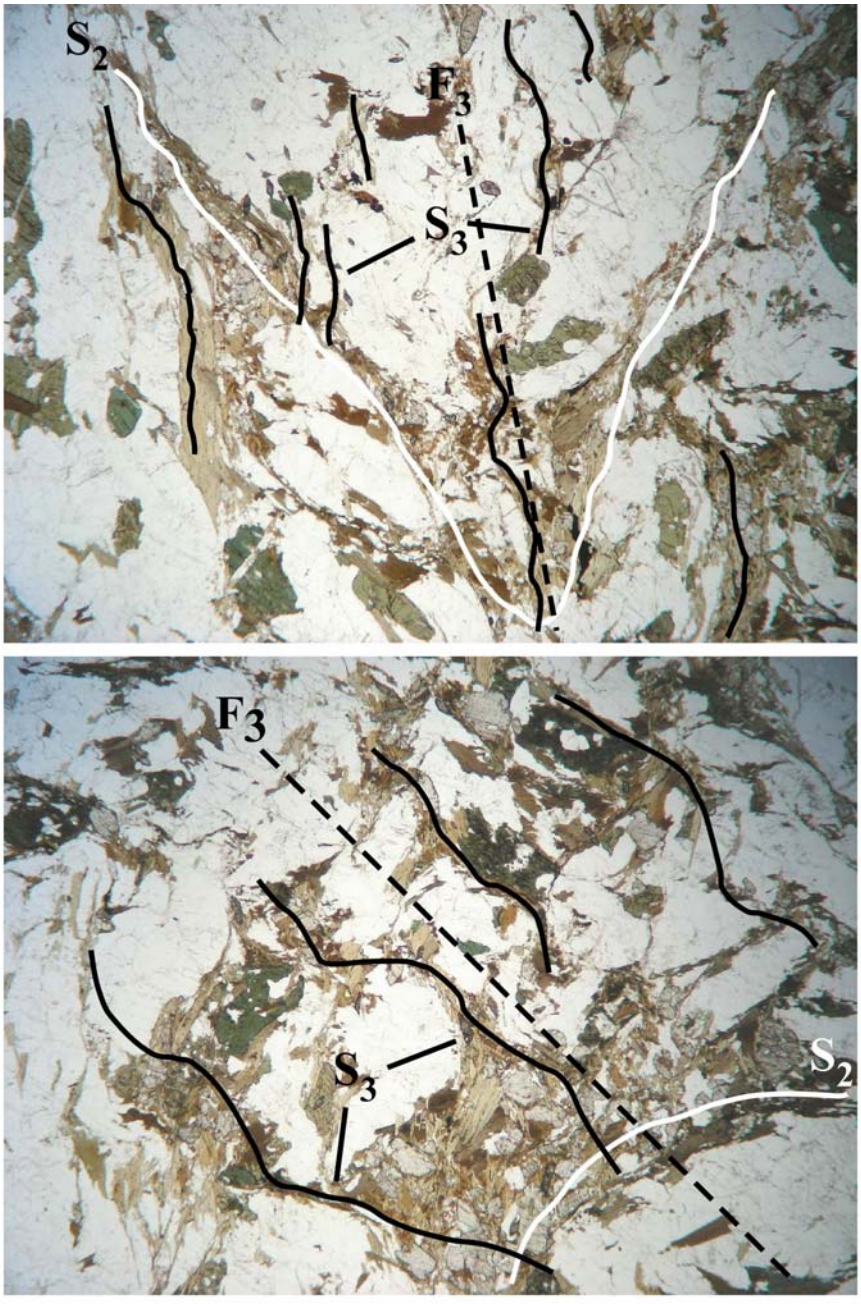

Figure 5.15. F_3 folds deform S_2 producing incipient S_3 anastomosing axial planar foliation in Hbl gneiss (DEL09-11gii). Width of view is 9.5 mm. Plane light.

SECTION VI. ANALYTICAL METHODS

Whole Rock Geochemistry

Whole rock X-ray fluorescence geochemistry was performed at the Kentucky Geological Survey on samples in order to determine major and trace element compositions for protolith identification. Samples visually deemed to be representative of the outcrop from which they were collected were washed and weathered surfaces were removed using a rock saw. Due to the mineral heterogeneity within a single sample of foliated and/or migmatitic gneiss, precautions were taken to ensure proper homogenization of each sample. A mass of 2-5 kg of material for each sample was crushed into pea-sized fragments using a jaw crusher and then manually homogenized and split. This portion was then pulverized into powder using a 3-puck shatterbox equipped with iron-alloy grinding pucks. A second homogenization and splitting technique was employed on the powder before preparing the fused discs for analysis.

X-ray fluorescence (XRF) geochemistry was carried out on a 4-kW Bruker S4 Pioneer wavelength dispersive XRF spectrometer at the Kentucky Geological Survey X-ray analytical lab in Lexington, KY. Fused glass discs were prepared by incorporating a 2:1 ratio of Premier Lab Supply GF-9010 Fluxite® (90% $Li_2B_4O_7$/ 10% LiF) and unknown sample powder in an automated fluxer equipped with a platinum crucible for heating. The concentrations of 10 major and 18 trace elements in the unknown samples were measured by comparing the X-ray intensity for each element with the intensities of reference material standards obtained from: United States Geological Survey (DNC-1, BIR-1, W2a, BCR-2, BHVO-1, BHVO-2, AVG-2, G-2, STM-1, GSP-1), Irish Geological

Association (OU-3, OU-4,AMH-1, YG-1, KPT-1), Canadian Certified References Materials Project (MRG-1, SY-2, SY-3), South African Reference Materials (SARM 4, SARM 50), Centre de Recherches Pétrographiques et Géochimiques (BE-N), Chinese National Standards (GBW 07105). Spectrum Plus®, the proprietary data reduction system software of Bruker, was used to calculate major and trace element compositions in the unknowns.

Geochronology

U-Pb zircon geochronology was carried out at the Keck Lab, UCLA on the Cameca 1270 ion microprobe (SIMS). Zircons were separated from eight basement gneiss samples for U-Pb zircon geochronology. Approximately 0.5 kg of rock was crushed for each sample into pea-sized fragments using a jaw crusher, and then semi-pulverized for ~10-15 seconds using a 3-puck shatterbox to allow for particle size heterogeneity. The samples were then ultrasonically washed and wet sieved using a 250 µm mesh. The mesh was changed between samples in order to avoid cross-contamination. Particles <250 µm were rinsed with water. Materials with low specific gravity (clay minerals, phyllosilicates, organic material) were decanted.

The remainder of the sample was dried in an oven and separated using bromoform ($CHBr_3$; specific gravity 2.85 g/mL). During this separation the sample was placed in a 500 mL glass separatory funnel equipped with a teflon stopcock that was filled with ~400 mL of bromoform. The sample was stirred 5-6 times during the first hour of separation,

then left undisturbed for >8 hours. The heavy portion was drained from the funnel, rinsed with acetone, and allowed to de-gas overnight in a fume hood.

The sample was further refined using a Frantz Isodynamic Magnetic Separator. Each sample was run through the separator three times under progressively stronger magnetic fields to ensure adequate removal of ferromagnetic minerals. Care was taken to prevent cross-contamination between samples. The separator channel and collection containers were cleaned with water then isopropanol before each sample change.

The final heavy liquid separation required the use of methylene iodide (diodomethane) (CH_2I_2; specific gravity 3.30 g/mL). The sample was placed in a 13 mL plastic centrifuge tube with ~11 mL of methylene iodide. The tube was capped and shaken for proper mixing and placed in a hand-cranked centrifuge for 4-5 minutes. The bottom ¼ of the tube was immediately placed in a liquid nitrogen bath for ~10 sec in order to retain the heaviest (zircon) portion of the sample. After the material with lower specific gravity was decanted, the remaining zircon separate was rinsed in acetone and dried under a heat lamp in a fume hood.

Ten to thirteen zircon grains of varying sizes were selected from each of the 8 samples for U-Pb geochronology. Zircons and standards (AS3, 1099.1 +/- 0.5 Ma, Paces and Miller, 1993) were hand-picked and placed on 3M® 701DL double-sided tape for mounting. An air-cured epoxy mount was produced by mixing 5 parts (by weight) Buehler® 20-8130 epoxide resin with 1 part (by weight) Buehler® 20-8132 epoxide hardener, pouring the mixture into a 1” ring surrounding the zircons, and allowing 6-8 hours to cure. The mount was polished using a standard silica polishing medium followed by a brief, final polish with 1µm diamond powder. The sample was

ultrasonically cleaned in 1N HCl for 1 minute to reduce common Pb contamination, and then ultrasonically cleaned in deionized water for ~ 5 minutes.

Individual grains were imaged by cathodoluminescence (CL) for internal zoning on a LEO 1430 VP Scanning Electron Microscope (SEM) equipped with a 4-quadrant backscattered electron detector (BSD) and an Oxford "mini-CL" cathodoluminescene detector at UCLA. The mount was sputter-coated with ~100Å of Au. The standard operating conditions used for analysis closely follow those outlined by Quidelleur et al. (1997). The primary O^- ion beam was focused to a spot with a diameter of ~15 µm. The secondary ion beam yielded a mass resolving power of ~5000, an energy window of 50 eV, and a 15 eV offset for $^{238}U^+$. The sample chamber was flooded with oxygen to enhance secondary ionization of Pb^+. Each grain analysis consists of 10 cycles of measurement of isotopic ratios.

Raw U-Th-Pb isotope data was reduced using Isoplot (Ludwig, 1999), which calculates elemental and isotopic concentrations, isotope ratios, apparent ages, uncertainties and error-correlations using the algorithms developed by Ludwig (1980).

SECTION VII. GEOCHEMISTRY

Whole rock major and trace element X-Ray fluorescence (XRF) spectrometric analysis was carried out on fifty samples of biotite gneiss, hornblende gneiss, and amphibolite within and near the Dellwood quadrangle (Figure 7.1) to elucidate geochemical trends associated with protolith type and tectonic setting of the rocks in the area. Detailed preparation procedures and operating conditions for analysis can be found in Section VI. An additional data set (E. Anderson, unpublished data) for basement gneisses and amphibolites collected from similar lithologies in the area (Figure 7.2) was incorporated so that geochemical trends within the basement suite could be more clearly resolved. Complete geochemical data can be found in Appendix B.

Results

Whole Rock Major Element Geochemistry

Collectively, all gneisses and some amphibolites define a calc-alkaline trend on the AFM diagram (Figure 7.3). The majority of amphibolites fall in the tholeiitic field (Figure 7.3). Harker variation diagrams of major element oxides vs. SiO_2 (Figure 7.4) illustrate that all samples are increasingly enriched in alkalis and progressively depleted in calcium, iron, magnesium and manganese with increasing silica content. A total alkali vs. silica (TAS) diagram (Le Maitre et al., 2002) (Figure 7.5) reveals that the biotite gneiss suite ranges in composition from andesite to rhyolite. The major element geochemistry is consistent with, but does not prove, a magmatic origin. However, gneisses derived primarily from immature, first-cycle volcanic and plutonic sediments resulting from basement weathering would exhibit the same geochemical signature as the

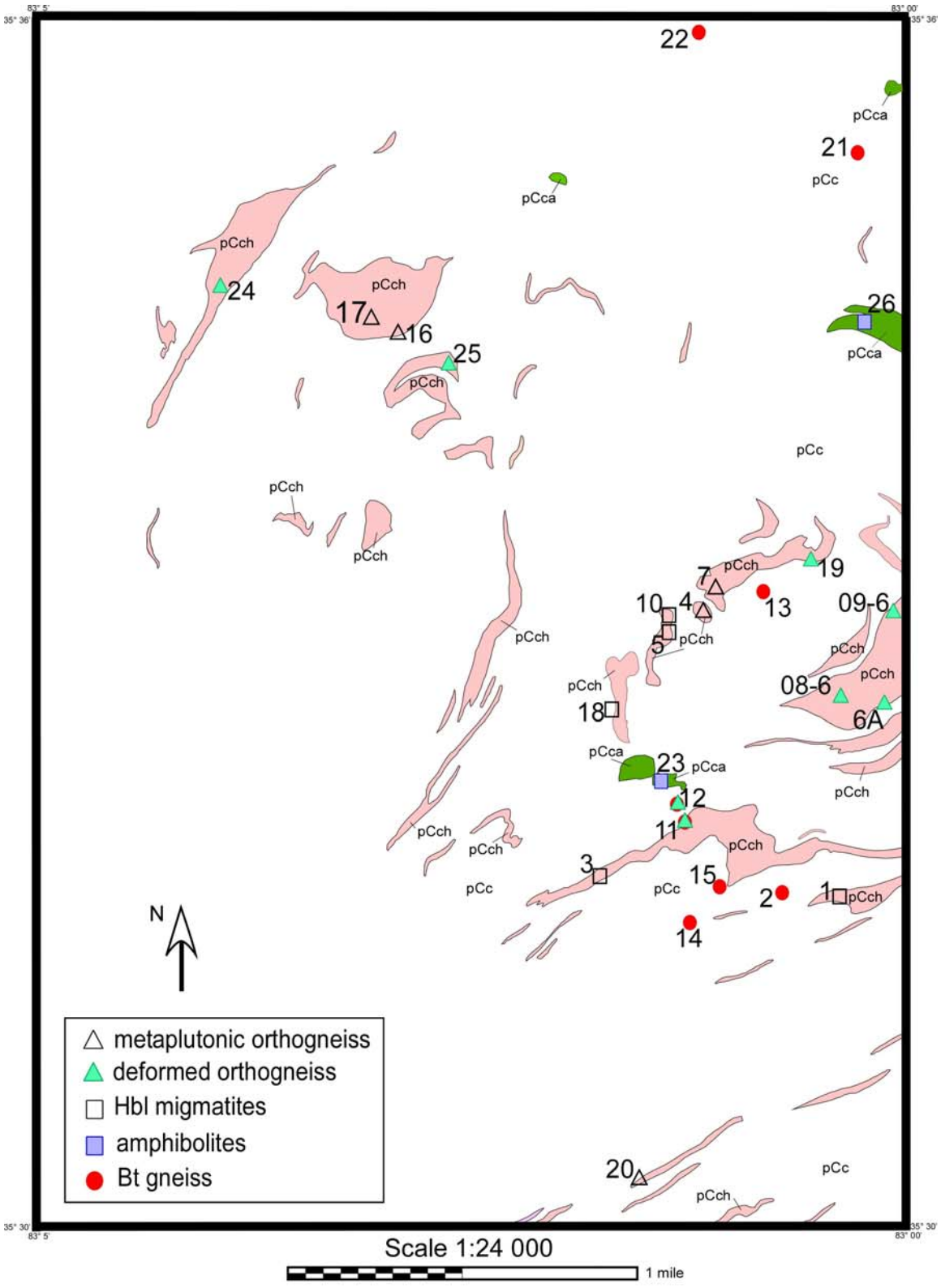

Figure 7.1 . Sample locations in the Dellwood Quadrangle, eastern Great Smoky Mountains, showing only hornblende gneisses (pink) and amphibolites (green) after Hadley and Goldsmith (1963). Location symbols correspond to lithologies.

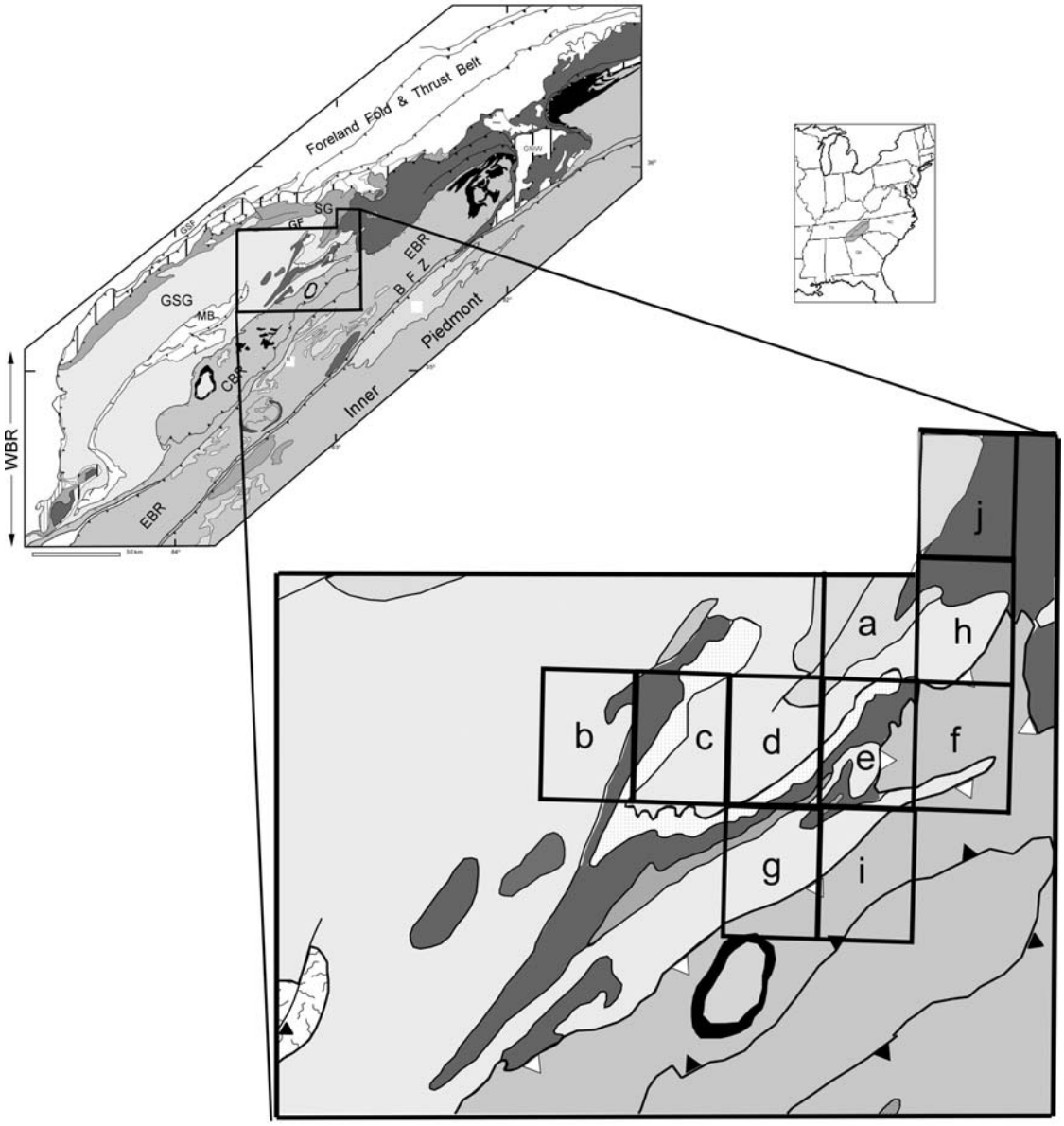

Figure 7.2. Regional geologic map showing the extent of the field sample area for samples obtained from E. Anderson (after Rankin et al., 1990). Black rectangles show locations of 7.5 minute quadrangles from which samples were collected: a-Cove Creek Gap, b-Clingmans Dome, c-Smokemont, d-Bunches Bald, e-Dellwood, f-Clyde, g-Sylva North, h-Fines Creek, i-Hazelwood, j-Lemons Gap.

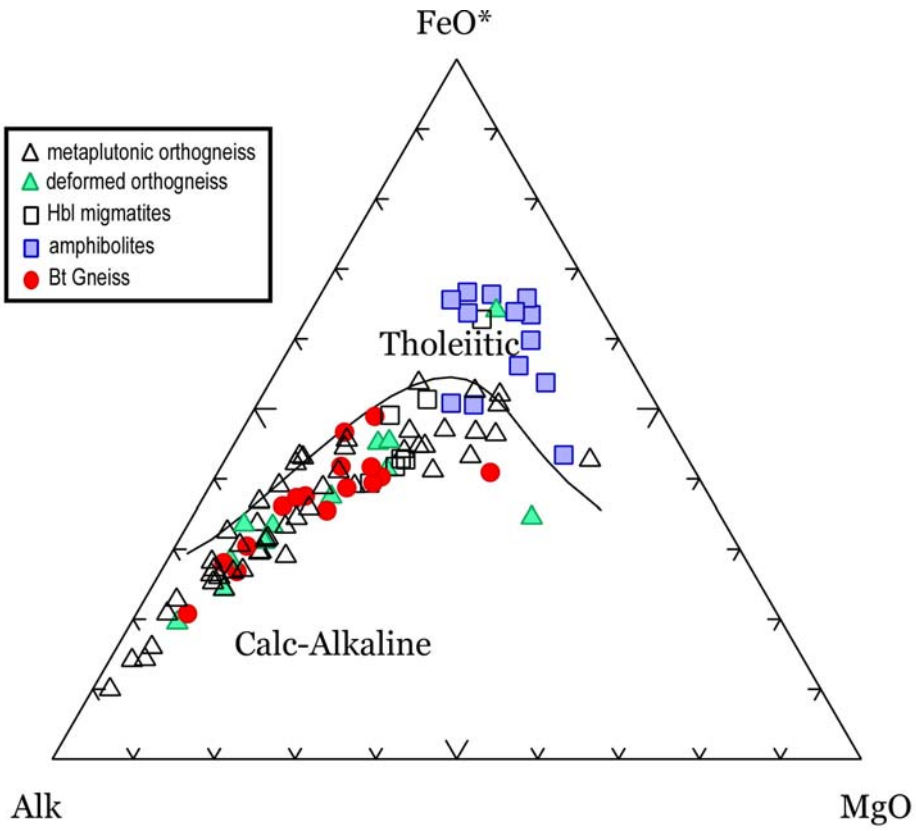

Figure 7.3. AFM diagram for whole rock geochemistry. Note most lithologies follow a calc-alkaline trend. Amphibolites of basaltic composition follow a tholeiitic trend.

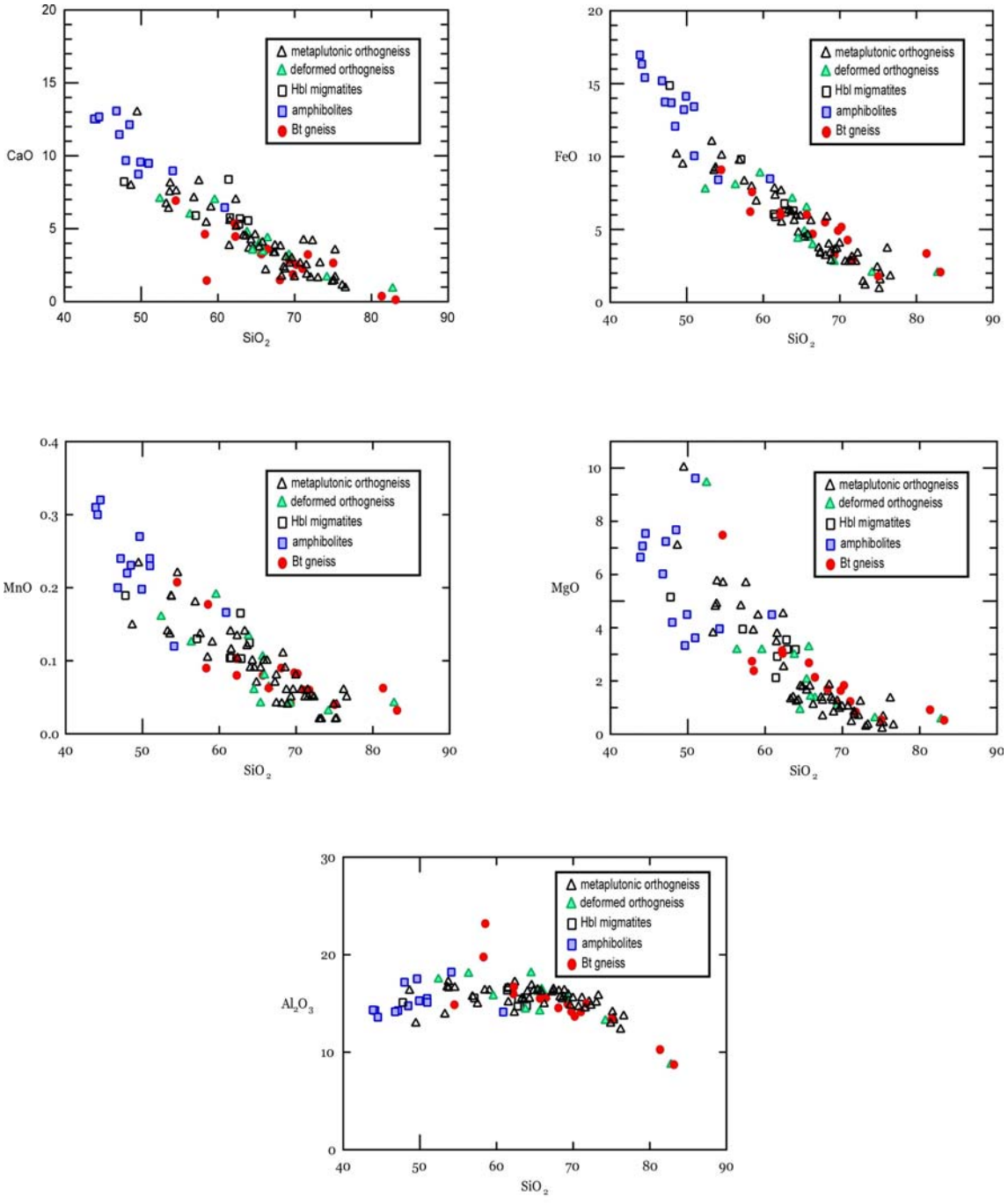

Figure 7.4. Harker variation diagrams for whole rock geochemistry for samples in and around the Dellwood area. Values are in weight percent oxide.

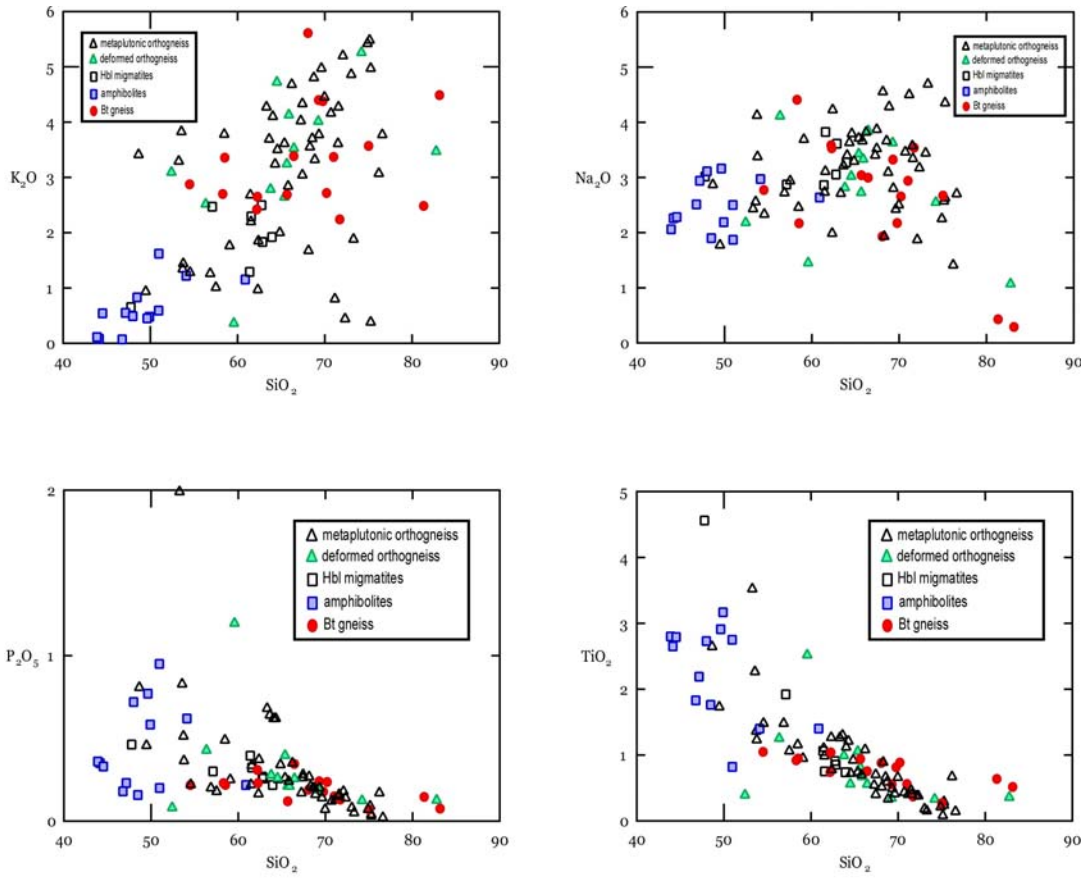

Figure 7.4. (continued)

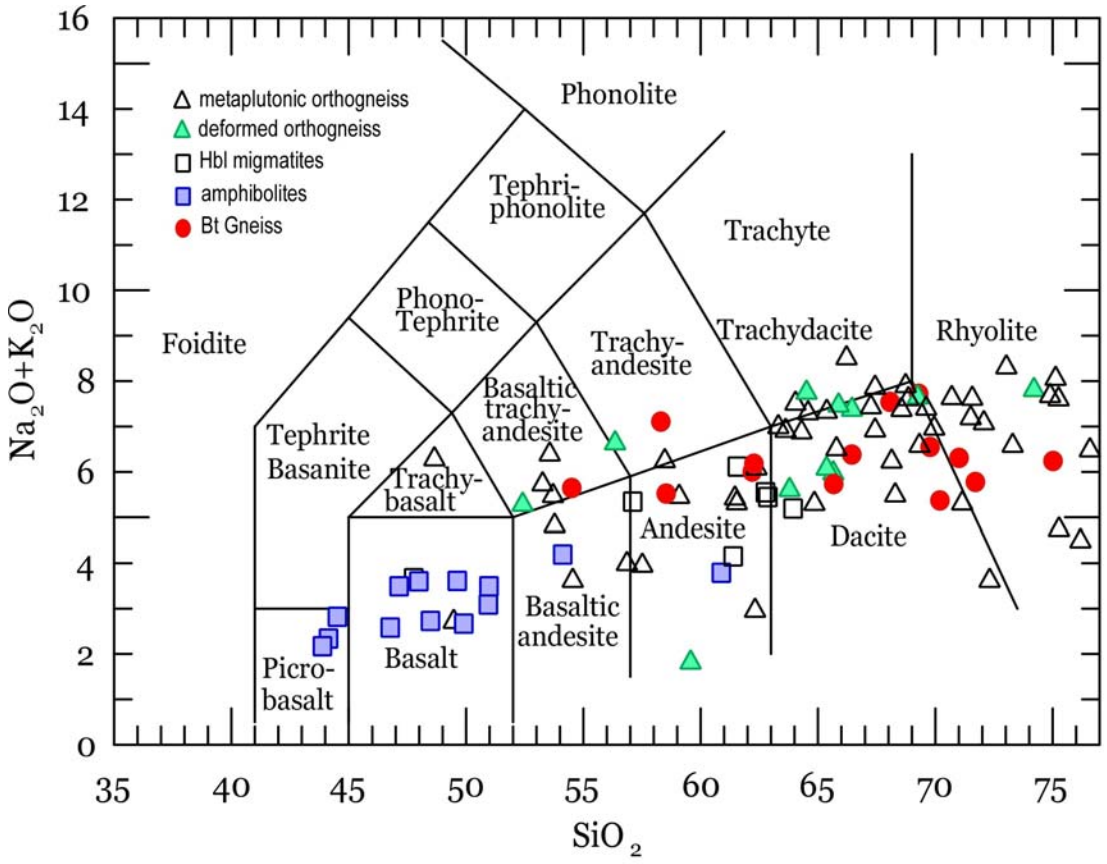

Figure 7.5. Total alkali vs. silica (TAS) diagram (Le Maitre et al., 2002) showing igneous compositional ranges for lithologies. Use of this diagram does not imply an original volcanic rock type for each type of basement lithology.

basement. The metaplutonic and intensely deformed hornblende orthogneisses and hornblende-bearing migmatites appear to be related, geochemically, though hornblende gneiss migmatites are a more mafic member of this suite possibly resulting from a loss of melt during peak temperature conditions. These rocks, ranging in composition from basalt to rhyolite (Figure 7.5), define a calc-alkaline trend with varying degrees of fractionation (Figure 7.3).

The hornblende gneisses and biotite gneisses exhibit slightly different geochemical trends. Quartz-albite-anorthite plots (Figure 7.6), based on the CIPW norm calculation (see Appendix A) show that the metaplutonic and deformed hornblende orthogneisses define an arcuate trend toward the albite endmember with increasing weight percentage of quartz. In contrast, the biotite gneisses define a linear trend with increasing weight percentage of quartz and are comprised of less albite-rich samples. Chemical alteration of feldspars (albitization) does not appear to be a factor as no petrographic evidence of such alteration was found in any of the hornblende gneisses. For biotite gneisses, total alkali weight percentages remain relatively constant with increasing silica; for hornblende gneisses, total alkali weight percentages increase in a linear fashion with increasing silica (Figure 7.5). However, the difference in geochemical trends is overshadowed by the obvious overlap in normative quartz range between the two lithologies (Figure 7.6a), excluding the most quartz-rich sample of biotite gneiss.

Amphibolites in the study area have a more distinct and restricted range of compositions than the other lithologies. Most samples are tholeiitic basalts of varying composition. However, two samples plotted as andesites in the TAS diagram (Figure

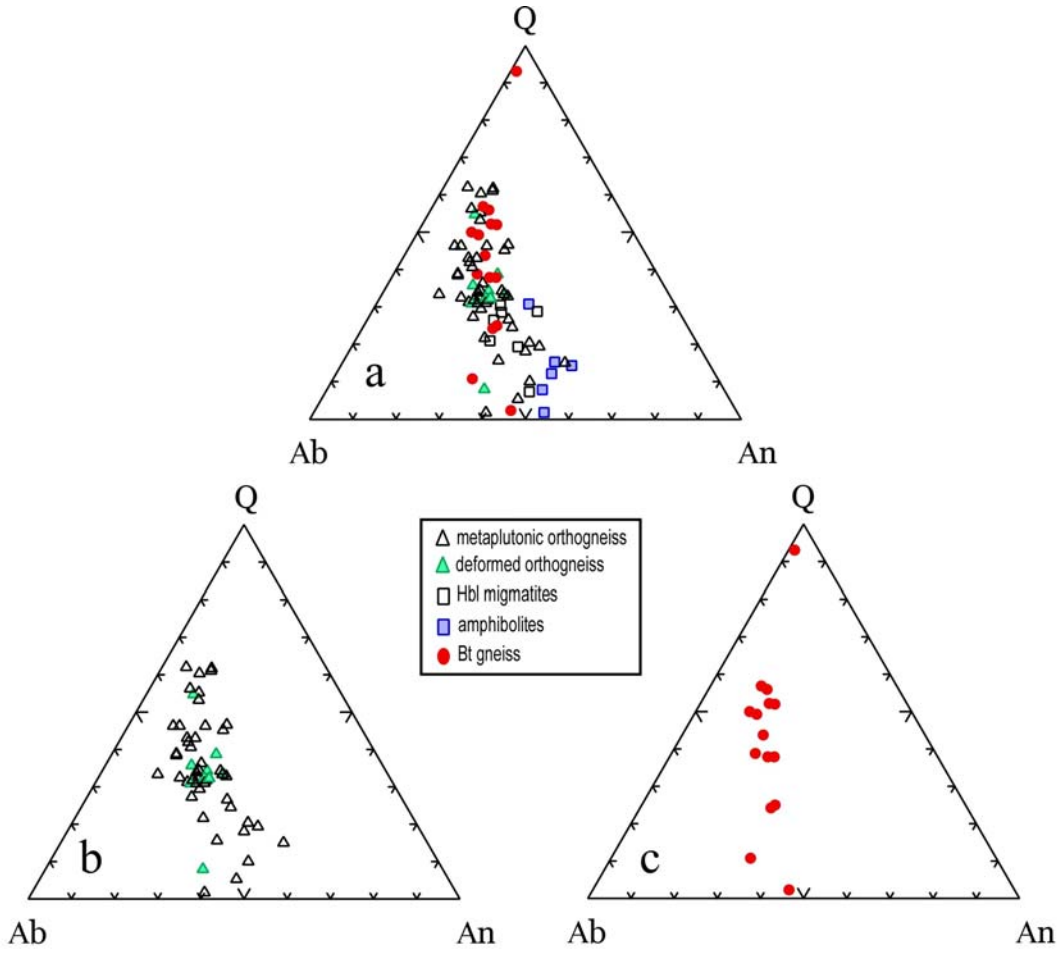

Figure 7.6. Normative quartz (Q) -albite (Ab) -anorthite (An) diagrams based on CIPW norm calculation. (a) all lithologies (b) metaplutonic orthogneisses and deformed equivalents and (c) biotite gneisses.

7.5). In contrast to the other lithologies, amphibolites exhibit a distinct tholeiitic trend (Figure 7.3).

Trace Element Geochemistry

Trace element compositions of orthogneisses, their deformed equivalents, and biotite gneisses overlap considerably (Figure 7.7). In contrast, the amphibolite geochemical trend increases from left (more incompatible elements) to right (less incompatible elements) on a chondrite normalized spider diagram. Amphibolites are extremely depleted in the large ion lithophile elements Rb and K compared to the other lithologies. Hornblende-bearing migmatites are anomalous as their respective trace element concentrations appear to be intermediate between the two other suites. All lithologies are extremely enriched in uranium and slightly enriched in zirconium, consistent with the zircon-rich nature of Grenvillian rocks (Moecher and Samson, 2006).

Additional plots separating the more felsic lithologies (biotite gneiss and orthogneisses) from the more mafic lithologies (Hbl-bearing migmatites and amphibolites) (see Figure 7.5) show similarities between the rock types more easily (Figure 7.8). Mafic to intermediate rocks, normalized to chondrites, exhibit similar but not identical trends.

A further geochemical test of protoliths presented in Figure 7.9 (Werner, 1987) suggests that both the hornblende gneisses and biotite gneisses have igneous protoliths, a finding that further substantiates an igneous origin for the biotite gneiss. The use of this test is geologically significant for two reasons: (1) common clastic sedimentary rocks,

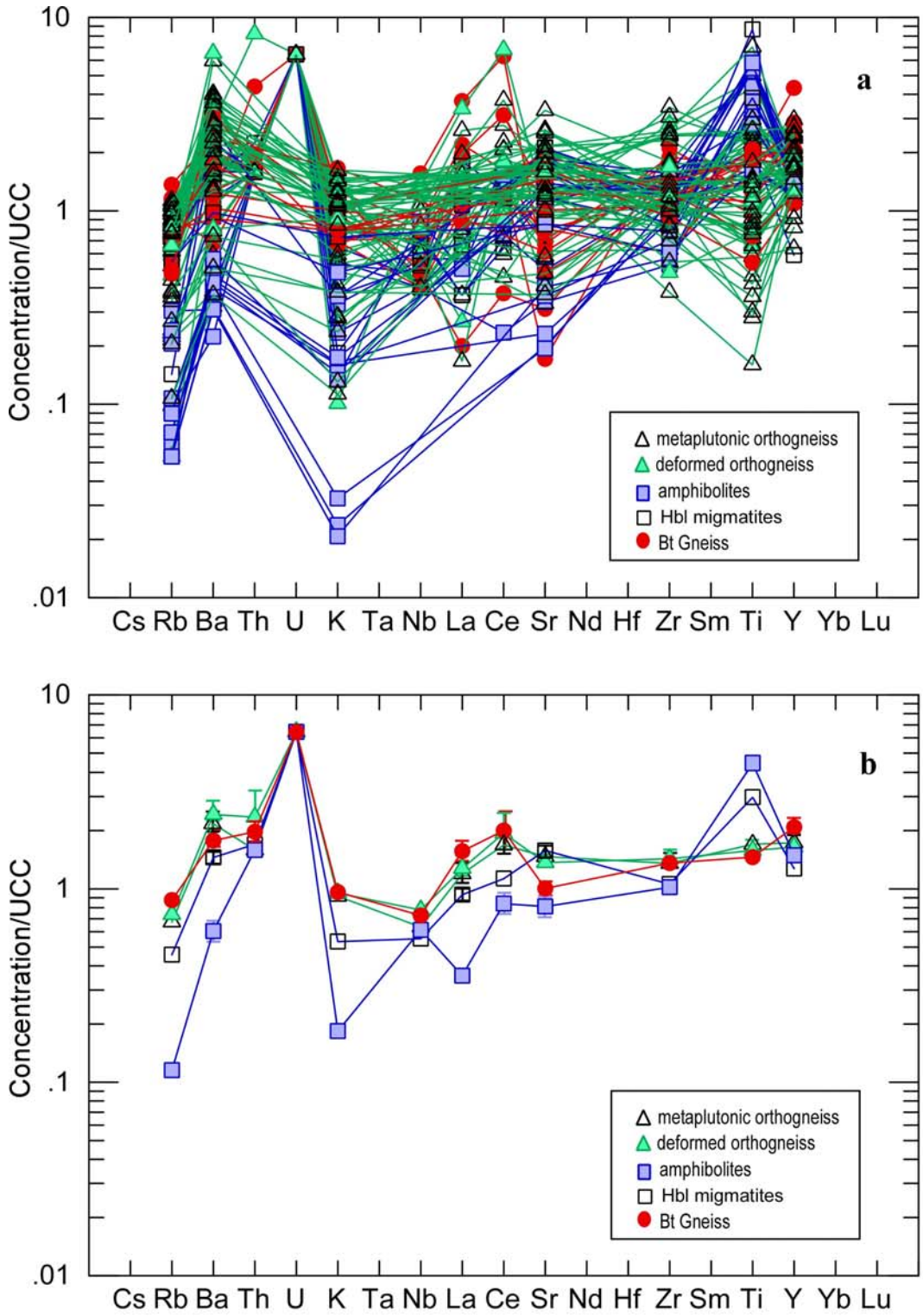

Figure 7.7. Trace element geochemistry a) of individual samples and b) of average compositions for five lithologies, normalized to upper continental crust (UCC) after Taylor and McLennan (1985). Error bars are 1 standard deviation. Concentrations are in ppm.

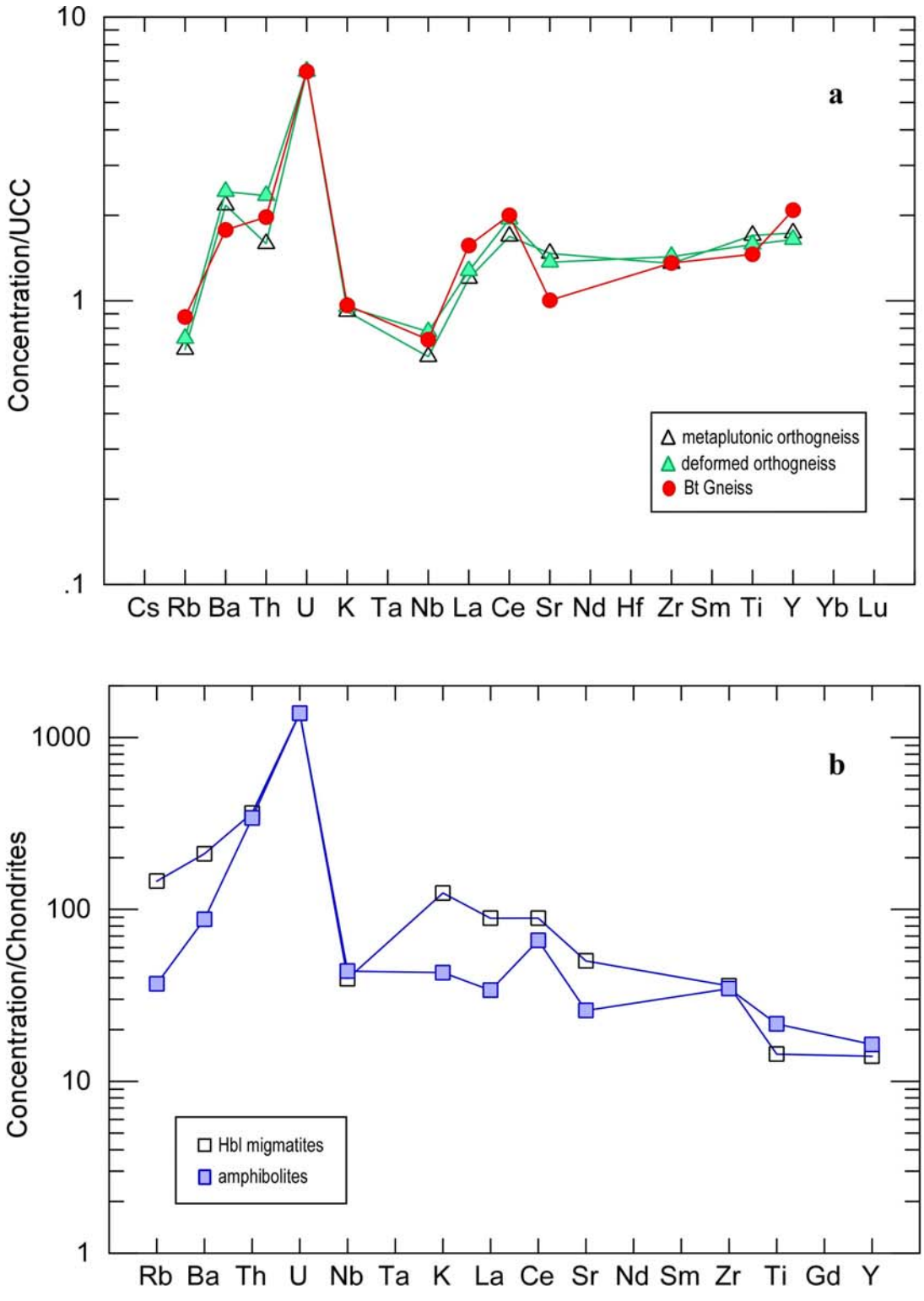

Figure 7.8. Trace element geochemistry of average compositions by lithology. a) Felsic to intermediate lithologies normalized to upper continental crust (UCC) after Taylor and McLennan (1985). b) Mafic to intermediate lithologies normalized to chondrite after Sun (1980). Concentrations given in ppm.

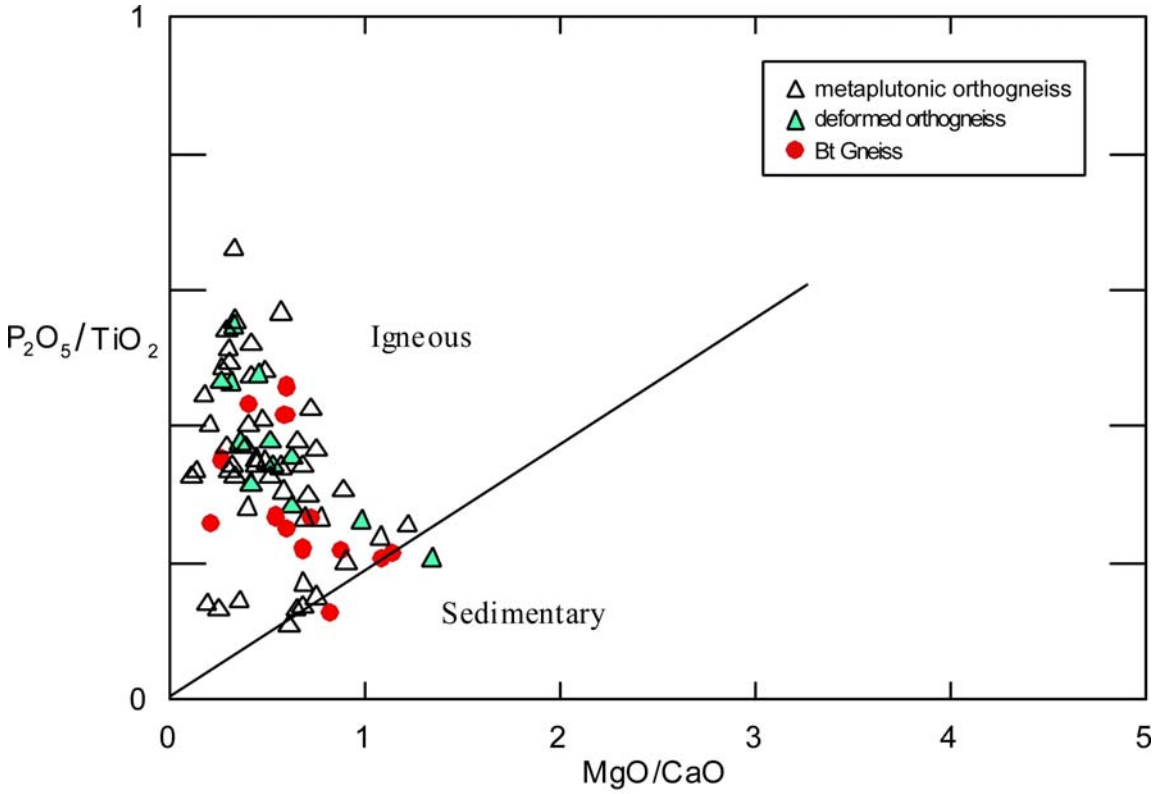

Figure 7.9. P_2O_5/TiO_2 plotted against MgO/CaO as a discriminator for felsic igneous versus clastic sedimentary protoliths in granulite facies rocks (Werner 1987, Ownby et al., 2004).

specifically shales and some sandstones, generally contain higher TiO_2 amounts than common felsic igneous rocks (Force, 1991) and (2) a worldwide average of granite chemical compositions (Blatt and Tracy, 1997) shows that the ratio of P_2O_5/TiO_2 is slightly higher than the ratio of MgO/CaO in granites. Since the compatibility displayed by Ti during fractionation results in enrichment in mafic and ultramafic rocks relative to felsic igneous rocks, this diagram should only be used to discriminate felsic igneous protoliths from clastic sedimentary protoliths.

SECTION VIII. GEOCHRONOLOGY

Cores of prismatic zircons from four samples of metaplutonic orthogneiss, two samples of intensely deformed orthogneiss interpreted to be the equivalent of the metaplutonic orthogneiss, one sample of migmatitic hornblende gneiss, and one sample of biotite gneiss were analyzed to determine crystallization ages of igneous protoliths and/or the age of deposition of the protolith of biotite gneiss. U-Pb zircon geochronology was carried out on a Cameca 1270 ion microprobe (SIMS) at the University of California at Los Angeles. Detailed preparation procedures and operating conditions for analysis can be found in Section VI. Data reduction was performed using Isoplot (Ludwig, 1999). All errors reported are 2σ. Complete geochronological data can be found in Appendix C.

Metaplutonic Orthogneiss

Zircon from metaplutonic orthogneiss samples has both oscillatory zoned and unzoned cores with Th/U values consistent with magmatic crystallization (> 0.1; Rubatto, 2002) (Figure 8.1), and thin (< 20 μm) unzoned rims consistent with metamorphic growth (Anderson and Moecher, 2009; Hanchar and Miller, 1993) (see grain 5, Figure 8.2a). All generations of zircon from each of the four samples reflect a single generation of zircon crystallization (MSWD ≤ 0.82).

DEL08-7a

This sample was taken from the western margin of a body mapped as hornblende gneiss by Hadley and Goldsmith (1963) that becomes progressively deformed toward the east (see Figure 3.2, location 7). The western margin of the body is much less deformed,

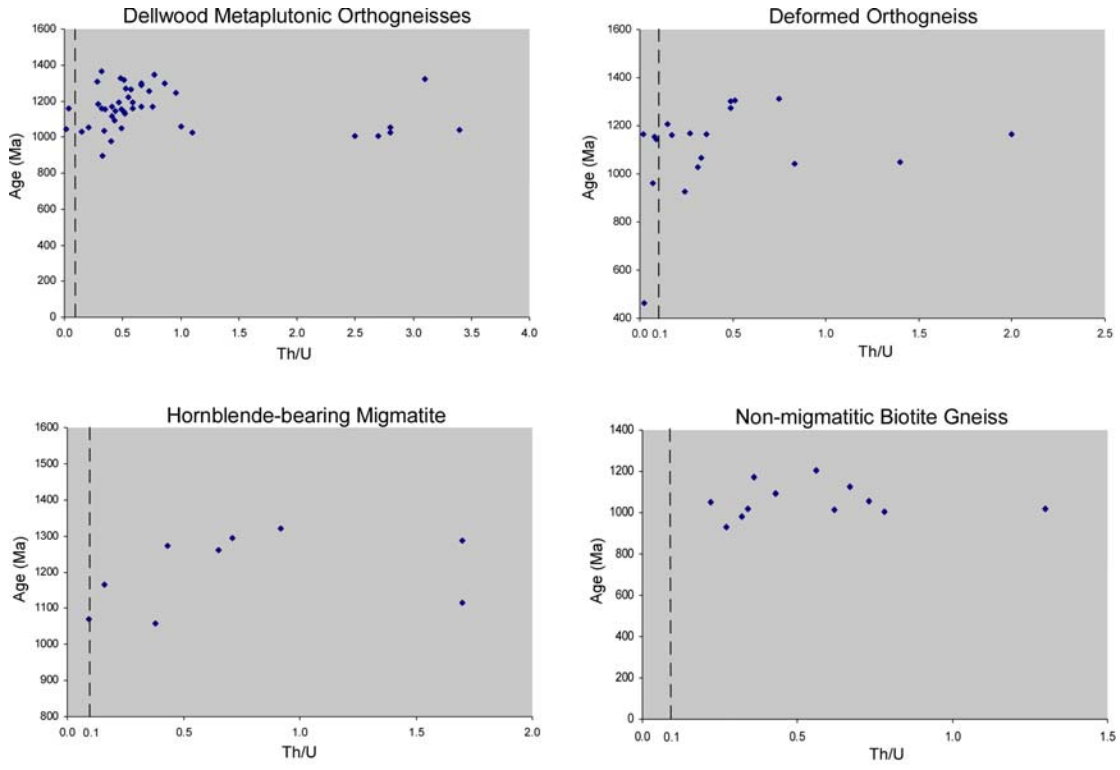

Figure 8.1. Th/U values vs. age for four Dellwood basement lithologies. Dashed line represents minimum Th/U value for magmatic zircons.

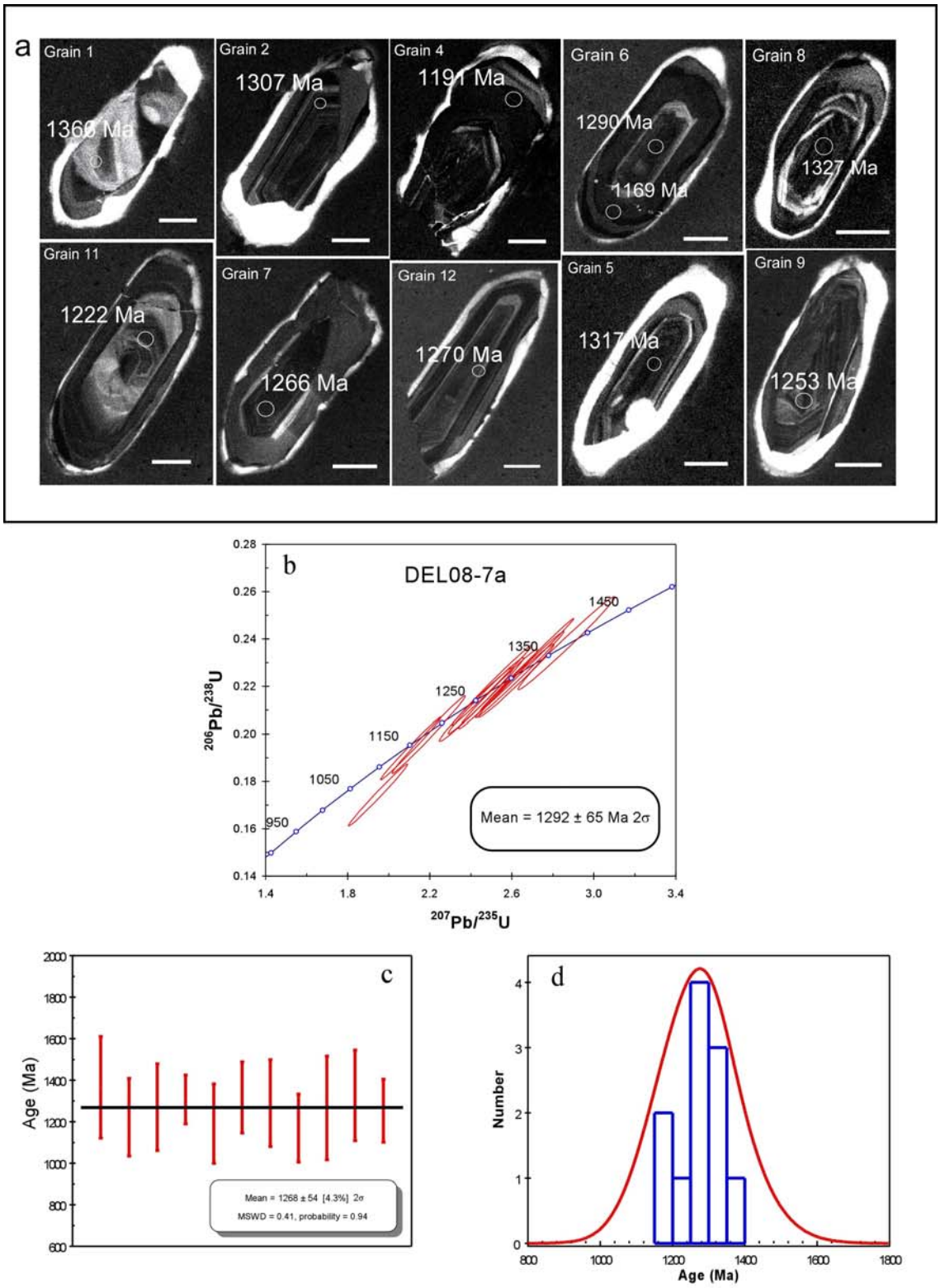

Figure 8.2. Geochronology of metaplutonic orthogneiss (DEL08-7a). a) CL images of zircon with analysis spot (circle) and age. Scale bar is 50 μm. b) concordia diagram, c) weighted mean plot and d) probability histogram.

retains igneous textures, and is non-migmatitic (Figure 3.10c). Additionally, zircons from this sample contain magmatic cores with relatively high Th/U values (Figure 8.1). Thus, zircon ages obtained from this sample are interpreted to reflect plutonic crystallization ages.

In addition to magmatic oscillatory zoning, some zircons have cores containing complicated, patchy zoning patterns (Figure 8.2a, grains 1 and 11). High angle truncations of oscillatory magmatic zonation are present (grains 2, 8, and 9). Ages in this sample range from 1191 Ma to 1366 Ma, with a dominant age mode at ~ 1300 Ma. The seven most tightly clustered ages, which also exhibit similar CL zoning patterns, were used to calculate a weighted mean age of 1292 ± 65 Ma (MSWD=0.101, probability=0.99) (Figure 8.2).

DEL08-7j

This sample was taken from the same location as sample DEL08-7a. Zircons from this sample contain magmatic cores with relatively high Th/U values (Figure 8.1). In addition to magmatic oscillatory zoning, some grains exhibit distinct anhedral cores bounded by thick oscillatory zones (Figure 8.3a, grains 8 and 13). Patchy zoning patterns (grains 2 and 12) are present as well as truncated oscillatory zoning (grains 1 and 5). Ages in this sample range from 897 Ma to 1345 Ma, with modes at ~ 1100 Ma and 1300 Ma (Figure 8.3 b and d). Two separate clusters of ages were used to calculate weighted mean age modes at 1170 ± 110 Ma and 1287 ± 79 Ma (Figure 8.3).

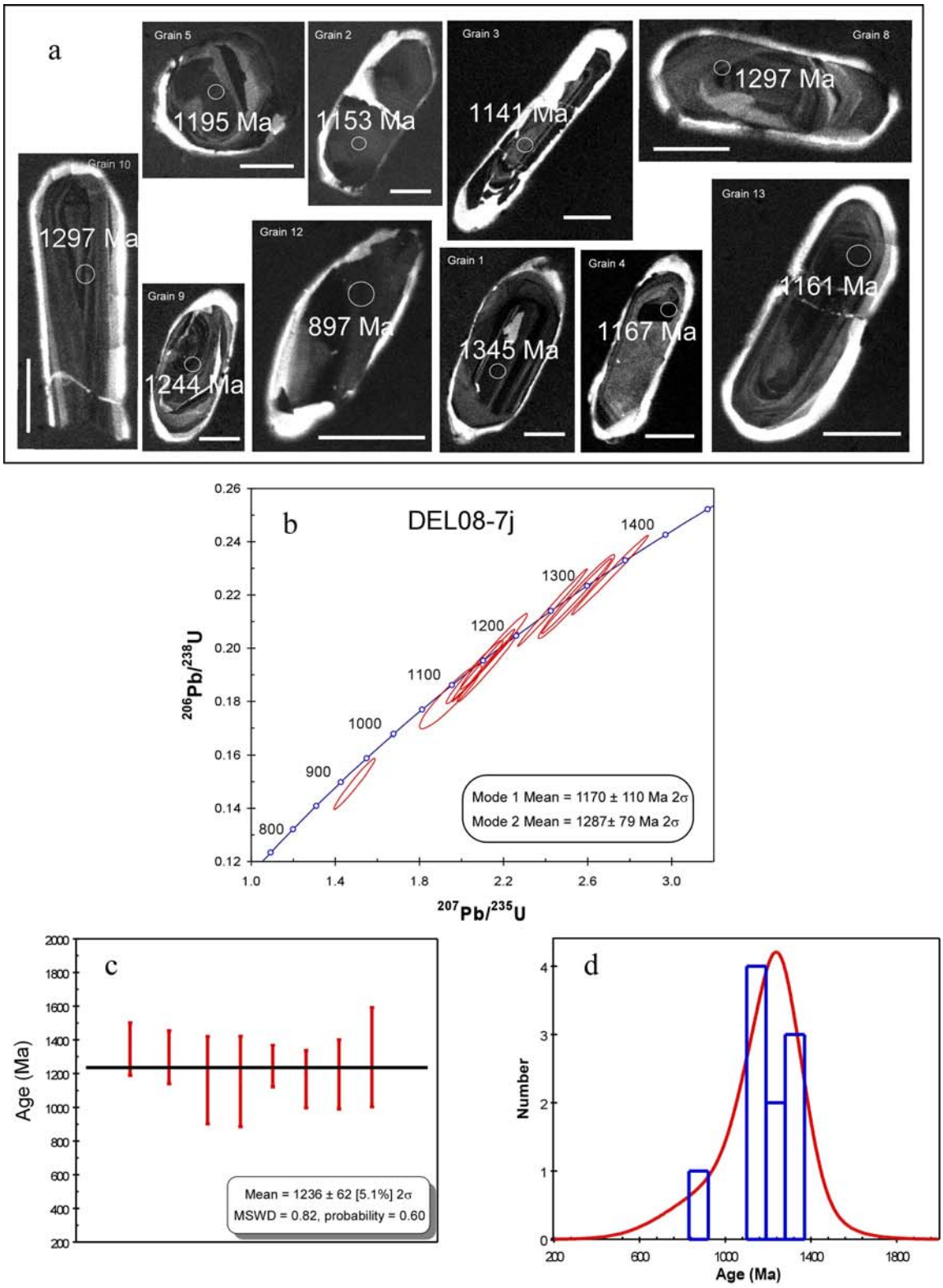

Figure 8.3. Geochronology of metaplutonic orthogneiss (DEL08-7j). a) CL images of zircon with analysis spot (circle) and age. Scale bar is 50 μm. b) concordia diagram, c) weighted mean plot and d) probability histogram. Concordia diagram and probability histogram suggest two modes are present.

DEL09-16b

This sample is taken from a large exposure of hornblende gneiss on the southeast flank of Purchase Knob. Magmatic cores and Th/U values for zircons obtained from this sample are consistent with igneous petrogenesis (Figure 8.1). Thus, zircon ages obtained from these rocks are interpreted to represent crystallization ages. In addition to magmatic oscillatory zoning, some zircons exhibit patchy unzoned cores (Figure 8.4a, grains 2, 3, 4, 8, and 12). All zircons exhibit thick (15-30 μm) metamorphic rims. Ages in this sample range from 978 Ma to 1181 Ma, with one dominant mode at ~1150 Ma. The six most tightly clustered ages were pooled and yielded a weighted mean age of 1153 ± 74 Ma (MSWD=0.070, probability=0.99) (Figure 8.4).

DEL09-17d

This sample was taken from the same hornblende gneiss body as the previous sample, DEL09-16b. Magmatic cores and Th/U values for zircons obtained from this sample are consistent with igneous petrogenesis (Figure 8.1). Thus, zircon ages obtained from these rocks are interpreted to represent crystallization ages. Although oscillatory zoning is present in some zircons in this sample, most exhibit bright unzoned anhedral cores. Most striking is the consistency in size and shape of these zircons and how different the CL zoning patterns are from zircons of other samples (Figure 8.5a). Ages in this sample range from 1004 Ma to 1324 Ma, with a dominant mode at ~1000 Ma. The ten mostly tightly clustered ages were pooled and yielded a weighted mean age of 1040 ± 100 Ma (MSWD=0.007, probability=1.0) (Figure 8.5).

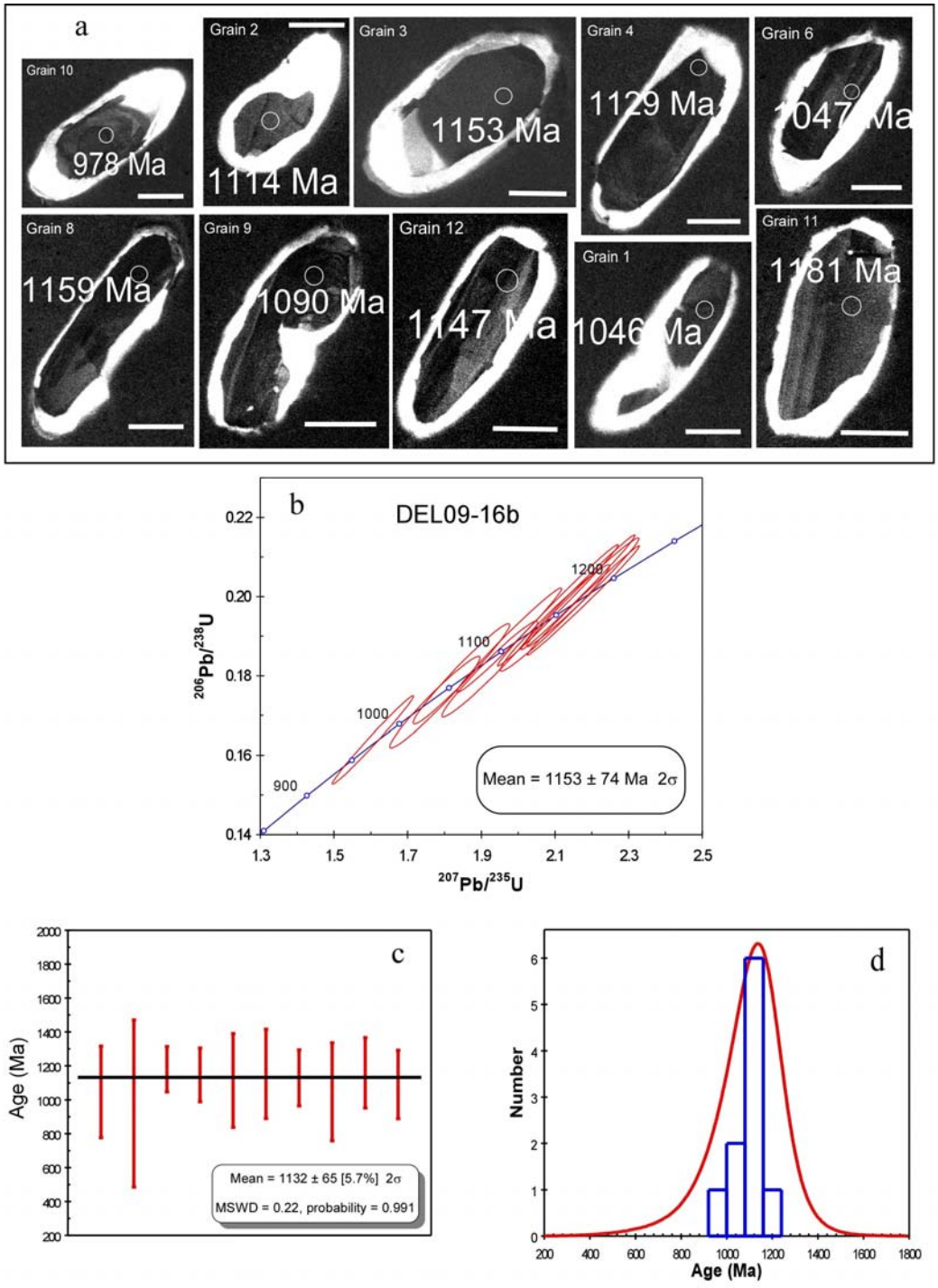

Figure 8.4. Geochronology of metaplutonic orthogneiss (DEL08-16b). a) CL images of zircon with analysis spot (circle) and age. Scale bar is 50 μm. b) concordia diagram, c) weighted mean plot and d) probability histogram.

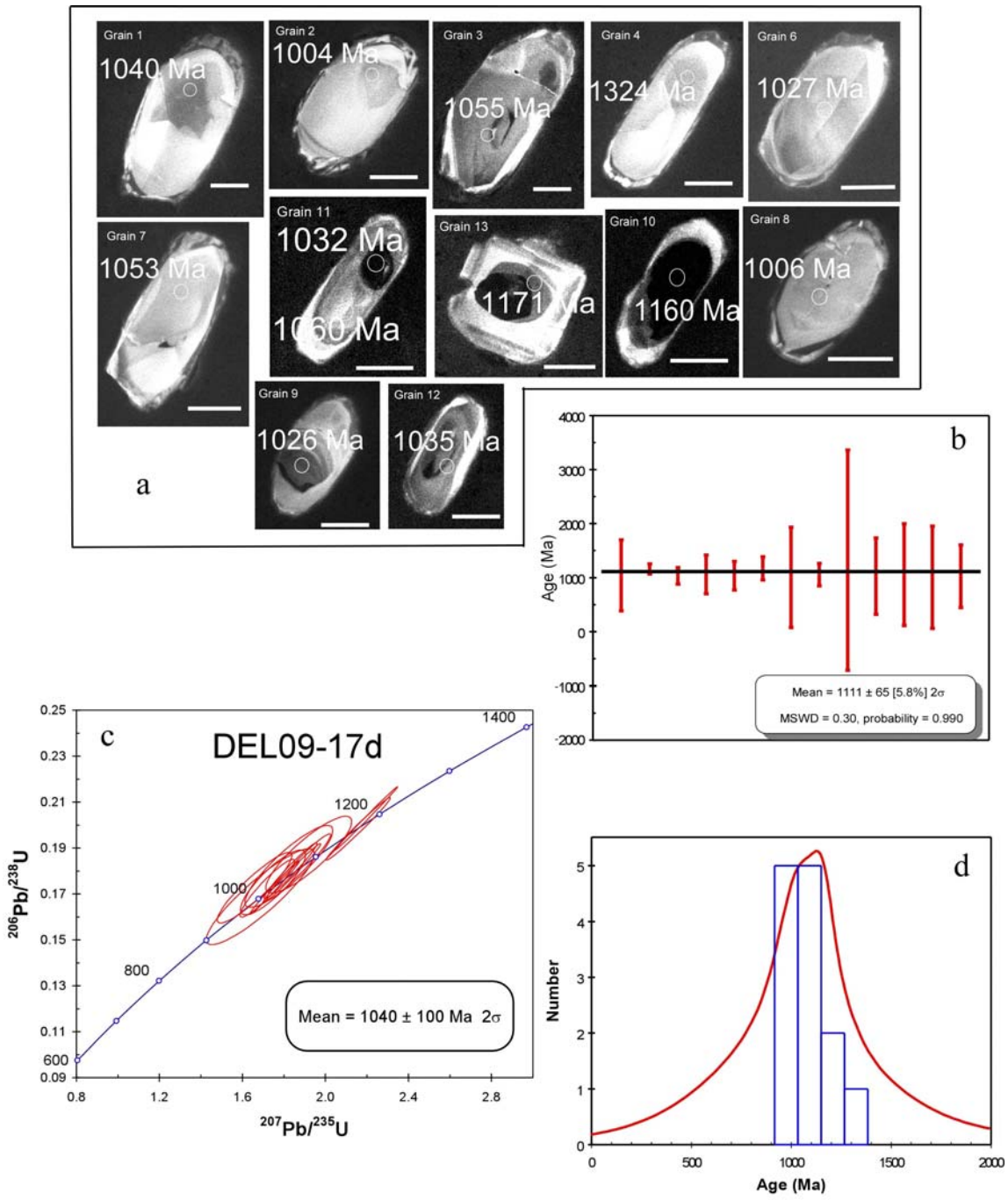

Figure 8.5. Geochronology of metaplutonic orthogneiss (DEL08-17d). a) CL images of zircon with analysis spot (circle) and age. Scale bar is 50 μm. b) weighted mean plot, c) concordia diagram and d) probability histogram.

Deformed Orthogneiss

Zircon from intensely deformed orthogneiss has both oscillatory zoned and unzoned cores with Th/U values consistent with magmatic crystallization and thin (< 20 μm) unzoned rims consistent with metamorphic growth. However, 25% (5 grains) of the zircons analyzed have Th/U values consistent with metamorphic growth. At least three Grenville-age modes are present in the two samples. Of the three modes, two are common to the samples.

DEL08-6c

This sample was taken from a large hornblende gneiss body located on Countryside Dr. Knob (location 08-6, Figure 3.2). In addition to oscillatory zonation, zircons from this sample exhibit patchy cores (Figure 8.6a, grains 3 and 4), embayments of metamorphic overgrowth within cores (bright CL pattern, grain 5), and truncated oscillatory zoning within cores (grains 1, 7, and 10). Ages in this sample range from 1042 Ma to 1313 Ma, with three dominant modes at ~1050 Ma, 1150 Ma, and 1300 Ma. Three separate age modes are proposed, based on weighted mean calculations and plots (Figure 8.7): 1052 ± 170 Ma (MSWD=0.021, probability=0.89), 1163 ± 72 Ma (MSWD=0.005, probability=0.99), and 1292 ± 59 Ma (MSWD=0.40, probability=0.81).

DEL09-19a

This sample of hornblende gneiss (Figure 3.11f, inset) was located at the end of Erwin Lane (location 19, Figure 3.2). Oscillatory zoning is generally absent in these zircons with the exception of grain 12. Patchy zoning (Figure 8.8a, grain 5) and anhedral cores (grains 2 and 3) are present. Ages in this sample range from 463 Ma to 1166 Ma, with two modes at ~1030 Ma and 1150 Ma. Two separate age modes are proposed,

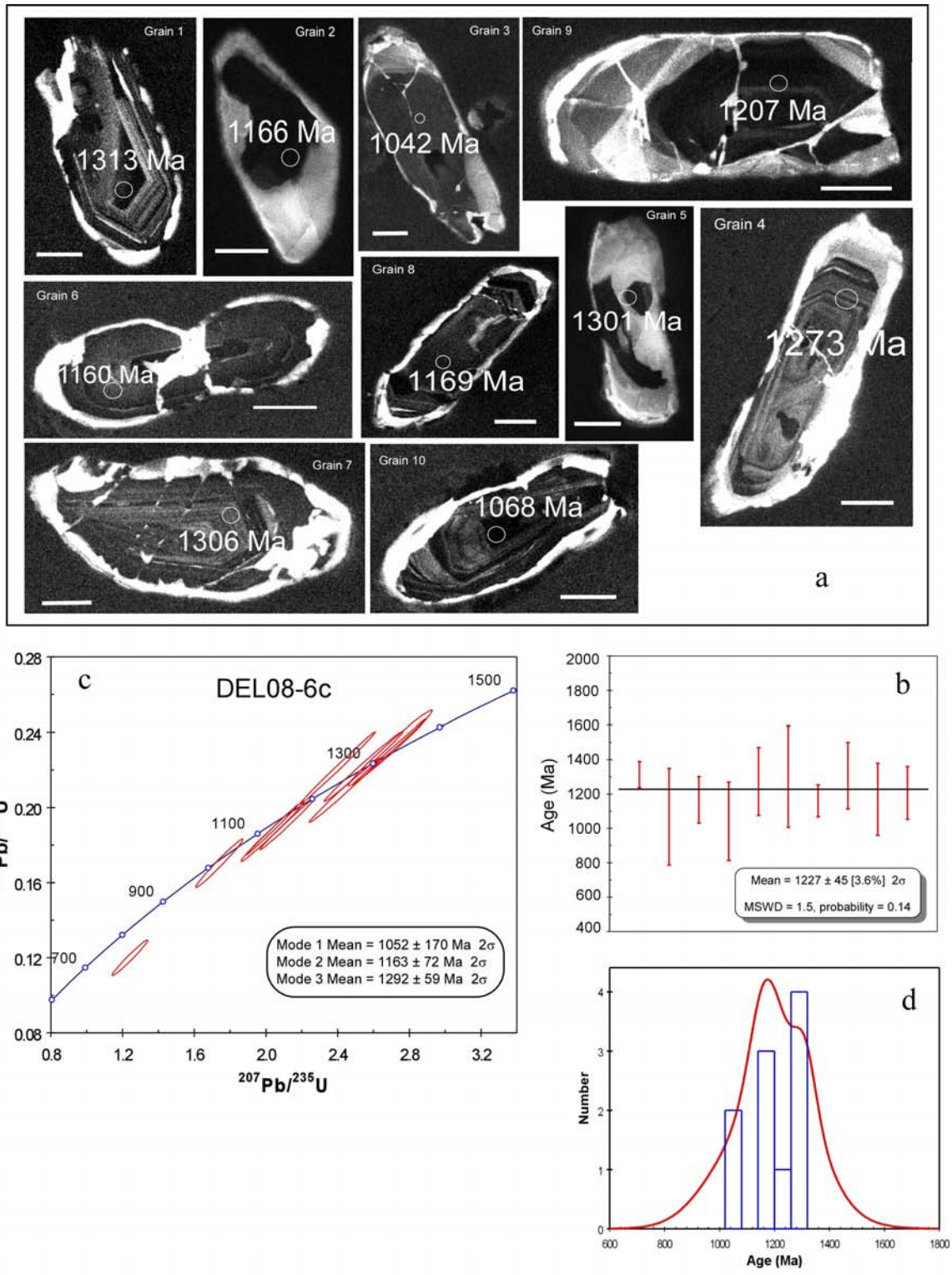

Figure 8.6. Geochronology of deformed orthogneiss (DEL08-6c). a) CL images of zircon with analysis spot (circle) and age. Scale bar is 50 μm. b) weighted mean plot, c) concordia diagram and d) probability histogram. Note probability histogram and weighted mean plot suggest multiple modes present.

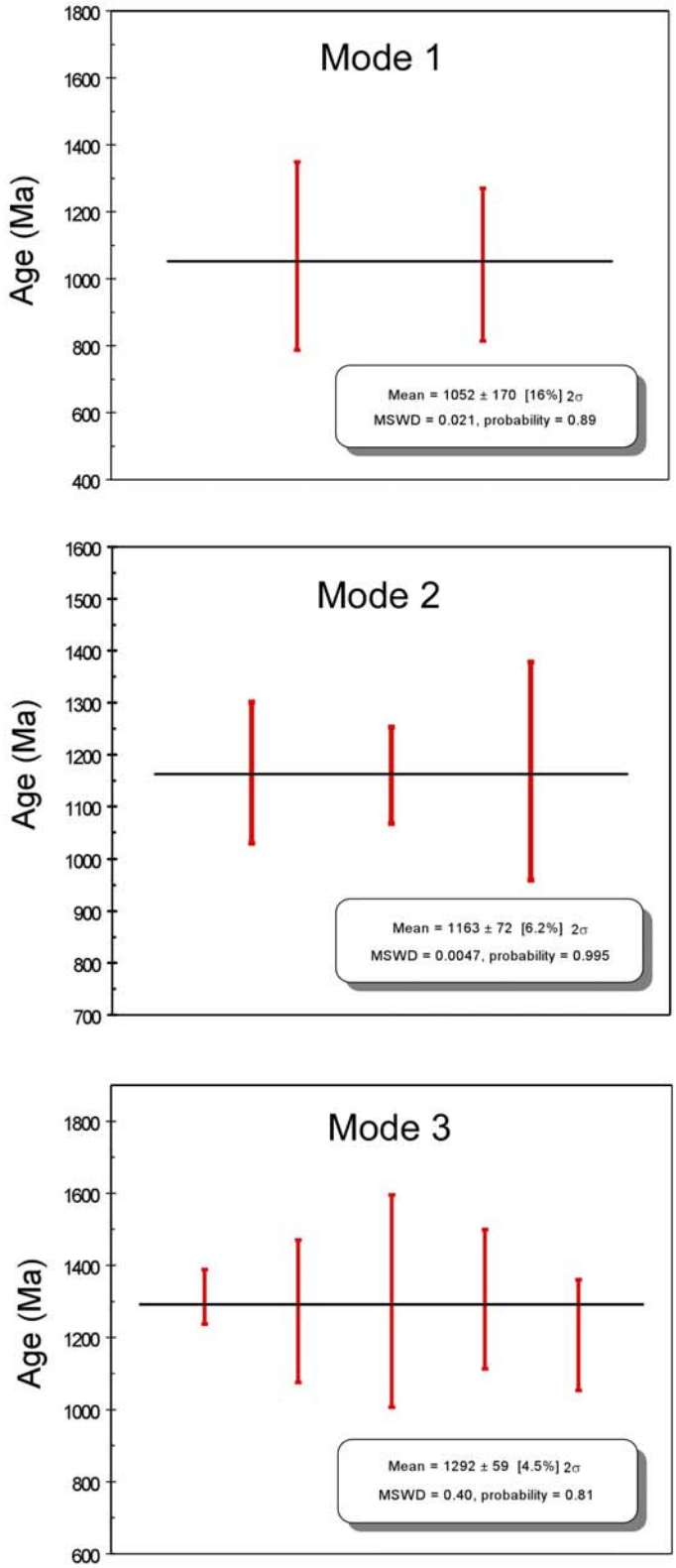

Figure 8.7. Weighted mean plots for deformed orthogneiss (DEL08-6c) showing three age modes present.

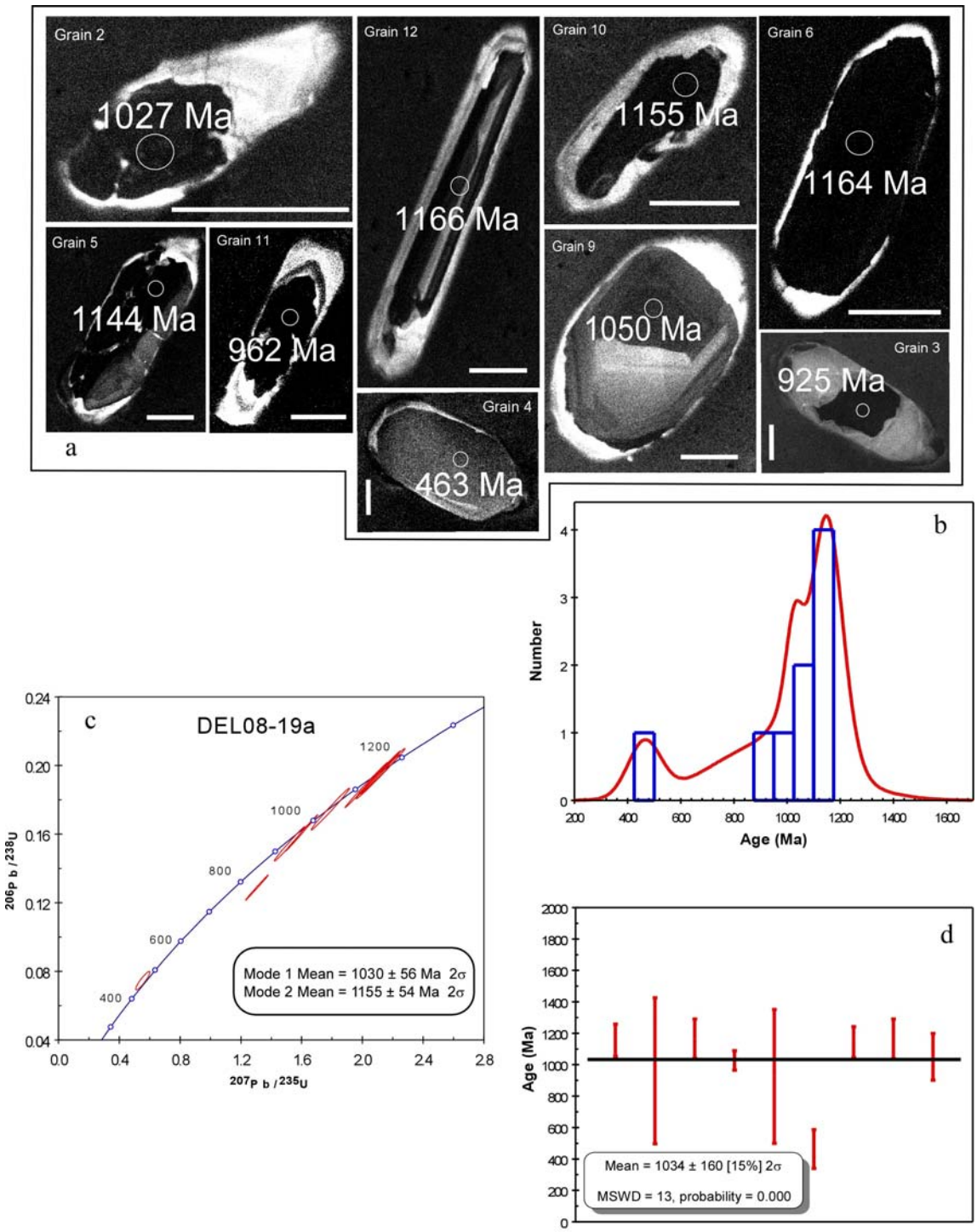

Figure 8.8. Geochronology of deformed orthogneiss (DEL09-19a). a) CL images of zircon with analysis spot (circle) and age. Scale bar is 50 μm. b) probability histogram, c) concordia diagram and d) weighted mean plot. Note probability histogram and weighted mean plot suggest multiple modes present.

based on CL zoning, weighted mean calculations, and plots (Figure 8.9): 1030 ± 56 Ma (MSWD=0.083, probability=0.77) and 1155 ± 54 Ma (MSWD=0.034, probability=0.99). These modes may correlate with the two youngest modes from sample DEL08-6c. One metamorphic zircon yielded an Ordovician age (463 ± 27 Ma) consistent with Taconian regional metamorphism (Anderson and Moecher, 2009).

Migmatitic Hornblende Gneiss

DEL08-10a

All zircons from the migmatitic hornblende gneiss sample exhibit zoned and unzoned cores with Th/U values consistent with magmatic crystallization and thin (< 20 μm) unzoned rims consistent with metamorphic growth. Although oscillatory zoning is present, most zircons in this sample exhibit unzoned or thick zones of diffuse (oscillatory?) zoning within cores (Figure 8.10a, grains 2, 3, 6, 9, and 10). Bright embayments appear to crosscut magmatic zoning in some zircons and are included within unzoned cores in other grains (Figure 8.10a; grains 5, 6, 9). Ages in this sample range from 1059 Ma to 1321 Ma, with modes at ~1050 Ma and 1270 Ma. Nine zircons from a sample of migmatitic hornblende gneiss collected along Boyd Farm Rd. (location 10, Figure 3.2) yielded a weighted mean age of 1125 ± 83 Ma (MSWD=2.2, probability=0.03) (Figure 8.10). The high MSWD value and low probability suggests this group of zircons did not originate from the same age population. Therefore, this age is not considered to be geologically significant. Two separate age modes are proposed, based on weighted mean calculations and plots (Figure 8.11): 1059 ± 58 Ma

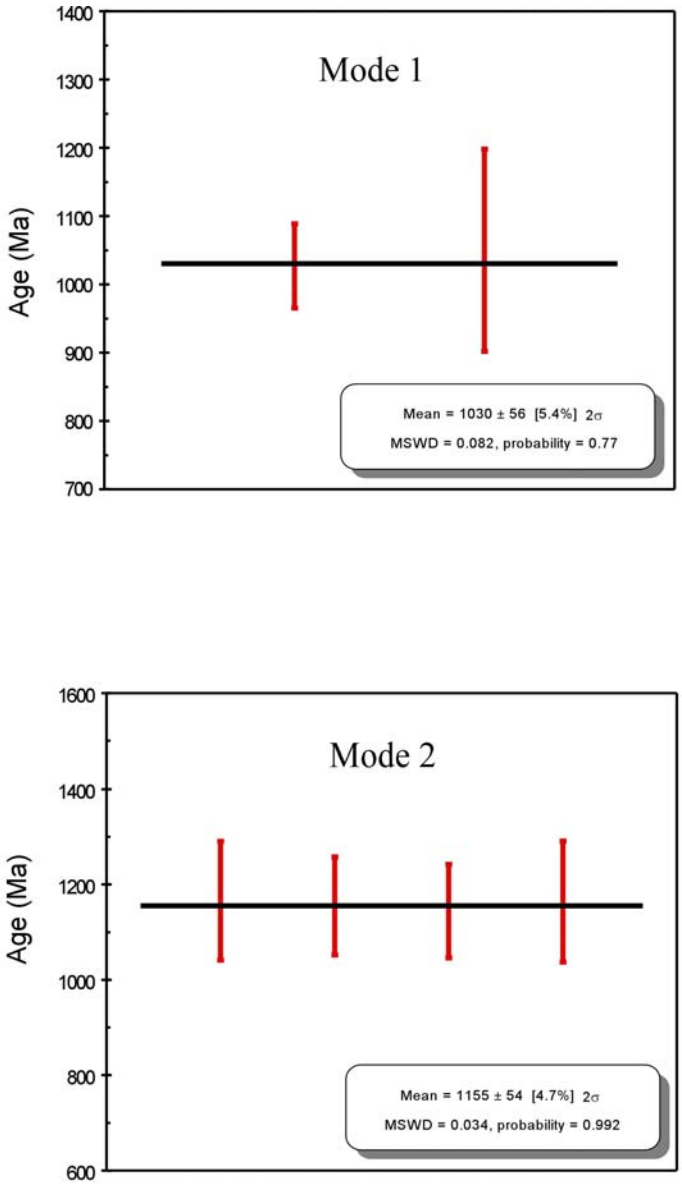

Figure 8.9. Weighted mean plots for deformed orthogneiss (DEL09-19a) showing two age modes present.

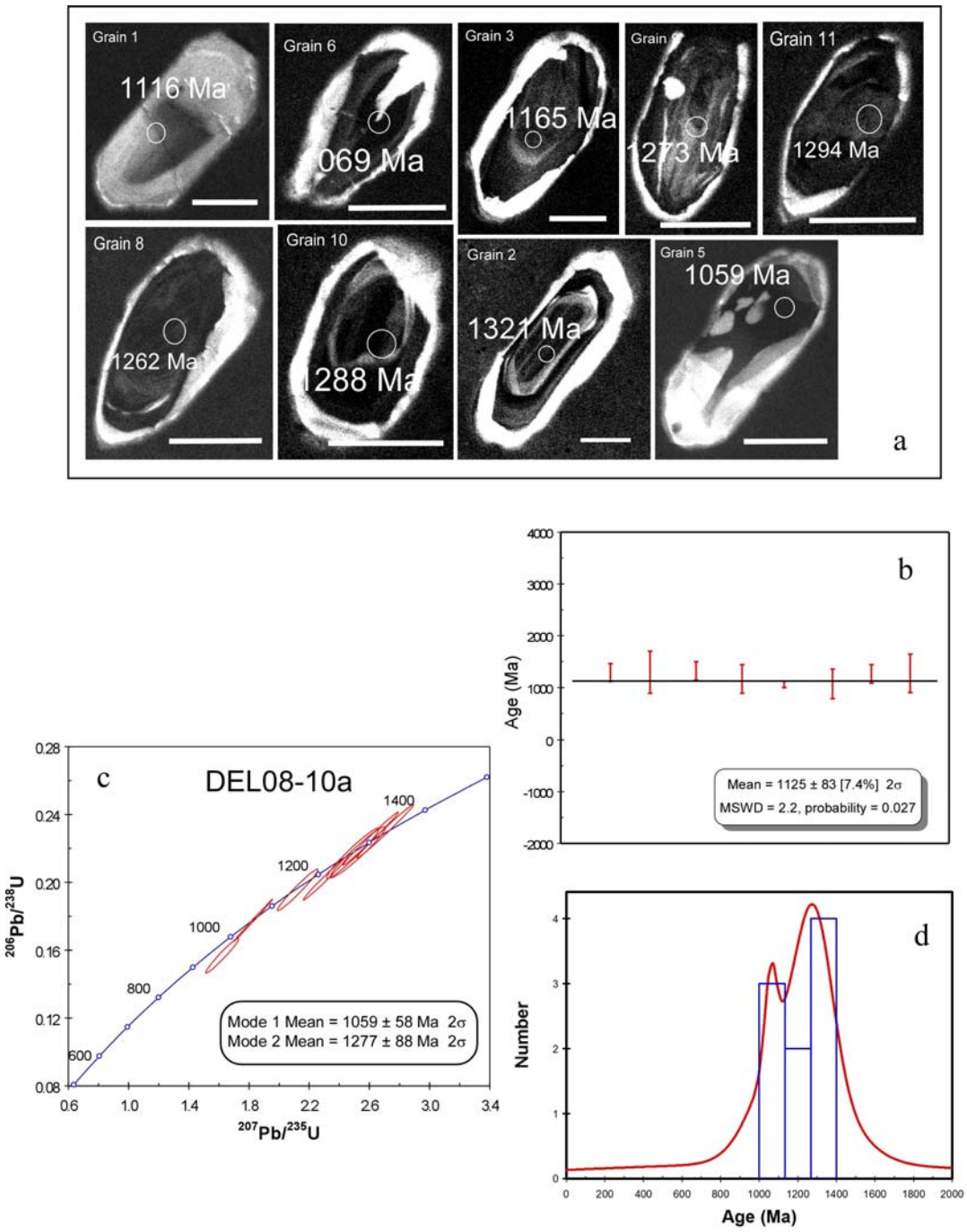

Figure 8.10. Geochronology of Hbl migmatite (DEL08-10a). a) CL images of zircon with analysis spot (circle) and age. Scale bar is 50 μm. b) weighted mean plot, c) concordia diagram and d) probability histogram. Note probability histogram and weighted mean plot suggest two modes present.

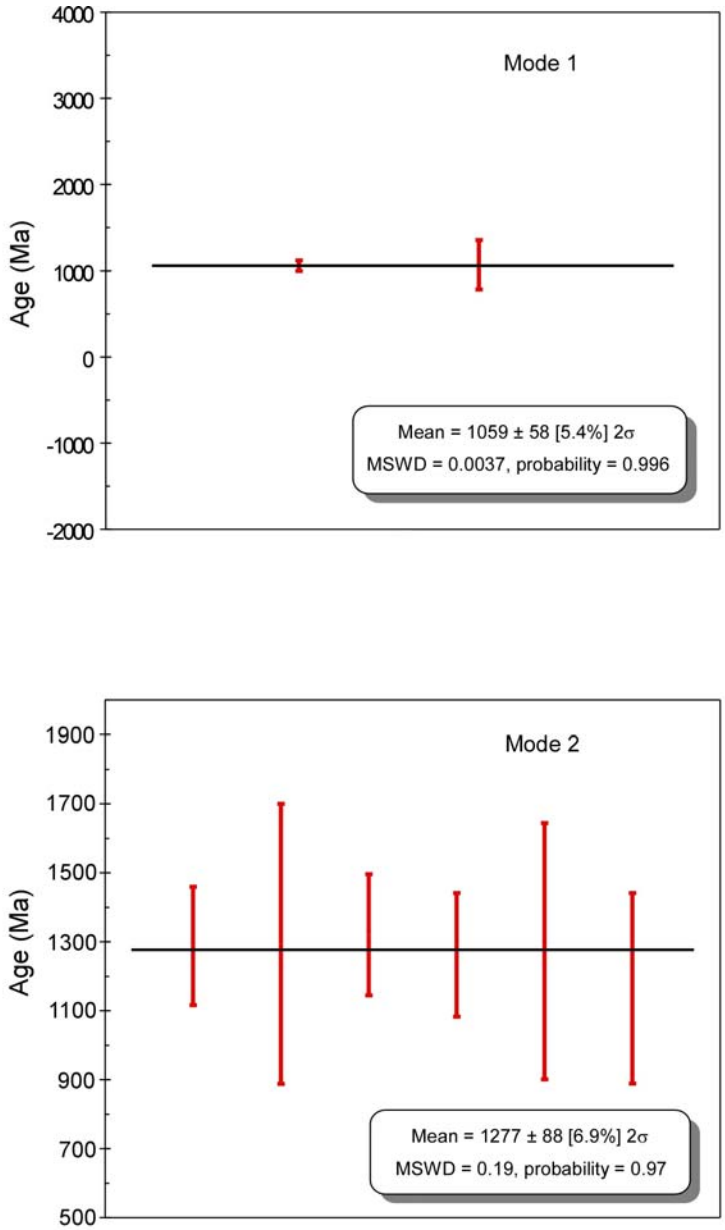

Figure 8.11. Weighted mean plots for hornblende migmatite (DEL08-10a) showing two age modes present.

(MSWD=0.004, probability=0.99) and 1277 ± 88 Ma (MSWD=0.19, probability=0.97). The older mode is consistent with prior age dating (1230 ± 20 Ma) of the same body at location 5 (E. Anderson, unpublished data).

Biotite Gneiss

DEL08-2d

Zircons from a sample of the least migmatitic biotite gneiss (Figure 5.2b) collected within the Trinity Cove housing development (location 2, Figure 3.2) exhibit mostly unzoned cores with Th/U values consistent with magmatic crystallization and very thin (< 10 μm) unzoned rims consistent with metamorphic growth. Additionally, elongate prismatic crystal morphology in some zircons of this sample is consistent with a magmatic origin (Figure 8.12a, grains 3, 8, 12, 10, 13, and 14). Patchy zonation is present (grains 2, 6, and 12). Truncation of magmatic cores is not recognized in these zircons. Ages range from 932 Ma to 1205 Ma, with a dominant mode at ~1050 Ma. Ten zircons yielded a weighted mean age of 1055 ± 65 Ma (MSWD=0.31, probability=0.99) (Figure 8.12).

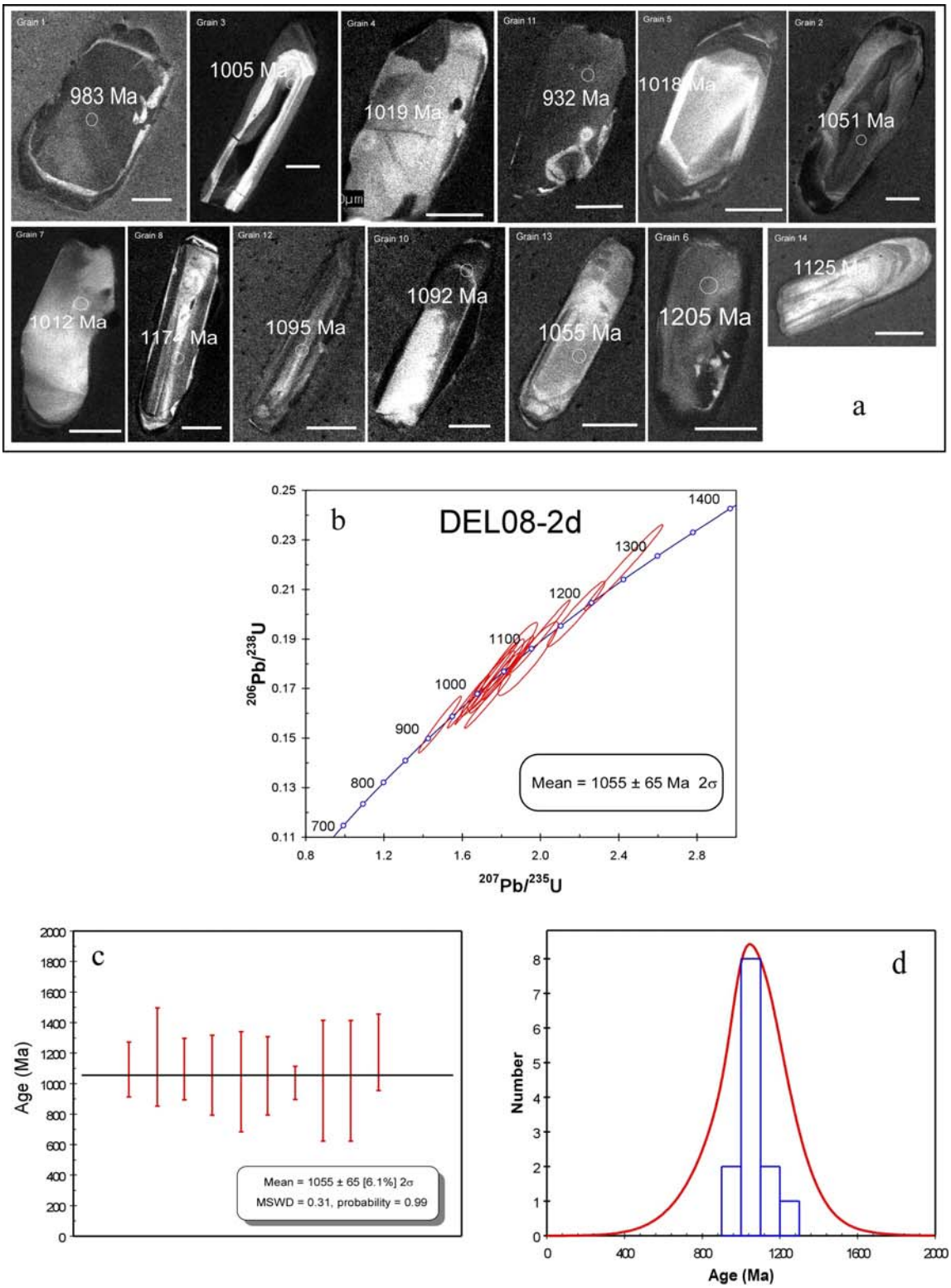

Figure 8.12. Geochronology of biotite gneiss (DEL08-2d). a) CL images of zircon with analysis spot (circle) and age. Scale bar is 50 μm. b) concordia diagram, c)weighted mean plot and d) probability histogram.

SECTION IX. DISCUSSION AND CONCLUSIONS

Textural and mineralogical similarities exist between the metaplutonic orthogneisses and their deformed equivalents that suggest these rocks are related via progressive deformation. The presence of clinopyroxene, garnet, and hornblende + quartz symplectites after clinopyroxene in orthogneiss and amphibolite, along with Taconian migmatization (Anderson and Moecher, 2009), suggest these rocks reached upper amphibolite facies regional metamorphism during the Taconian Orogeny. The prevalent compositional banding related to S_2 is a result of migmatization under these conditions. Dynamic recrystallization of quartz, brittle behavior of feldspar and titanite, and retrogression of garnet and clinopyroxene suggests these rocks were overprinted by one or more lower temperature (400-500 °C) tectonometamorphic events characterized by dynamic recrystallization of quartz, fracture of feldspar and titanite, and recrystallization of biotite. The abundance of biotite and epidote in highly deformed orthogneisses, disparate sets of inclusion trails in garnet, and mylonitization fabrics in migmatitic hornblende gneiss substantiate a late retrograde event. Structurally, strain is accommodated during this event by dynamic recrystallization of quartz in fold limbs and slip along mica-rich zones within fold hinges, taking advantage of differences in physical properties between the alternating compositional bands. The S_3 axial planar foliation and related incipient axial planar crenulation is a result of this late-stage deformation event. These observations are consistent with those of previous workers in the area (Massey, 2003; Massey and Moecher, 2005).

Field relationships, textural observations, and geochemical data suggest that the hornblende gneiss bodies are igneous in origin and are related by being progressively

deformed variants of granitic metaplutonic rocks. The nature of the biotite gneiss is more ambiguous. The calc-alkaline trend observed in this suite supports an igneous origin. However, due to a lack of preserved igneous texture and intensive migmatization of these rocks, the geochemistry does not preclude a source as immature clastic detritus derived directly from basement. The virtually identical trace element geochemical trends of the hornblende gneisses and biotite gneisses and the overlap in major element trends indicate a common igneous source.

Ryan et al. (2005) carried out whole rock geochemical analyses on amphibolites and hornblende migmatites in the Sylva North quadrangle immediately to the southwest of Dellwood quadrangle that are correlative to both the basement rocks in this study and the eastern Blue Ridge migmatitic gneiss of Massey (2003). These rocks plot along a distinctly calc-alkaline trajectory and have bulk chemical and trace element signatures consistent with igneous rocks of intermediate composition.

Field relationships, textural observations, and the distinctive tholeiitic trend of the amphibolite suite indicate that most amphibolites represent ancient fragments of oceanic crust that became disaggregated within a subduction setting. Two scenarios can explain their presence in this area: (1) amphibolites may represent fragments of uppermost oceanic crust that were scraped off the subducting slab and were caught up in the accretionary wedge or (2) they represent xenoliths of oceanic crust incorporated into arc-related magmatism. Biotite gneiss geochronology, geochemistry, and field relationships (mafic enclaves present within the biotite gneiss at a variety of scales and over a wide area) suggest the latter explanation. A small number of amphibolites are calc-alkaline basalts and may be related to the hornblende gneisses.

The preserved igneous texture in the metaplutonic hornblende orthogneisses suggests these bodies were more competent than the enveloping biotite gneisses. Thus, the interiors of these bodies were somewhat shielded from the deformation associated with both the peak thermal event (Taconian) and the late-stage, lower temperature event. As such, these rocks are useful for obtaining U-Pb zircon crystallization ages, as the absence of migmatization ensures that zircons in these rocks are magmatic, rather than metamorphic (Moecher and Samson, 2006; Moecher et al., 2004; Oliver et al., 1999). This, however, does not preclude the presence of metamorphic overgrowths on magmatic zircons nucleated under upper amphibolite to granulite facies conditions. Even so, the cores of magmatic zircons with metamorphic overgrowths are likely to preserve magmatic U and Pb concentrations (Moecher and Samson, 2006), due to the high closure temperature of zircon (~900 °C) (Cherniak and Watson, 2001).

Three dominant age modes are resolved in the four lithologies in this study: 1030 – 1055 Ma, 1153 – 1170 Ma, and 1287 – 1292 Ma. Pooled together, the four metaplutonic orthogneiss samples contain representatives of all three modes. One of the deformed orthogneisses (DEL08-6c) exhibits all three age modes. The oldest age mode is absent in the other deformed orthogneiss (DEL09-19a). The intermediate age mode is absent in the migmatitic hornblende gneiss sample. The biotite gneiss sample has only the youngest age mode.

Of the three modes listed above, the two youngest modes correspond to the widely observed dominant Grenville age modes of ~1050 Ma and ~1150 – 1190 Ma (Berquist et al., 2005; Carrigan et al., 2003; Easton, 1992; McLelland et al., 1996; McLelland et al., 2004; Ratcliffe et al., 1991; Walsh et al., 2004). The oldest age mode,

observed in metaplutonic orthogneiss (DEL08-7a and DEL08-7j), deformed orthogneiss (DEL08-6c) and migmatitic hornblende gneiss (DEL08-10a), has not previously been recognized in southern Appalachian Blue Ridge basement rocks. Tollo et al. (2006) reported three separate magmatic intervals consistent with the age modes in this study in charnockites, leucogranites, and granitoid rocks in the northern Virginia Blue Ridge. Southworth et al. (2005) concluded that the ages of the Mesoproterozoic basement rocks in the Great Smoky Mountain National Park area comprise three age groups consistent with age modes in this study (1192 – 1194 Ma, 1117 – 1168 Ma, 1029 – 1056 Ma). Neither of these studies recognized the earliest age mode discovered in the present study (1287 – 1292 Ma).

Similar ages (~1250 – 1300 Ma) are reported in calc-alkaline AMCG granitoids of the Adirondacks (McLelland et al., 2004), the Green Mountains of Vermont (Ratcliffe et al., 1991), in western Connecticut (Walsh et al., 2004), and within the western Central Metasedimentary Belt of the Canadian Grenville province (Easton, 1992). All of these calc-alkaline orthogneisses are interpreted as arc-related crustal additions emplaced during the (Elzeverian?) interval ca. 1400 – 1220 Ma (McLelland et al., 2004).

In this study, all lithologies exhibiting the oldest age mode contain zircons with internally zoned cores that are separated from their rims by geometrically irregular surfaces which truncate internal zoning (DEL08-7a, grains 2, 5, 8, 9; DEL08-7j, grains 1, 8, 9; DEL08-6c, grains 1, 7; DEL08-10a, grains 9, 10) or distinct, euhedrally-shaped cores separated from the rim by later magmatic zoning (DEL08-10a, grain 2; DEL08-7a, grains 5 and 6) consistent with xenocrystic zircons (Corfu et al., 2003). Thus, the oldest

age mode observed in this study may be related to the Grenvillian magmatism (Elzeverian) in the northern Appalachians.

Three geochronological observations suggest that the protolith of the biotite gneiss sample (DEL08-2d) is igneous. (1) The prismatic-shaped zircons are consistent with magmatic zircon growth, (2) the sample contains only one dominant Grenville age mode (1055 Ma), and (3) no zircons of Neoproterozoic age were found in the sample. If this sample were a highly deformed and metamorphosed Neoproterozoic clastic rock derived from weathering and erosion of Grenville basement rocks, it should contain all Grenville age modes. Chakraborty et al. (2010) showed that Neoproterozoic (Ocoee) sediment derived from Grenville basement has, in addition to all Grenville age modes, Neoproterozoic-aged (620 – 800 Ma) zircons derived from Neoproterozoic rift-related magmatic rocks (Aleinikoff et al., 1995; Tollo and Hutson, 1996). The Ashe suite metaclastic rocks have a similar zircon distribution as the Ocoee metaclastic rocks (dominantly Grenville modes with a few Neoproterozoic ages; Moecher et al., in review). Thus, the definitive test for the origin of the biotite gneiss protolith would be to analyze ≥100 zircon grains separated from the biotite gneiss to determine if Neoproterozoic grains are present.

Modal data and XRF major and trace element geochemistry show that metaplutonic rocks, hornblende gneisses, and biotite gneisses are related and therefore may have a common source. U-Pb zircon geochronology suggests metaplutonic orthogneisses, their deformed equivalents, migmatitic hornblende gneisses, and biotite gneisses are all derived from Grenvillian magmatism. Petrographic observations (widespread replacement of hornblende by biotite) suggest that the biotite gneiss may

simply be retrograded hornblende gneiss. The presence of gradational contacts between hornblende gneiss bodies and the enveloping biotite gneiss is consistent with this interpretation. Field relationships, textural observations, geochemical trends, and geochronological data suggest that the protoliths of the hornblende gneisses are Grenville-age granitic plutons and are related by progressive deformation. Major and trace element geochemistry, geochronology (along with the presence of magmatic zircons), and field relationships suggest an alternative (igneous) origin for the biotite gneiss. Evidence presented in this study suggests that there is a larger exposure of Grenville basement in this region than previously thought. A previously unknown age mode for Mesoproterozoic plutonism in the southern Appalachian Blue Ridge was discovered in this study (~1250-1300 Ma).

Future Work

Future work in the area should include a detrital zircon study of the Great Smoky Group schists and Longarm/Wading Branch formations exposed in the Dellwood quadrangle to compare with the geochronology of the biotite gneiss. Absent Neoproterozoic ages in the biotite gneiss would confirm an igneous origin for these rocks. U-Pb zircon geochronology should be carried out on some large amphibolite bodies within the quad to provide constraints on their emplacement. A Sm-Nd isotopic analysis for obtaining depleted mantle model ages of the basement rocks would be useful for determining if these rocks are derived from juvenile crust or reworked older crust. $^{207}Pb/^{204}Pb$ isotopic analysis of the basement rocks would be useful to test the hypothesis

that these rocks are of Laurentian affinity. Elevated ratios may suggest a pre-Grenvillian (Gondwanan?) crustal heritage.

SECTION X. APPENDICES

APPENDIX A

Structural Data

The following is a compilation of structural data taken from field locations in Dellwood quadrangle. Location numbers correspond to locations given in Figure 3.2.

Location	Foliation Orientation strike (azimuth) / dip (°), dip direction	Fold Axis Orientation plunge (°) / trend (azimuth)
2	092/52 SW	44/226
	081/65 SE	54/223
	058/50 SE	60/226
	090/80 S	76/206
	059/54 SE	26/074
	076/52 SE	32/097
	064/52 SE	
	072/52 SE	
	142/52 NE	
	155/50 NE	
	072/77 SE	
	066/50 SE	
	134/33 NE	
10	144/60 SW	No data
	164/52 SW	
	144/63 SW	
	170/36 SW	
08-6	122/78 SW	4/120
	130/52 SW	11/120
	152/72 SW	10/130
	053/40 SE	10/090
	042/36 SE	0/100
	110/64 SW	21/130
	122/78 SW	
	095/25 SW	
	120/76 SW	
	090/36 S	
	130/80 SW	
	084/48 SE	
	112/24 SW	
	094/34 SW	
	052/32SE	

Location	Foliation Orientation strike (azimuth) / dip (°), dip direction	Fold Axis Orientation plunge (°) / trend (azimuth)
11	027/48 SE	55/130
	060/44 SE	61/097
	047/55 SE	52/114
	057/53 SE	70/118
	044/50 SE	42/102
	078/56 SE	36/114
	082/52 SE	52/140
	070/55 SE	27/122
	065/38 SE	
	046/40 SE	
	040/40 SE	
	043/44 SE	
	060/52 SE	
	048/48 SE	
	044/58 SE	
	048/50 SE	
12	No data	28/068
		26/076
		32/052
		20/068
		20/064
		22/066
09-6	051/27 SE	43/143
	036/21 SE	28/127
	051/18 SE	17/125
	031/19 SE	
	032/29 SE	
	022/21 SE	
	082/24 SE	
6A	047/39 SE	38/250
	067/15 SE	17/115
	150/33 NE	
	010/18 SE	

Location	Foliation Orientation strike (azimuth) / dip (°), dip direction	Fold Axis Orientation plunge (°) / trend (azimuth)
13	001/76 NW 015/44 NW 175/60 SW 018/43 NW 160/21 SW	16/205 1/239 28/354
15	052/66 SE 070/69 SE 088/38 SE 112/40 SW 095/34 SW 121/83 SW 119/47 SW	66/120 55/147 4/304
16	084/86 NW 068/65 NW	No data
17	050/55 NW	No data
18	007/48 NW 175/64 SW	30/345 37/103
19	110/20 SW	No data
21	020/77 SE	No data
23	10838 SW 122/22 SW 121/42 SW	No data
25	127/39 NE	No data

APPENDIX B

XRF Spectrometric Analysis

The following whole rock major element oxide and trace element geochemistry for basement samples was performed at the Kentucky Geological Survey, Lexington, KY. Major element oxide concentrations are given in weight percents. Trace element concentrations are given in ppm. The standard error for major element oxides is 1-2%, for minor element oxides is < 5%, and for trace elements is 5-10%. Error values were calculated at 95% confidence level. Sample numbers with asterisks were obtained from E. Anderson (unpublished data). Quadrangle codes are as follows: a = Cove Creek Gap, b = Clingmans Dome, c = Smokemont, d = Bunches Bald, e = Dellwood, f = Clyde, g = Sylva North, h = Fines Creek, i = Hazelwood, j = Lemons Gap. Lithology codes are as follows: 1 = metaplutonic orthogneiss, 2 = deformed orthogneiss, 3 = migmatitic hornblende gneiss, 4 = amphibolite, 5 = biotite gneiss, 6 = pegmatite dike.

SAMPLE	DEL08-2d	DEL08-10A	DEL08-11B	DEL08-7H	DEL09-6A	DEL09-15A	DEL08-7A	DEL09-18A	CG09-1-1A	DEL09-19B	SN09-1	DEL08-7D
Quadrangle	**e**	**e**	**e**	**e**	**e**	**e**	**e**	**e**	**f**	**e**	**g**	**e**
Lithology	**5**	**3**	**5**	**1**	**2**	**5**	**1**	**3**	**4**	**2**	**5**	**1**
SiO2	66.78	59.09	66.3	46.63	62.18	77.94	64.51	61.11	58.66	78.97	68.19	58.81
TiO2	0.78	0.72	0.53	1.63	0.77	0.61	0.38	0.83	1.35	0.34	0.86	0.94
Al2O3	13.56	15.94	14.28	12.2	13.43	9.84	15.74	14.99	13.61	8.31	13.29	14.44
MnO	0.08	0.1	0.04	0.22	0.1	0.06	0.04	0.1	0.16	0.04	0.08	0.11
FeO	4.71	5.63	3.11	8.91	6.14	3.21	3.26	6.01	8.16	1.93	5.02	6.98
MgO	1.57	2.8	1.09	9.44	3.09	0.88	1.2	3.1	4.33	0.53	1.78	3.6
CaO	1.79	5.52	2.72	12.24	3.15	0.36	3.67	5.53	6.22	0.85	2.47	5.29
Na2O	2.08	3.67	3.18	1.67	2.58	0.41	3.7	3.51	2.54	1.02	2.58	2.97
K2O	4.19	2.2	4.21	0.88	3.07	2.38	2.91	1.78	1.11	3.31	2.64	2.1
P2O5	0.17	0.31	0.23	0.43	0.2	0.14	0.25	0.25	0.21	0.12	0.23	0.32
LOI	3.77	3.4	3.96	4.76	4.6	3.82	4	2.12	2.72	4.38	2.31	3.67
TOTAL	99.48	99.38	99.66	99.01	99.31	99.66	99.66	99.33	99.08	99.8	99.46	99.24
%AN	30.62	39.79	30.83	62.14	39.61	20.07	34.61	40.11	51.10	28.46	33.00	44.15
Q	33.47	14.03	25.96	0.00	23.76	67.43	23.53	18.00	19.91	60.77	35.77	16.86
or	25.81	13.51	25.95	5.50	19.11	14.64	17.94	10.80	6.79	20.46	16.02	12.95
ab	18.35	32.28	28.06	14.94	23.00	3.61	32.67	30.48	22.24	9.03	22.42	26.23
an	8.10	21.33	12.51	24.53	15.08	0.91	17.29	20.41	23.24	3.59	11.04	20.74
ne	0.00	0.00	0.00	0.00	0.00	0.00	0.00	0.00	0.00	0.00	0.00	0.00
C	2.87	0.00	0.10	0.00	0.65	6.53	0.45	0.00	0.00	1.87	2.31	0.00
di	0.00	4.08	0.00	29.29	0.00	0.00	0.00	4.92	5.91	0.00	0.00	3.64
hy	6.01	9.25	2.83	14.18	12.91	2.28	3.93	9.72	14.49	1.38	6.71	13.24
ol	0.00	0.00	0.00	2.45	0.00	0.00	0.00	0.00	0.00	0.00	0.00	0.00
mt	3.45	3.35	2.85	4.80	3.47	2.76	2.84	3.47	4.28	0.03	3.51	3.69
il	1.54	1.42	1.05	3.27	1.54	1.21	0.75	1.62	2.65	0.68	1.68	1.86
hem	0.00	0.00	0.15	0.00	0.00	0.29	0.00	0.00	0.00	1.90	0.00	0.00
ap	0.41	0.75	0.56	1.05	0.49	0.34	0.60	0.59	0.50	0.29	0.55	0.77
ru	0.00	0.00	0.00	0.00	0.00	0.00	0.00	0.00	0.00	0.00	0.00	0.00
Pb	29	13	24	7	11	23	19	13	5	21	22	12
Cu	10	9	10	0	20	11	13	67	20	6	9	41
Co	13	18	6	38	18	6	11	26	33	5	12	32
Ni	29	35	18	118	95	27	19	68	55	18	32	48
Cr	95	103	96	938	240	215	87	174	238	129	165	222
Ce	104	82	100	95	66	90	77	81	48	80	81	109
V	73	112	53	239	116	52	59	111	184	30	85	138
La	66	40	44	35	20	47	40	54	17	8	33	41
Ba	1018	1218	1499	176	869	937	1989	639	170	1129	692	1025
Nb	22	11	11	17	15	18	10	12	14	16	19	20
Zr	340	219	289	170	251	401	259	203	230	268	359	223
Y	63	32	33	25	34	55	20	27	40	33	58	48
Sr	247	745	449	321	367	60	907	657	173	256	236	615
Rb	127	63	101	11	126	82	76	60	34	66	98	52
U	18	18	18	18	18	18	18	18	18	18	18	18
Th	21	17	17	17	19	20	17	17	17	17	17	17
Ga	22	26	26	19	24	21	28	20	18	15	20	20
Zn	83	74	46	112	88	101	42	76	68	20	87	89

SAMPLE	DEL08-7E	DEL08-6C dm	DEL09-17B	DEL09-6A-1	DEL09-25A	DEL08-7J	DEL09-14A	DEL09-16B	DEL09-17D	DEL09-16A	DEL09-26A	DEL09-6F
Quadrangle	**e**	**e**	**e**	**e**	**e**	**e**	**e**	**e**	**e**	**e**	**e**	**e**
Lithology	**1**	**2**	**1**	**2**	**2**	**1**	**5**	**1**	**1**	**1**	**4**	**3**
SiO2	51.31	66.46	68.62	54	62.58	66.32	77.45	56.2	72.83	51.12	46.24	60.85
TiO2	1.3	0.33	0.36	1.2	1.01	0.5	0.48	1.11	0.23	2.16	1.68	0.88
Al2O3	16.43	14.9	14.43	17.29	15.49	15.83	8.13	15.7	12.83	15.9	14.07	14.26
MnO	0.18	0.04	0.05	0.12	0.04	0.04	0.03	0.1	0.02	0.13	0.22	0.16
FeO	8.76	2.66	2.64	7.7	4.64	3.1	1.93	7.61	1.47	8.6	11.52	6.57
MgO	4.67	1	0.65	3.03	1.96	1.54	0.49	3.74	0.4	4.57	7.32	3.44
CaO	7.17	3.06	1.56	5.72	3.82	3.68	0.12	5.19	1.61	6.07	11.57	5.15
Na2O	3.94	3.48	1.78	3.94	3.28	4.43	0.27	2.36	2.54	2.44	1.81	2.96
K2O	1.28	3.48	4.95	2.41	2.53	1.63	4.18	3.63	4.81	3.65	0.79	2.42
P2O5	0.49	3.48	0.17	0.41	0.38	0.26	0.07	0.47	0.03	0.79	0.15	0.26
LOI	3.49	3.48	4.5	3.33	3.76	2.31	6.63	3.07	3.06	3.61	3.34	2.32
TOTAL	99.02	3.48	99.7	99.15	99.49	99.63	99.78	99.18	99.83	99.04	98.71	99.27
%AN	41.20	31.70	30.56	40.16	37.24	30.64	5.70	51.87	26.61	51.19	64.59	42.45
Q	1.21	24.98	37.21	4.55	24.45	25.50	63.31	11.20	36.82	4.73	0.00	18.34
or	7.90	23.67	30.67	14.82	15.58	9.88	26.46	22.26	29.33	22.52	4.88	14.72
ab	34.80	30.63	15.79	34.70	28.92	38.44	2.45	20.72	22.17	21.55	16.01	25.77
an	24.39	14.21	6.95	23.29	17.16	16.98	0.15	22.34	8.04	22.60	29.19	19.01
ne	0.00	0.00	0.00	0.00	0.00	0.00	0.00	0.00	0.00	0.00	0.00	0.00
C	0.00	0.00	3.89	0.00	1.38	0.73	3.33	0.00	0.61	0.00	0.00	0.00
di	7.66	0.28	0.00	2.84	0.00	0.00	0.00	0.97	0.00	2.75	24.23	4.50
hy	16.06	2.46	1.70	12.38	5.82	3.93	1.31	15.27	1.03	14.11	13.26	11.78
ol	0.00	0.00	0.00	0.00	0.00	0.00	0.00	0.00	0.00	0.00	3.93	0.00
mt	4.24	2.54	2.34	4.07	3.79	2.95	0.00	3.93	0.00	5.54	4.82	3.55
il	2.58	0.65	0.72	2.37	2.00	0.97	0.40	2.19	0.04	4.28	3.33	1.72
hem	0.00	0.15	0.33	0.00	0.00	0.02	2.12	0.00	1.69	0.00	0.00	0.00
ap	1.18	0.43	0.41	0.99	0.92	0.62	0.17	1.13	0.07	1.91	0.36	0.62
ru	0.00	0.00	0.00	0.00	0.00	0.00	0.30	0.00	0.21	0.00	0.00	0.00
Pb	14	23	28	10	24	23	36	6	29	8	10	15
Cu	26	13	5	7	15	20	20	19	10	6	22	24
Co	31	7	5	24	15	17	2	30	2	43	45	23
Ni	50	16	14	25	30	36	19	49	18	62	44	51
Cr	97	61	114	47	108	129	186	226	171	85	327	220
Ce	133	58	29	84	100	46	24	105	38	177	15	46
V	186	52	48	151	92	67	34	152	24	184	307	140
La	56	25	18	38	44	23	6	39	19	78	0	11
Ba	587	2043	2212	452	1014	1085	1134	1650	1456	1460	123	802
Nb	27	10	10	32	22	10	12	19	10	25	10	19
Zr	229	227	200	235	309	252	301	278	236	476	100	277
Y	43	30	32	56	26	20	36	54	20	44	26	41
Sr	724	738	329	398	512	886	109	627	313	687	118	462
Rb	26	81	121	112	87	58	112	102	90	107	11	78
U	18	18	18	18	18	18	18	18	18	18	18	18
Th	17	17	17	17	17	17	17	17	17	17	17	24
Ga	22	19	19	24	21	20	14	20	17	21	16	20
Zn	101	38	41	99	90	41	33	81	22	116	114	87

SAMPLE	DEL09-19A	DEL08-12A	DEL08-6C	DEL09-20	DEL08-7dmaf	DEL08-5	DEL09-13a	SN09-2a	DEL08-7dfel	DEL08-7c-2	DEL08-7c-3maf	DEL08-7c-1f
Quadrangle	**e**	**e**	**e**	**e**	**e**	**e**	**e**	**g**	**e**	**e**	**e**	**e**
Lithology	**2**	**5**	**2**	**1**	**4**	**3**	**5**	**1**	**1**	**1**	**4**	**1**
SiO2	71.99	60.39	62.23	60.6	47.75	61.57	63.4	54.84	66.91	56.72	49.97	64.52
TiO2	0.32	0.72	0.52	1.23	1.94	0.71	0.72	1.01	0.28	0.91	1.47	0.46
Al2O3	12.82	15.53	14.68	13.66	13.85	14.23	14.87	14.24	15.29	15.65	13.75	15.56
MnO	0.03	0.1	0.06	0.13	0.21	0.12	0.06	0.13	0.04	0.12	0.2	0.07
FeO	1.97	5.99	3.67	7.42	12.71	6.04	4.47	7.91	2.06	6.64	10.94	4.02
MgO	0.58	3.05	1.27	4.39	6.98	3.06	2.04	5.41	0.98	4.28	6.84	1.98
CaO	1.61	5.18	4.07	6.78	7.33	5.35	3.44	7.88	3.64	6.2	8.25	5.17
Na2O	2.47	3.48	3.6	1.93	1.56	3.15	2.86	2.8	3.71	3.54	2.25	3.99
K2O	5.1	2.35	3.3	0.94	2.86	1.85	3.23	0.96	2.76	1.69	1.59	1.2
P2O5	0.12	0.3	0.24	0.16	0.45	0.21	0.33	0.17	0.19	0.24	0.17	0.24
LOI	2.78	2.23	5.94	1.92	2.95	3.05	4.07	3.77	3.92	3.27	3.34	2.34
TOTAL	99.79	99.32	99.59	99.16	98.59	99.34	99.5	99.12	99.78	99.26	98.77	99.55
%AN	25.63	40.22	31.72	61.27	62.86	41.90	38.12	49.74	34.88	42.14	54.41	38.35
Q	35.12	15.58	20.51	24.93	0.00	20.62	25.28	10.90	27.12	10.41	2.33	23.79
or	31.01	14.27	20.78	5.70	17.61	11.33	19.96	5.93	16.98	10.38	9.82	7.28
ab	21.51	30.26	32.46	16.75	13.75	27.62	25.30	24.78	32.69	31.13	19.89	34.66
an	7.41	20.36	15.08	26.49	23.28	19.92	15.59	24.53	17.51	22.68	23.74	21.56
ne	0.00	0.00	0.00	0.00	0.00	0.00	0.00	0.00	0.00	0.00	0.00	0.00
C	0.61	0.00	0.00	0.00	0.00	0.00	1.26	0.00	0.04	0.00	0.00	0.00
di	0.00	3.28	3.81	5.60	9.44	5.02	0.00	12.31	0.00	6.19	14.56	2.54
hy	1.49	10.83	2.60	13.71	25.29	10.29	7.02	15.32	2.54	13.22	21.85	5.79
ol	0.00	0.00	0.00	0.00	0.51	0.00	0.00	0.00	0.00	0.00	0.00	0.00
mt	0.25	3.31	3.12	4.06	5.20	3.32	3.37	3.81	0.83	3.63	4.50	2.92
il	0.63	1.41	1.05	2.40	3.84	1.40	1.43	2.01	0.55	1.80	2.92	0.90
hem	1.70	0.00	0.00	0.00	0.00	0.00	0.00	0.00	1.28	0.00	0.00	0.00
ap	0.29	0.71	0.59	0.38	1.09	0.50	0.80	0.41	0.46	0.58	0.41	0.57
ru	0.00	0.00	0.00	0.00	0.00	0.00	0.00	0.00	0.00	0.00	0.00	0.00
Pb	25	14	25	8	8	10	19	15	26	13	8	19
Cu	7	30	6	29	41	2	5	17	43	24	32	78
Co	5	26	12	31	45	25	14	37	9	19	36	15
Ni	13	47	24	66	59	47	38	100	31	44	56	37
Cr	90	245	124	260	443	175	78	255	107	133	167	116
Ce	106	76	73	106	377	106	200	72	92	116	145	75
V	32	116	80	170	233	120	72	151	35	126	262	65
La	19	31	41	5	74	20	59	11	30	24	19	20
Ba	1550	968	1491	211	724	875	981	186	2064	712	377	564
Nb	10	10	16	15	37	10	13	13	10	15	18	10
Zr	291	205	229	213	206	160	285	120	244	175	110	144
Y	30	30	30	39	72	28	37	30	25	28	34	14
Sr	425	612	717	145	339	556	421	216	817	582	381	662
Rb	111	63	52	26	53	74	111	24	65	42	30	23
U	18	18	18	18	18	18	18	18	18	18	18	18
Th	88	17	17	17	17	17	17	17	17	17	17	17
Ga	18	20	20	19	20	21	21	20	21	20	20	22
Zn	20	71	43	71	153	63	72	86	28	72	106	42

SAMPLE	DEL09-22a	DEL08-7c-3fel	CLY09-2a	DEL08-7k	DEL09-24a	DEL08-7f	CLY09-1	DEL08-1	DEL08-11c	DEL08-11g	DEL08-1m	DEL08-3c
Quadrangle	**e**	**e**	**f**	**e**	**e**	**e**	**f**	**e**	**e**	**e**	**e**	**e**
Lithology	**5**	**1**	**4**	**1**	**2**	**1**	**6**	**3**	**5**	**2**	**3**	**3**
SiO2	56.16	58.03	47.91	60.4	56.32	51.63	72.31	45.46	52.51	61.9	47.59	59.03
TiO2	0.91	0.79	3.04	0.75	2.38	1.18	0.15	4.34	1.01	0.96	1.96	1.02
Al2O3	22.25	16.27	14.66	16.62	14.88	15.9	14.4	14.37	14.32	13.96	13.83	15.73
MnO	0.17	0.11	0.19	0.1	0.18	0.18	0.01	0.18	0.2	0.13	0.23	0.1
FeO	7.27	5.81	13.57	5.3	8.36	8.86	0.97	14.15	8.76	6.89	13.02	5.81
MgO	2.29	3.77	4.32	2.44	2.99	5.51	0.39	4.9	7.21	2.89	6.34	2.04
CaO	1.39	5.72	9.19	4.97	6.59	7.78	2.42	7.83	6.68	4.61	10.27	8.06
Na2O	2.08	3.88	2.1	4.09	1.37	3.24	4.91	2.87	2.67	2.73	2.42	2.75
K2O	3.22	1.72	0.46	1.79	0.34	1.38	1.03	0.62	2.77	2.7	0.28	1.24
P2O5	0.21	0.24	0.56	0.36	1.13	0.35	0.05	0.44	0.21	0.27	0.2	0.38
LOI	3.24	3.02	2.48	2.58	4.52	3.02	3.27	3.26	2.68	2.21	2.42	3.18
TOTAL	99.19	99.35	98.49	99.4	99.06	99.03	99.91	98.42	99.02	99.24	98.57	99.35
%AN	23.89	40.01	62.18	38.54	68.59	47.46	21.94	50.22	45.56	43.61	55.98	53.63
Q	24.04	11.36	8.33	15.67	32.33	2.54	35.33	4.07	0.81	21.17	0.98	20.75
or	19.78	10.53	2.82	10.90	2.12	8.47	6.29	3.83	16.95	16.40	1.71	7.60
ab	18.30	34.00	18.42	35.66	12.21	28.48	42.95	25.37	23.39	23.75	21.22	24.14
an	5.74	22.68	30.29	22.37	26.66	25.72	12.07	25.59	19.58	18.36	27.00	27.92
ne	0.00	0.00	0.00	0.00	0.00	0.00	0.00	0.00	0.00	0.00	0.00	0.00
C	13.85	0.00	0.00	0.00	3.14	0.00	0.96	0.00	0.00	0.00	0.00	0.00
di	0.00	4.10	10.84	0.50	0.00	9.75	0.00	9.64	10.77	2.73	20.08	8.93
hy	12.37	11.78	15.15	9.22	10.10	17.83	1.00	13.00	22.26	11.42	19.48	3.96
ol	0.00	0.00	0.00	0.00	0.00	0.00	0.00	0.00	0.00	0.00	0.00	0.00
mt	3.63	3.44	6.82	3.36	5.93	4.04	0.00	8.84	3.77	3.67	5.20	3.79
il	1.80	1.55	5.99	1.47	4.76	2.33	0.02	8.61	1.99	1.87	3.86	2.01
hem	0.00	0.00	0.00	0.00	0.00	0.00	1.11	0.00	0.00	0.00	0.00	0.00
ap	0.51	0.58	1.35	0.86	2.76	0.84	0.12	1.06	0.50	0.64	0.48	0.91
ru	0.00	0.00	0.00	0.00	0.00	0.00	0.14	0.00	0.00	0.00	0.00	0.00
Pb	34	12	6	14	9	11	15	5	6	13	0	14
Cu	10	20	8	25	1	22	10	6	8	21	28	1
Co	6	24	48	21	25	43	2	62	46	24	41	13
Ni	15	39	31	40	22	51	12	38	168	42	32	15
Cr	164	114	66	136	130	206	9	97	507	161	277	90
Ce	403	81	98	145	435	239	15	41	75	115	25	78
V	103	107	236	104	204	180	13	313	140	115	312	136
La	111	25	15	45	101	59	5	11	26	48	5	32
Ba	654	800	210	905	607	432	251	284	372	1051	71	1246
Nb	39	12	22	16	34	21	10	18	20	20	10	13
Zr	215	196	201	237	534	179	187	160	115	282	124	240
Y	95	23	28	29	41	40	6	22	44	48	29	13
Sr	168	621	631	706	370	576	611	410	283	379	117	739
Rb	130	45	7	38	6	25	19	6	108	70	4	16
U	18	18	18	18	18	18	18	18	18	18	18	18
Th	47	17	17	17	17	17	17	17	17	17	17	17
Ga	30	21	20	23	20	21	23	18	20	21	18	22
Zn	129	64	151	65	79	106	33	142	130	91	82	62

SAMPLE	DEL08-3eNorth	DEL09-17c	CCG03-3*	CCG03-5*	CG03-1*	CG03-2*	CH02-1*	CH02-2*	CH02-4*	CT04-3B*	DEL03-1*	DEL03-1L*
Quadrangle	**e**	**e**	**a**	**a**	**f**	**f**	**c**	**c**	**c**	**f**	**e**	**e**
Lithology	**3**	**1**	**1**	**1**	**1**	**1**	**1**	**1**	**1**	**4**	**5**	**1**
SiO2	44.03	45.82	66.23	76.58	61.46	56.87	63.31	64.31	64.04	54.12	71.01	75.13
TiO2	1.22	2.49	1.08	0.14	1.10	1.48	1.26	1.21	1.12	1.40	0.56	0.08
Al2O3	16.36	15.35	14.94	13.68	16.59	15.68	15.50	15.48	16.20	18.21	14.14	14.10
MnO	0.26	0.14	0.10	0.05	0.14	0.18	0.14	0.10	0.09	0.12	0.06	0.02
FeO	12.59	9.55	5.57	1.78	7.80	9.71	6.30	5.93	5.58	8.41	4.27	0.91
MgO	7.25	6.67	1.10	0.33	3.46	4.81	1.31	1.27	1.22	3.96	1.23	0.20
CaO	8.49	7.48	2.15	0.93	3.82	7.10	4.51	4.22	3.63	8.97	2.27	1.42
Na2O	2.48	2.7	3.82	2.70	2.73	2.72	2.71	3.63	3.40	2.97	2.94	2.57
K2O	2.34	3.21	4.68	3.77	2.68	1.26	4.27	3.24	4.10	1.22	3.37	5.48
P2O5	0.24	0.76	0.35	0.02	0.22	0.20	0.68	0.62	0.62	0.62	0.15	0.09
LOI	3.33	4.77	0.84	1.27	1.59	1.34	2.57	0.62	2.20	1.71	0.03	0.40
TOTAL	98.59	98.94	100.00	100.00	100.00	100.00	100.00	100.00	100.00	100.00	100.00	100.00
%AN	69.01	48.52	20.68	16.46	43.22	53.90	43.36	34.80	32.74	56.62	29.21	22.83
Q	0.00	0.00	19.81	43.93	19.69	12.17	20.29	20.62	19.81	7.66	33.80	36.10
or	14.48	20.06	27.57	22.27	15.82	7.43	25.15	19.10	24.14	7.20	19.85	32.33
ab	12.50	22.76	32.20	22.80	23.00	22.91	22.85	30.60	28.66	25.04	24.87	21.75
an	27.84	21.45	8.40	4.49	17.51	26.79	17.49	16.34	13.95	32.68	10.26	6.43
ne	5.13	0.76	0.00	0.00	0.00	0.00	0.00	0.00	0.00	0.00	0.00	0.00
C	0.00	0.00	0.51	3.50	2.76	0.00	0.00	0.00	1.05	0.00	1.88	1.58
di	12.01	9.97	0.00	0.00	0.00	5.72	0.29	0.44	0.00	6.27	0.00	0.00
hy	0.00	0.00	4.92	0.83	14.84	17.38	5.90	5.26	5.00	12.85	4.93	0.50
ol	20.92	12.03	0.00	0.00	0.00	0.00	0.00	0.00	0.00	0.00	0.00	0.00
mt	4.13	6.12	3.76	0.67	3.81	4.35	4.06	3.94	3.85	4.25	3.00	0.00
il	2.43	5.00	2.04	0.27	2.08	2.79	2.39	2.28	2.12	2.64	1.07	0.04
hem	0.00	0.00	0.00	1.20	0.00	0.00	0.00	0.00	0.00	0.00	0.00	1.01
ap	0.58	1.86	0.80	0.05	0.50	0.47	1.58	1.43	1.43	1.42	0.35	0.21
ru	0.00	0.00	0.00	0.00	0.00	0.00	0.00	0.00	0.00	0.00	0.00	0.06
Pb	9	10										
Cu	7	15										
Co	50	49										
Ni	99	74	5	14	52	54	8	19	6	52	31	9
Cr	339	149	303	439	495	442	332	418	260	304	469	268
Ce	63	132										
V	229	213	60	19	159	206	74	69	65	172	65	16
La	23	46										
Ba	730	2107	1672	984	841	325	2179	1395	2070	1485	675	1830
Nb	15	10										
Zr	176	340	652	237	219	195	462	467	579	296	225	72
Y	34	30	65	30	42	36	52	56	60	28	53	32
Sr	422	1156	337	116	196	166	557	507	549	650	280	502
Rb	53	83	99	86	69	27	86	80	93	23	121	111
U	18	18										
Th	17	17										
Ga	20	19	21	24	21	18	20	21	22	21	22	19
Zn	133	105										

SAMPLE	DEL03-2*	DEL03-3*	DEL03-3B*	DEL03-3C*	DEL03-3D*	DEL04-5*	DEL05-3B2*	FC04-1A*	FC04-1B*	FC04-2*	H03-1*	H03-2*
Quadrangle	**e**	**e**	**e**	**e**	**e**	**e**	**e**	**h**	**h**	**h**	**e**	**e**
Lithology	**5**	**4**	**4**	**4**	**4**	**1**	**4**	**1**	**1**	**1**	**1**	**1**
SiO2	68.06	47.15	44.15	43.88	44.52	68.85	46.77	53.26	69.96	67.25	76.20	71.16
TiO2	0.88	2.19	2.65	2.80	2.79	0.33	1.83	3.52	0.66	0.54	0.67	0.40
Al2O3	14.54	14.26	14.28	14.33	13.59	16.32	14.15	13.87	15.54	16.13	12.31	15.54
MnO	0.09	0.24	0.30	0.31	0.32	0.04	0.20	0.14	0.08	0.07	0.06	0.05
FeO	5.50	13.74	16.34	16.97	15.41	2.84	15.20	11.01	4.03	3.70	3.68	2.77
MgO	1.70	7.24	7.07	6.65	7.54	0.82	6.02	3.79	1.03	1.37	1.34	0.46
CaO	1.49	11.46	12.53	12.53	12.67	3.03	13.07	6.69	1.68	3.34	1.10	4.20
Na2O	1.93	2.94	2.26	2.06	2.28	4.28	2.51	2.43	2.50	3.40	1.41	4.50
K2O	5.61	0.55	0.08	0.11	0.54	3.32	0.07	3.29	4.45	4.02	3.07	0.80
P2O5	0.19	0.23	0.35	0.36	0.33	0.16	0.18	1.99	0.07	0.17	0.17	0.13
LOI	3.04	0.13	0.75	0.92	1.53	0.66	1.29	2.90	0.00	0.32	2.91	1.83
TOTAL	100.00	100.00	100.00	100.00	100.00	100.00	100.00	100.00	100.07	100.00	100.00	100.00
%AN	27.49	51.26	61.75	62.93	62.52	27.83	56.10	45.60	27.09	34.94	26.80	34.31
Q	28.80	0.00	0.00	0.00	0.00	23.86	0.00	11.79	32.91	22.88	52.15	32.61
or	33.10	3.23	0.48	0.67	3.16	19.60	0.42	19.37	26.22	23.70	18.11	4.70
ab	16.29	22.84	17.64	17.33	15.08	36.17	21.14	20.45	21.10	28.75	11.88	37.97
an	6.18	24.02	28.47	29.42	25.15	13.95	27.01	17.14	7.84	15.44	4.35	19.83
ne	0.00	1.05	0.75	0.00	2.25	0.00	0.03	0.00	0.00	0.00	0.00	0.00
C	3.01	0.00	0.00	0.00	0.00	0.56	0.00	0.00	3.73	0.50	5.06	0.00
di	0.00	25.44	25.67	24.94	28.90	0.00	30.32	2.34	0.00	0.00	0.00	0.07
hy	6.99	0.00	0.00	0.85	0.00	2.20	0.00	10.33	3.65	4.33	3.58	1.11
ol	0.00	13.39	15.14	14.43	13.17	0.00	12.32	0.00	0.00	0.00	0.00	0.00
mt	3.53	5.36	6.04	6.26	6.26	2.67	4.88	7.34	3.14	2.97	3.22	2.33
il	1.67	4.14	5.01	5.29	5.27	0.63	3.47	6.66	1.26	1.03	1.27	0.76
hem	0.00	0.00	0.00	0.00	0.00	0.00	0.00	0.00	0.00	0.00	0.00	0.32
ap	0.43	0.54	0.80	0.83	0.76	0.37	0.40	4.59	0.16	0.40	0.38	0.31
ru	0.00	0.00	0.00	0.00	0.00	0.00	0.00	0.00	0.00	0.00	0.00	0.00
Pb												
Cu												
Co												
Ni	21	47	64	53	55	11	48	14	17	9	31	6
Cr	126	453	455	417	313	196	405	126	420	166	351	299
Ce												
V	90	365	355	340	407	48	291	227	51	62	64	56
La												
Ba	1304	243	174	221	217	1580	170	3276	1169	1880	725	278
Nb												
Zr	293	134	184	212	169	185	108	492	206	187	273	198
Y	59	30	40	43	38	31	34	40	47	36	53	26
Sr	215	127	70	68	81	918	141	755	342	600	143	651
Rb	153	12	6	8	8	73	6	49	95	86	111	40
U												
Th												
Ga	21	17	16	16	18	22	16	19	20	21	20	25
Zn												

SAMPLE	H03-4B*	H03-4D*	H03-4E*	HM03-2*	HM03-3*	HM03-4*	HM03-5A*	HM03-5B*	JUN04-1A*	MLL04-1A*	MLL04-1B*	MLL04-1C*
Quadrangle	e	e	e	f	f	f	f	f	f	i	i	i
Lithology	4	4	4	5	1	1	4	1	1	5	5	3
SiO2	50.96	47.99	49.63	71.71	64.84	73.29	50.98	75.27	54.56	62.26	58.31	57.10
TiO2	2.75	2.73	2.91	0.37	0.92	0.15	0.82	0.29	1.48	1.04	0.92	1.92
Al2O3	15.50	17.17	17.52	14.98	16.29	15.78	15.12	13.48	16.61	16.71	19.77	15.55
MnO	0.24	0.22	0.27	0.06	0.07	0.02	0.23	0.04	0.22	0.08	0.09	0.13
FeO	13.42	13.69	13.22	2.90	5.90	1.15	10.05	1.97	10.06	5.99	6.22	9.80
MgO	3.62	4.20	3.33	0.84	1.77	0.35	9.62	0.66	5.68	3.03	2.74	3.95
CaO	9.48	9.68	8.74	3.23	4.57	2.63	9.49	3.52	7.57	4.47	4.63	5.90
Na2O	2.50	3.11	3.16	3.54	3.29	4.69	1.87	4.35	2.33	3.53	4.41	2.87
K2O	0.59	0.49	0.45	2.24	2.00	1.88	1.62	0.38	1.28	2.65	2.70	2.47
P2O5	0.95	0.72	0.77	0.13	0.34	0.05	0.20	0.04	0.22	0.23	0.23	0.30
LOI	1.16	2.18	2.43	0.69	1.85	0.55	3.08	0.00	1.69	2.55	0.00	2.23
TOTAL	100.00	100.00	100.00	100.00	100.00	100.00	100.00	101.68	100.00	100.00	100.10	100.00
%AN	58.16	54.42	54.70	33.66	42.37	24.25	64.00	30.50	61.13	40.92	36.52	47.75
Q	9.12	0.84	5.24	34.63	24.97	32.74	0.00	40.27	9.03	16.69	7.16	11.36
or	3.44	2.87	2.63	13.23	11.79	11.11	9.53	2.27	7.51	15.65	15.89	14.55
ab	21.02	26.23	26.63	29.86	27.79	39.66	15.77	36.72	19.70	29.82	37.19	24.24
an	29.23	31.31	32.16	15.15	20.43	12.69	28.03	16.12	30.98	20.65	21.39	22.15
ne	0.00	0.00	0.00	0.00	0.00	0.00	0.00	0.00	0.00	0.00	0.00	0.00
C	0.00	0.00	0.00	1.17	1.20	1.36	0.00	0.00	0.00	0.44	1.74	0.00
di	9.45	9.81	4.96	0.00	0.00	0.00	14.30	0.82	4.12	0.00	0.00	4.15
hy	14.15	15.93	14.64	2.22	7.74	0.88	22.57	1.26	21.00	10.51	10.86	14.21
ol	0.00	0.00	0.00	0.00	0.00	0.00	4.34	0.00	0.00	0.00	0.00	0.00
mt	6.20	6.19	6.46	2.73	3.56	0.00	3.46	0.53	4.37	3.75	3.51	5.02
il	5.20	5.16	5.51	0.71	1.75	0.04	1.56	0.54	2.80	1.98	1.73	3.64
hem	0.00	0.00	0.00	0.00	0.00	1.28	0.00	1.40	0.00	0.00	0.00	0.00
ap	2.20	1.65	1.78	0.30	0.78	0.12	0.46	0.09	0.50	0.53	0.53	0.69
ru	0.00	0.00	0.00	0.00	0.00	0.13	0.00	0.00	0.00	0.00	0.00	0.00
Pb												
Cu												
Co												
Ni	21	18	11	17	16	10	177	5	54	47	35	32
Cr	281	80	106	250	297	145	620	304	295	289	217	240
Ce												
V	203	209	198	49	99	16	156	38	223	111	103	158
La												
Ba	257	234	310	1709	1120	404	513	202	278	501	569	538
Nb												
Zr	297	229	245	236	330	147	115	103	169	201	269	149
Y	34	28	31	27	35	18	26	14	40	37	46	33
Sr	389	486	460	675	440	738	298	687	129	353	507	298
Rb	10	10	6	53	85	43	27	12	30	89	85	61
U												
Th												
Ga	20	20	20	21	20	24	18	20	20	21	23	19
Zn												

SAMPLE	MP04-2*	MV02-2*	MV02-3*	MV02-4A*	MV02-6B*	MV02-6HB*	MV02-7*	MV02-8*	NB04-1B*	OS03-1B*	OS03-1GN*	PK03-1*
Quadrangle	j	e	e	e	e	e	e	e	e	g	g	e
Lithology	1	5	1	2	5	2	1	1	1	1	1	2
SiO2	63.63	65.66	64.57	65.89	75.02	52.41	68.29	65.37	65.79	73.03	71.57	64.51
TiO2	1.30	0.94	0.72	0.67	0.27	0.39	0.89	0.74	0.70	0.18	0.40	0.56
Al2O3	15.32	15.51	16.84	16.45	13.39	17.45	15.63	16.40	16.21	15.09	14.51	18.11
MnO	0.12	0.08	0.09	0.08	0.04	0.16	0.11	0.09	0.10	0.02	0.05	0.06
FeO	6.24	6.01	4.77	4.43	1.78	7.74	5.84	4.45	4.62	1.41	3.10	4.35
MgO	1.38	2.68	1.80	1.41	0.54	9.44	1.84	1.64	1.79	0.28	0.74	0.91
CaO	4.48	3.26	3.66	3.41	2.65	7.04	1.71	3.72	4.05	1.61	1.85	3.50
Na2O	3.21	3.04	3.79	3.33	2.67	2.18	1.93	3.71	3.66	3.44	3.34	3.02
K2O	3.69	2.69	3.50	4.13	3.57	3.09	3.55	3.61	2.84	4.86	4.27	4.72
P2O5	0.64	0.12	0.25	0.21	0.07	0.08	0.21	0.26	0.24	0.08	0.16	0.26
LOI	1.44	0.00	2.40	3.55	0.92	1.20	4.33	0.35	0.26	1.94	1.41	2.58
TOTAL	100.00	100.28	100.00	100.00	100.00	100.00	100.00	100.00	100.00	100.00	100.00	100.00
%AN	37.80	37.43	34.00	35.52	35.95	60.81	30.45	34.78	37.43	20.42	22.34	37.98
Q	20.13	25.35	18.29	21.10	39.49	0.00	36.10	19.53	21.99	30.73	30.96	19.80
or	21.74	15.86	20.65	24.33	21.06	18.24	20.90	21.28	16.76	28.68	25.21	27.86
ab	27.07	25.67	32.00	28.15	22.55	18.45	16.25	31.33	30.88	29.07	28.20	25.52
an	16.45	15.36	16.49	15.51	12.66	28.63	7.12	16.71	18.48	7.46	8.11	15.63
ne	0.00	0.00	0.00	0.00	0.00	0.00	0.00	0.00	0.00	0.00	0.00	0.00
C	0.00	1.95	0.76	0.80	0.48	0.00	6.00	0.26	0.33	1.43	1.41	2.28
di	1.23	0.00	0.00	0.00	0.00	4.59	0.00	0.00	0.00	0.00	0.00	0.00
hy	5.35	10.22	6.61	5.15	1.33	16.13	7.88	5.64	6.50	0.69	2.20	4.22
ol	0.00	0.00	0.00	0.00	0.00	10.26	0.00	0.00	0.00	0.00	0.00	0.00
mt	4.09	3.54	3.28	3.23	0.00	2.78	3.58	3.25	3.19	0.00	2.78	3.04
il	2.46	1.79	1.37	1.26	0.45	0.74	1.69	1.39	1.32	0.04	0.75	1.06
hem	0.00	0.00	0.00	0.00	1.79	0.00	0.00	0.00	0.00	1.56	0.00	0.00
ap	1.49	0.28	0.57	0.48	0.16	0.19	0.49	0.61	0.56	0.19	0.38	0.60
ru	0.00	0.00	0.00	0.00	0.04	0.00	0.00	0.00	0.00	0.16	0.00	0.00
Pb												
Cu												
Co												
Ni	3	89	8	9	10	279	27	12	9	6	13	9
Cr	199	403	184	187	238	654	334	178	104	238	500	379
Ce												
V	65	123	72	65	27	84	91	71	80	18	38	52
La												
Ba	1467	957	1384	1765	1666	443	879	1570	827	1512	1326	3589
Nb												
Zr	472	223	267	226	176	91	302	252	189	133	238	320
Y	59	37	37	38	24	28	55	38	44	27	35	40
Sr	559	432	562	608	577	426	203	595	478	554	446	545
Rb	92	82	101	113	55	74	111	97	89	87	93	92
U												
Th												
Ga	22	20	20	20	19	18	22	20	22	21	21	21
Zn												

SAMPLE	PK03-2*	PK03-5*	PR04-1*	SC04-1*	SC04-2*	SC04-3*	SC04-4*	SC04-5*	SC04-6*
Quadrangle	e	e	e	e	e	e	e	e	e
Lithology	1	1	1	1	1	1	1	1	1
SiO2	69.60	68.55	67.43	74.89	70.70	71.51	69.33	72.32	68.74
TiO2	0.41	0.66	0.70	0.21	0.43	0.46	0.49	0.38	0.59
Al2O3	14.79	15.43	16.31	12.94	14.63	14.51	15.91	14.77	15.67
MnO	0.06	0.09	0.08	0.04	0.06	0.06	0.05	0.05	0.06
FeO	3.67	3.97	3.34	2.38	2.78	2.81	3.60	3.36	3.38
MgO	0.95	1.37	0.67	0.42	1.04	0.83	1.24	1.22	1.26
CaO	2.97	2.35	3.33	1.37	2.61	2.49	2.61	4.15	2.21
Na2O	2.42	3.66	3.52	2.25	3.46	3.57	2.80	3.17	3.09
K2O	4.97	3.70	4.33	5.42	4.16	3.61	3.77	0.44	4.80
P2O5	0.14	0.20	0.28	0.07	0.12	0.15	0.20	0.14	0.20
LOI	2.12	1.78	3.08	0.68	0.48	1.70	2.58	0.15	2.82
TOTAL	100.00	100.00	100.00	100.00	100.00	100.00	100.00	100.00	100.00
%AN	40.29	25.01	33.06	25.00	29.25	27.31	32.95	42.34	27.04
Q	28.46	26.12	22.98	37.61	27.81	30.72	31.28	41.38	26.26
or	29.29	21.82	25.52	31.98	24.56	21.30	22.24	2.61	28.32
ab	20.45	30.91	29.72	19.02	29.20	30.16	23.67	26.75	26.08
an	13.79	10.31	14.68	6.34	12.07	11.33	11.63	19.64	9.66
ne	0.00	0.00	0.00	0.00	0.00	0.00	0.00	0.00	0.00
C	0.37	1.61	0.44	1.04	0.00	0.56	2.94	1.86	1.84
di	0.00	0.00	0.00	0.00	0.05	0.00	0.00	0.00	0.00
hy	3.72	4.33	1.67	1.05	2.56	2.05	3.90	3.98	3.19
ol	0.00	0.00	0.00	0.00	0.00	0.00	0.00	0.00	0.00
mt	2.82	3.18	2.46	2.18	2.27	2.15	2.95	2.74	3.09
il	0.78	1.26	1.33	0.40	0.82	0.87	0.94	0.72	1.12
hem	0.00	0.00	0.56	0.22	0.38	0.50	0.00	0.00	0.00
ap	0.33	0.47	0.65	0.16	0.28	0.35	0.45	0.33	0.45
ru	0.00	0.00	0.00	0.00	0.00	0.00	0.00	0.00	0.00
Pb									
Cu									
Co									
Ni	11	6	1	28	9	6	24	18	10
Cr	246	149	152	953	237	164	225	235	170
Ce									
V	47	68	33	31	42	42	61	48	51
La									
Ba	2208	1114	1611	1233	692	880	1010	405	1990
Nb									
Zr	188	223	438	156	160	204	190	200	225
Y	53	46	54	32	42	38	36	20	37
Sr	557	445	752	354	401	415	428	698	609
Rb	93	121	118	126	112	85	107	23	86
U									
Th									
Ga	19	22	23	19	21	21	22	21	21
Zn									

APPENDIX C

U-Pb Zircon Geochronology

The following U-Pb zircon geochronologic analyses were carried out at the Keck Lab, University of California at Los Angeles.

U-Pb Geochronologic Analyses

DEL08-7a					Isotope ratios							Apparent ages (Ma)							
Analysis	U (ppm)	206Pb 204Pb	U/Th	Th/U	206Pb* 207Pb*	± (%)	207Pb* 235U*	± (%)	206Pb* 238U	± (%)	error corr.	206Pb* 238U*	± (Ma)	207Pb* 235U	± (Ma)	206Pb* 207Pb*	± (Ma)	Best age (Ma)	± (Ma)
DEL08-7a-1	300	136407	3.1	0.32	11.4626	12.3	2.8660	6.7	0.2382	6.8	0.99	1378.0	83.7	1373.0	50.7	1366.0	17.9	1366.0	17.9
DEL08-7a-2	530	28385	3.6	0.28	11.8133	25.5	2.6750	7.0	0.2292	7.0	1.00	1330.0	83.7	1321.0	51.5	1307.0	9.0	1307.0	9.0
DEL08-7a-4	540	28353	2.1	0.47	12.5408	15.5	2.1950	6.7	0.1997	6.7	0.99	1174.0	71.9	1180.0	46.4	1191.0	16.0	1191.0	16.0
DEL08-7a-5	480	92507	2.0	0.51	11.7550	17.6	2.6390	6.7	0.2250	6.7	1.00	1308.0	78.9	1311.0	49.3	1317.0	13.0	1317.0	13.0
DEL08-7a-6c	610	72098	1.5	0.66	11.9190	14.3	2.5340	6.2	0.2190	6.3	0.99	1277.0	72.7	1282.0	45.4	1290.0	16.2	1290.0	16.2
DEL08-7a-6r	590	30941	2.4	0.41	12.6791	18.0	2.1080	5.7	0.1939	5.6	0.99	1142.0	58.4	1152.0	39.5	1169.0	14.0	1169.0	14.0
DEL08-7a-7	510	48948	1.8	0.57	12.0700	11.9	2.4280	6.1	0.2125	6.0	0.99	1242.0	67.9	1251.0	43.9	1266.0	19.7	1266.0	19.7
DEL08-7a-8	440	7418	2.1	0.48	11.6959	13.8	2.6220	5.8	0.2224	5.7	0.99	1295.0	67.2	1307.0	42.4	1327.0	16.4	1327.0	16.4
DEL08-7a-9	520	69979	1.4	0.73	12.1477	19.6	2.5040	6.4	0.2206	6.3	1.00	1285.0	73.6	1273.0	46.4	1253.0	12.1	1253.0	12.1
DEL08-7a-11	330	61013	1.8	0.55	12.3411	15.9	1.9480	6.1	0.1743	6.2	0.99	1036.0	59.2	1098.0	40.7	1222.0	15.3	1222.0	15.3
DEL08-7a-12	460	5959	1.9	0.53	12.0453	14.4	2.4740	6.1	0.2161	6.1	0.99	1261.0	69.4	1264.0	44.1	1270.0	16.4	1270.0	16.4

DEL08-7j					Isotope ratios							Apparent ages (Ma)							
Analysis	U (ppm)	206Pb 204Pb	U/Th	Th/U	206Pb* 207Pb*	± (%)	207Pb* 235U*	± (%)	206Pb* 238U	± (%)	error corr.	206Pb* 238U*	± (Ma)	207Pb* 235U	± (Ma)	206Pb* 207Pb*	± (Ma)	Best age (Ma)	± (Ma)
DEL08-7j-1	530	46447	1.3	0.77	11.5888	19.2	2.7060	5.5	0.2275	5.4	0.99	1321.0	64.5	1330.0	41.1	1345.0	11.6	1345.0	11.6
DEL08-7j-2	320	32206	2.0	0.49	12.7796	10.9	2.0620	5.3	0.1911	5.1	0.98	1128.0	52.7	1136.0	36.5	1153.0	23.3	1153.0	23.3
DEL08-7j-3	230	1617	2.0	0.51	12.8601	5.5	1.9480	6.2	0.1817	5.4	0.93	1076.0	53.4	1098.0	41.5	1141.0	46.8	1141.0	46.8
DEL08-7j-4	660	16565	1.3	0.76	12.6887	17.2	2.1030	5.9	0.1935	5.8	0.99	1141.0	60.5	1150.0	40.4	1167.0	14.6	1167.0	14.6
DEL08-7j-5	510	15528	1.7	0.59	12.5156	14.3	2.1250	5.6	0.1929	5.6	0.99	1137.0	58.3	1157.0	38.6	1195.0	17.2	1195.0	17.2
DEL08-7j-8	520	4606	1.5	0.66	11.8779	10.2	2.5470	5.9	0.2194	5.9	0.98	1279.0	68.5	1286.0	42.7	1297.0	22.7	1297.0	22.7
DEL08-7j-9	840	229938	1.0	0.96	12.2026	24.2	2.4330	5.6	0.2153	5.6	1.00	1257.0	63.5	1252.0	40.1	1244.0	9.9	1244.0	9.9
DEL08-7j-10	670	43840	1.2	0.86	11.8807	19.1	2.5480	5.4	0.2196	5.3	0.99	1280.0	61.2	1286.0	39.1	1297.0	12.1	1297.0	12.1
DEL08-7j-12	670	6109	3.0	0.33	13.7988	11.8	1.4910	5.4	0.1492	5.3	0.98	896.6	44.0	926.8	32.7	999.2	23.7	896.6	44.0
DEL08-7j-13	510	24728	1.7	0.59	12.7275	11.3	2.1540	6.1	0.1988	5.9	0.98	1169.0	62.7	1166.0	42.0	1161.0	22.3	1161.0	22.3

U-Pb Geochronologic Analyses

DEL09-16b					Isotope ratios							Apparent ages (Ma)							
Analysis	U (ppm)	206Pb 204Pb	U/Th	Th/U	206Pb* 207Pb*	± (%)	207Pb* 235U*	± (%)	206Pb* 238U	± (%)	error corr.	206Pb* 238U*	± (Ma)	207Pb* 235U	± (Ma)	206Pb* 207Pb*	± (Ma)	Best age (Ma)	± (Ma)
DEL09-16b-1	480	14422	55.6	0.02	13.4844	10.6	1.8460	5.8	0.1805	5.7	0.98	1070.0	56.6	1062.0	38.1	1046.0	25.8	1046.0	25.8
DEL09-16b-2	280	9042	2.4	0.41	13.0310	10.5	1.9230	5.5	0.1817	5.5	0.97	1077.0	54.1	1089.0	36.9	1114.0	24.8	1114.0	24.8
DEL09-16b-3	340	10407	2.9	0.35	12.7779	11.1	2.1000	5.8	0.1946	5.6	0.98	1146.0	59.3	1149.0	39.8	1153.0	22.8	1153.0	22.8
DEL09-16b-4	910	56593	1.9	0.52	12.9383	17.7	2.1080	6.4	0.1978	6.4	0.99	1163.0	67.8	1151.0	43.9	1129.0	14.6	1129.0	14.6
DEL09-16b-6	400	8361	2.0	0.49	13.4789	9.9	1.7740	5.7	0.1734	5.4	0.97	1031.0	51.8	1036.0	36.7	1047.0	27.6	1047.0	27.6
DEL09-16b-8	660	25432	28.6	0.04	12.7437	14.1	2.1760	5.7	0.2011	5.6	0.99	1181.0	60.4	1173.0	39.8	1159.0	17.9	1159.0	17.9
DEL09-16b-9	620	21716	2.3	0.43	13.1891	14.2	1.9760	5.9	0.1890	5.7	0.99	1116.0	58.5	1107.0	39.6	1090.0	18.5	1090.0	18.5
DEL09-16b-10	590	14403	2.5	0.40	14.0706	17.9	1.6060	5.6	0.1639	5.6	0.99	978.2	50.4	972.5	35.3	959.4	16.1	978.2	50.4
DEL09-16b-11	480	37106	3.4	0.29	12.6024	22.1	2.1770	5.7	0.1990	5.7	1.00	1170.0	60.9	1174.0	39.9	1181.0	11.3	1181.0	11.3
DEL09-16b-12	530	32765	2.3	0.44	12.8189	18.5	2.1630	5.9	0.2011	5.9	0.99	1181.0	63.8	1169.0	40.8	1147.0	13.8	1147.0	13.8

DEL09-17d					Isotope ratios							Apparent ages (Ma)							
Analysis	U (ppm)	206Pb 204Pb	U/Th	Th/U	206Pb* 207Pb*	± (%)	207Pb* 235U*	± (%)	206Pb* 238U	± (%)	error corr.	206Pb* 238U*	± (Ma)	207Pb* 235U	± (Ma)	206Pb* 207Pb*	± (Ma)	Best age (Ma)	± (Ma)
DEL09-17d-1	60	4415	0.3	3.40	13.8160	3.5	1.7470	7.3	0.1750	6.6	0.85	1040.0	63.2	1026.0	47.4	996.5	79.9	1040.0	63.2
DEL09-17d-2	50	3207	0.4	2.50	13.7646	3.0	1.8240	9.5	0.1820	8.0	0.88	1078.0	79.6	1054.0	62.2	1004.0	92.5	1004.0	92.5
DEL09-17d-3	280	121007	4.8	0.21	13.4246	13.7	1.8380	6.2	0.1790	5.9	0.99	1061.0	57.9	1059.0	40.8	1055.0	19.8	1055.0	19.8
DEL09-17d-4	30	1397	0.3	3.10	11.7123	1.5	1.9140	10.6	0.1626	7.6	0.66	971.2	68.8	1086.0	70.8	1324.0	154.0	1324.0	154.0
DEL09-17d-6	50	3948	0.4	2.80	14.3575	3.9	1.6590	8.9	0.1727	7.3	0.91	1027.0	68.9	992.9	56.2	918.0	75.9	1027.0	68.9
DEL09-17d-7	40	4274	0.4	2.80	13.4354	3.0	1.9200	8.8	0.1871	7.3	0.86	1106.0	74.2	1088.0	58.8	1053.0	89.5	1053.0	89.5
DEL09-17d-8	50	3047	0.4	2.70	13.8064	2.4	1.6860	12.6	0.1688	10.1	0.90	1006.0	94.1	1003.0	80.6	998.1	116.0	1006.0	94.1
DEL09-17d-9	160	7231	0.9	1.10	13.8255	6.1	1.7200	6.3	0.1725	6.0	0.93	1026.0	56.4	1016.0	40.1	995.3	46.2	1026.0	56.4
DEL09-17d-10	2,100	59347	3.1	0.32	12.7340	31.7	2.1970	5.6	0.2029	5.6	1.00	1191.0	60.6	1180.0	39.2	1160.0	8.0	1160.0	8.0
DEL09-17d-11c	790	32415	6.7	0.15	13.5740	18.3	1.7550	5.6	0.1728	5.6	0.99	1027.0	52.9	1029.0	36.4	1032.0	14.9	1032.0	14.9
DEL09-17d-11r	140	17553	1.0	1.00	13.3869	8.0	1.8710	6.8	0.1817	6.5	0.97	1076.0	64.5	1071.0	44.7	1060.0	33.7	1060.0	33.7
DEL09-17d-12	270	11137	2.9	0.34	13.5538	10.8	1.8320	5.7	0.1801	5.6	0.98	1067.0	54.6	1057.0	37.5	1035.0	25.4	1035.0	25.4
DEL09-17d-13	580	37665	1.5	0.66	12.6662	13.8	2.1590	5.9	0.1984	5.6	0.99	1166.0	60.1	1168.0	40.8	1171.0	18.2	1171.0	18.2

U-Pb Geochronologic Analyses

DEL08-6c					Isotope ratios							Apparent ages (Ma)							
Analysis	U (ppm)	206Pb 204Pb	U/Th	Th/U	206Pb* 207Pb*	± (%)	207Pb* 235U*	± (%)	206Pb* 238U	± (%)	error corr.	206Pb* 238U*	± (Ma)	207Pb* 235U	± (Ma)	206Pb* 207Pb*	± (Ma)	Best age (Ma)	± (Ma)
DEL08-6c-1	790	18430	1.3	0.75	11.777	39.5	2.6880	6.2	0.2296	6.3	1.00	1332.0	75.3	1325.0	46.2	1313.0	5.8	1313.0	5.8
DEL08-6c-2	1,200	89445	55.6	0.02	12.695	21.7	2.4000	7.2	0.2210	7.2	1.00	1287.0	83.8	1243.0	51.6	1166.0	11.6	1166.0	11.6
DEL08-6c-3	220	80841	1.2	0.83	13.506	12.5	1.7400	6.2	0.1704	6.2	0.98	1015.0	58.3	1023.0	39.8	1042.0	21.9	1042.0	21.9
DEL08-6c-4	400	84317	2.0	0.49	12.022	15.2	2.5450	7.1	0.2219	6.9	0.99	1292.0	80.8	1285.0	51.6	1273.0	15.5	1273.0	15.5
DEL08-6c-5	360	7013	2.0	0.49	11.853	10.2	2.6940	7.1	0.2316	7.1	0.99	1343.0	86.4	1327.0	52.8	1301.0	22.6	1301.0	22.6
DEL08-6c-6	670	56948	5.9	0.17	12.739	31.5	2.0360	5.8	0.1882	5.8	1.00	1111.0	59.1	1128.0	39.5	1160.0	8.0	1160.0	8.0
DEL08-6c-7	520	290360	2.0	0.51	11.820	15.5	2.4400	6.7	0.2092	6.7	0.99	1225.0	74.9	1255.0	47.9	1306.0	14.8	1306.0	14.8
DEL08-6c-8	370	29949	3.7	0.27	12.677	14.0	2.0370	7.1	0.1873	7.0	0.99	1107.0	71.4	1128.0	48.3	1169.0	17.9	1169.0	17.9
DEL08-6c-9	860	53390	6.7	0.15	12.438	19.2	2.1190	5.9	0.1912	5.9	0.99	1128.0	60.7	1155.0	40.8	1207.0	12.7	1207.0	12.7
DEL08-6c-10	2,100	867	3.0	0.33	13.335	10.2	1.2410	6.6	0.1200	6.5	0.98	730.8	44.9	819.4	36.9	1068.0	26.3	1068.0	26.3

DEL09-19a					Isotope ratios							Apparent ages (Ma)							
Analysis	U (ppm)	206Pb 204Pb	U/Th	Th/U	206Pb* 207Pb*	± (%)	207Pb* 235U*	± (%)	206Pb* 238U	± (%)	error corr.	206Pb* 238U*	± (Ma)	207Pb* 235U	± (Ma)	206Pb* 207Pb*	± (Ma)	Best age (Ma)	± (Ma)
DEL09-19a-2	2,400	21973	3.2	0.31	13.6129	45.9	1.3060	4.7	0.1289	4.7	1.00	781.8	34.8	848.4	27.2	1027.0	6.0	1027.0	6.0
DEL09-19a-3	1,200	62775	4.2	0.24	13.9938	20.0	1.5210	5.4	0.1543	5.3	0.99	925.3	46.0	938.8	33.2	970.6	14.2	925.3	46.0
DEL09-19a-4	340	6693	41.7	0.02	18.5322	6.7	0.5545	6.9	0.0745	6.0	0.92	463.4	26.6	447.9	25.0	369.2	62.6	463.4	26.6
DEL09-19a-5	1,800	39651	11.5	0.09	12.8370	29.7	2.0260	5.7	0.1886	5.7	1.00	1114.0	58.6	1124.0	38.6	1144.0	8.6	1144.0	8.6
DEL09-19a-6	1,400	90090	0.5	2.00	12.7113	23.1	2.1340	5.6	0.1967	5.5	1.00	1158.0	58.6	1160.0	39.0	1164.0	10.9	1164.0	10.9
DEL09-19a-9	700	177873	0.7	1.40	13.4571	19.2	1.7890	5.8	0.1746	5.7	0.99	1037.0	54.7	1041.0	37.5	1050.0	14.1	1050.0	14.1
DEL09-19a-10	2,100	117592	13.0	0.08	12.7698	28.5	2.1090	5.5	0.1953	5.5	1.00	1150.0	58.2	1152.0	38.1	1155.0	8.9	1155.0	8.9
DEL09-19a-11	2,000	37908	14.1	0.07	13.8485	46.5	1.6010	5.4	0.1608	5.4	1.00	961.5	48.3	970.7	33.8	991.7	6.1	961.5	48.3
DEL09-19a-12	1,100	144051	2.8	0.36	12.6968	23.4	2.1010	5.6	0.1934	5.5	1.00	1140.0	57.1	1149.0	38.4	1166.0	10.7	1166.0	10.7

U-Pb Geochronologic Analyses

DEL08-10a					Isotope ratios							Apparent ages (Ma)							
Analysis	U (ppm)	206Pb 204Pb	U/Th	Th/U	206Pb* 207Pb*	± (%)	207Pb* 235U*	± (%)	206Pb* 238U	± (%)	error corr.	206Pb* 238U*	± (Ma)	207Pb* 235U	± (Ma)	206Pb* 207Pb*	± (Ma)	Best age (Ma)	± (Ma)
DEL08-10a-1	70	433	0.6	1.70	13.019	1.3	1.2050	11.7	0.1138	5.4	0.56	694.6	35.7	802.9	64.8	1116.0	194.0	1116.0	194.0
DEL08-10a-2	590	55249	1.1	0.92	11.729	17.0	2.7050	5.7	0.2301	5.7	0.99	1335.0	68.3	1330.0	42.5	1321.0	13.3	1321.0	13.3
DEL08-10a-3	340	12952	6.3	0.16	12.702	10.6	2.1240	5.2	0.1956	5.1	0.97	1152.0	54.1	1157.0	36.0	1165.0	23.7	1165.0	23.7
DEL08-10a-5	1,800	222767	2.6	0.38	13.396	47.6	1.8290	5.8	0.1777	5.8	1.00	1054.0	56.1	1056.0	37.9	1059.0	5.7	1059.0	5.7
DEL08-10a-6	810	3187	10.6	0.09	13.330	10.0	1.6220	5.5	0.1568	5.4	0.97	938.9	46.8	978.7	34.8	1069.0	26.7	1069.0	26.7
DEL08-10a-8	700	18755	1.5	0.65	12.093	16.7	2.3090	5.3	0.2025	5.3	0.99	1189.0	57.1	1215.0	37.4	1262.0	14.2	1262.0	14.2
DEL08-10a-9	210	6780	2.3	0.43	12.026	8.1	2.4890	5.7	0.2171	5.6	0.96	1266.0	64.3	1269.0	41.1	1273.0	29.2	1273.0	29.2
DEL08-10a-10	1,400	4706	0.6	1.70	11.930	17.5	2.6080	5.8	0.2257	5.7	0.99	1312.0	67.8	1303.0	42.5	1288.0	13.3	1288.0	13.3
DEL08-10a-11	300	4941	1.4	0.71	11.895	7.4	2.5240	5.9	0.2178	5.6	0.96	1270.0	65.0	1279.0	43.2	1294.0	31.4	1294.0	31.4

DEL08-2d					Isotope ratios							Apparent ages (Ma)							
Analysis	U (ppm)	206Pb 204Pb	U/Th	Th/U	206Pb* 207Pb*	± (%)	207Pb* 235U*	± (%)	206Pb* 238U	± (%)	error corr.	206Pb* 238U*	± (Ma)	207Pb* 235U	± (Ma)	206Pb* 207Pb*	± (Ma)	Best age (Ma)	± (Ma)
DEL08-2d-1	540	374813	3.1	0.32	13.935	17.3	1.6310	5.4	0.1648	5.3	0.99	983.4	48.7	982.1	33.7	979.1	16.4	983.4	48.7
DEL08-2d-2	400	24402	4.5	0.22	13.450	11.1	1.7670	6.0	0.1723	5.8	0.98	1025.0	55.0	1033.0	39.0	1051.0	24.4	1051.0	24.4
DEL08-2d-3	330	108155	1.3	0.78	13.761	25.8	1.7250	7.7	0.1722	8.0	1.00	1024.0	75.4	1018.0	49.7	1005.0	10.8	1005.0	10.8
DEL08-2d-4	180	7457	2.9	0.34	13.663	7.1	1.7720	6.7	0.1756	6.7	0.96	1043.0	64.3	1035.0	43.6	1019.0	38.8	1019.0	38.8
DEL08-2d-5	110	28433	0.8	1.30	13.669	7.1	1.8410	6.4	0.1826	6.3	0.95	1081.0	62.8	1060.0	41.8	1018.0	38.8	1018.0	38.8
DEL08-2d-6	290	65274	1.8	0.56	12.4486	11.8	2.4250	6.8	0.2189	6.5	0.99	1276.0	75.1	1250.0	48.7	1205.0	20.8	1205.0	20.8
DEL08-2d-7	110	28571	1.6	0.62	13.7155	8.6	1.7300	6.5	0.1721	6.3	0.97	1023.0	59.2	1020.0	41.7	1012.0	32.4	1012.0	32.4
DEL08-2d-8	220	15513	2.8	0.36	12.6438	9.2	2.1820	5.5	0.2001	5.4	0.97	1176.0	58.1	1175.0	38.5	1174.0	27.4	1174.0	27.4
DEL08-2d-10	530	147297	2.3	0.43	13.180	16.0	1.9990	6.3	0.1911	6.3	0.99	1127.0	65.3	1115.0	42.3	1092.0	16.5	1092.0	16.5
DEL08-2d-11	350	14436	3.7	0.27	14.436	11.9	1.4860	6.1	0.1555	6.0	0.98	932.0	52.5	924.5	36.7	906.8	25.0	932.0	52.5
DEL08-2d-12	330	5341880	2.3	0.43	13.156	14.3	1.7300	5.6	0.1650	5.5	0.99	984.7	49.9	1020.0	35.8	1095.0	18.4	1095.0	18.4
DEL08-2d-13	150	19128	1.4	0.73	13.425	10.9	1.8320	5.9	0.1783	5.9	0.98	1058.0	57.9	1057.0	38.9	1055.0	24.9	1055.0	24.9
DEL08-2d-14	90	12749	1.5	0.67	12.962	5.2	1.9370	6.5	0.1821	6.7	0.93	1079.0	66.3	1094.0	43.5	1125.0	49.4	1125.0	49.4

SECTION XI. REFERENCES

Aleinikoff, J.N., Zartman, R.E., Walter, M., Rankin, D.W., Lyttle, P.T., and Burton, W.C., 1995, U-Pb ages of metarhyolites of the Catoctin and Mount Rogers Formations, central and southern Appalachians: evidence for two pulses of Iapetan rifting: American Journal of Science, v. 295, p. 428-454.

Anderson, E.D., and Moecher, D.P., 2008, Geochronology and geochemistry of basement rocks, Dellwood area, eastern Great Smoky Mountains, NC: Geological Society of America Abstracts with Programs, v. 40, p. 19.

—, 2009, Formation of high-pressure metabasites in the southern Appalachian Blue Ridge via Taconic continental subduction beneath the Laurentian margin: Tectonics, p. in press.

Berquist, P.J., Fisher, C.M., Miller, C.F., Wooden, J.L., Fullagar, P.D., and Loewy, S.L., 2005, Geochemistry and U-Pb zircon geochronology of Blue Ridge basement, western North Carolina and eastern Tennessee: Implications for tectonic assembly, *in* Hatcher, R.D., Jr., and Merschat, A.J., eds., Blue Ridge Geology Geotraverse East of the Great Smoky Mountains National Park, Western North Carolina: North Carolina Geological Survey, Carolina Geological Society Annual Field Trip Guidebook, p. 33-44.

Blatt, H., and Tracy, R.J., 1997, Petrology: Igneous, sedimentary, and metamorphic: New York, Freeman, 529 p.

Bream, B.R., 2003, Tectonic implications of geochronology and geochemistry of para- and orthogneisses from the southern Appalachian crystalline core [Ph.D. dissertation]: Knoxville, University of Tennessee.

Bream, B.R., Hatcher, R.D., Jr., Miller, C.F., and Fullagar, P.D., 2004, Detrital zircon ages and Nd isotopic data from the southern Appalachian crystalline core, GA-SC-NC-TN: New provenance constraints for part of the Laurentian margin, *in* Tollo, R.P., Corriveau, L., McLelland, J., and Bartholomew, M.J., eds., Proterozoic evolution of the Grenville orogen in North America: Boulder, Colorado, Geological Society of America Memoir 197, p. 459-475.

Carrigan, C.W., Miller, C.F., Fullagar, P.D., Bream, B.R., Hatcher, R.D., Jr., and Coath, C.D., 2003, Ion microprobe age and geochemistry of southern Appalachian basement, with implications for Proterozoic and Paleozoic reconstructions: Precambrian Research, v. 120, p. 1-36.

Cattanach, B.L., and Merschat, C.E., 2005, An overview of the Middle Proterozoic basement complex on the west half of the Asheville 1:100,000 scale geologic map, *in* Hatcher, R.D., Jr., and Merschat, A.J., eds., Blue Ridge Geology Geotraverse East of the Great Smoky Mountains National Park, Western North

Carolina: North Carolina Geological Survey, Carolina Geological Society Annual Field Trip Guidebook, p. 25-32.

Chakraborty, S., Moecher, D.P., and Samson, S.D., 2010, Provenance analysis of the Neoproterozoic Ocoee Supergroup, eastern Great Smoky Mountains, NC/TN: Geological Society of America Abstracts with Programs, v. 42.

Cherniak, D.J., and Watson, E.B., 2001, Pb diffusion in zircon: Chemical Geology, v. 172, p. 5-24.

Clemons, K.M., and Moecher, D.P., 2008, Re-interpretation of the deformation history of the Greenbrier fault, Great Smoky Mountains: critical assessment of previous work: Southeastern Geology, v. 45, p. 203-224.

Corfu, F., Hanchar, J.M., Hoskin, P.W.O., and Kinny, P.D., 2003, Atlas of Zircon Textures: Reviews in Mineralogy and Geochemistry, v. 53, p. 469-500.

Easton, R.M., 1992, The Grenville province and the Proterozoic history of central and southern Ontario, *in* Thurston, P.C., Williams, H.R., Sutcliffe, R.H., and Stott, G.M., eds., The Geology of Ontario, Canada: Ontario, Ontario Geological Survey Special Volume 4, Part 2, p. 715-904.

Eckert, J.O., Jr., 1984, Stratigraphy, structure, and metamorphism of the east half of the Wayah Bald quadrangle, North Carolina: Evidence for Paleozoic granulite facies metamorphism in the southern Appalachians: Columbia, University of South Carolina.

Force, E.R., 1991, Geology of titanium-mineral deposits: Boulder, Geological Society of America Special Paper 259, 113 p.

Gulley, G.L., 1985, A Proterozoic granulite facies terrane on Roan Mountain, Western Blue Ridge belt, North Carolina--Tennessee Geological Society of America Bulletin, v. 96, p. 1428-1439.

Hadley, J.B., and Goldsmith, R., 1963, Geology of the eastern Great Smoky Mountains, North Carolina and Tennessee: U.S. Geological Survey Professional Paper 349-B, p.1-107

Hanchar, J.M., and Miller, C.F., 1993, Zircon zonation patterns as revealed by cathodoluminescence and backscattered electron images: Implications for interpretation of complex crustal histories: Chemical Geology, v. 110, p. 1-13.

Hatcher, R.D., Jr., 1978, Tectonics of the western Piedmont and Blue Ridge: Review and speculation: American Journal of Science, v. 278, p. 276-304.

—, 1987, Tectonics of the southern and central Appalachian internides: Annual Reviews in Earth and Planetary Science, v. 15, p. 337-362.

Hatcher, R.D., Jr., Bream, B.R., Miller, C.F., Eckert, J.O., Jr., Fullagar, P.D., and Carrigan, C.W., 2004, Paleozoic structure of internal basement massifs, southern Appalachian Blue Ridge, incorporating new geochronologic, Nd and Sr isotopic, and geochemical data, *in* Tollo, R.P., Corriveau, L., McLelland, J., and Bartholomew, M.J., eds., Proterozoic tectonic evolution of the Grenville orogen in North America: Boulder, Colorado, Geological Society of America Memoir 197, p. 525-547.

Hatcher, R.D., Jr., Merschat, A.J., and Thigpen, J.R., 2005, Blue Ridge Primer, *in* Hatcher, R.D., Jr., and Merschat, A.J., eds., Blue Ridge Geology Geotraverse east of the Great Smoky Mountains National Park, western North Carolina: North Carolina Geological Survey, Carolina Geological Society Annual Field Trip Guidebook, p. 1-24.

Holcombe, R., 2009, Georient 32 version 9.4.4.

King, P.B., 1964, Geology of the central Great Smoky Mountains, Tennessee: U.S. Geological Society Professional Paper 349-C.

Klein, C., 2002, Analytical methods in mineral science, *in* Mills, C., and Tavares, K., eds., Manual of Mineral Science, John Wiley & Sons, Inc., p. 290-332.

Le Breton, N., and Thompson, A.B., 1988, Fluid-absent (dehydration) melting of biotite in metapelites in the early stages of crustal anatexis.: Contributions to Mineralogy and Petrology, v. 99, p. 226-237.

Le Maitre, R.W., Streckeisen, A., Zanettin, B., Le Bas, M.J., Bonin, B., Bateman, P., Bellieni, G., Dudek, A., Efremova, S., Keller, J., Lamere, J., Sabine, P.A., Schmid, R., Sorensen, H., and Woolley, A.R., 2002, Igneous rocks: A classification and glossary of terms, recommendations of the International Union of Geological Sciences, Subcommission of the Systematics of Igneous Rocks: Cambridge, Cambridge University Press, 256 p.

Ludwig, K., 1980, Calculation of uncertainties of U-Pb isotope data: Earth and Planetary Science Letters, v. 46, p. 212-220.

—, 1999, Isoplot/Ex v. 2.10b.

Massey, M.A., 2003, Metamorphic, fabric, and structural evolution of rocks defining the Eastern Blue Ridge-Western Blue Ridge boundary, western North Carolina: Implications for the Hayesville Fault, Earth and Environmental Sciences: Lexington, University of Kentucky, p. 180.

Massey, M.A., and Moecher, D.P., 2005, Deformation and metamorphic history of the Western Blue Ridge-Eastern Blue Ridge terrane boundary, southern Appalachian Orogen: Tectonics, v. 24, p. 1-18.

McLelland, J., Daly, J.S., and McLelland, J.M., 1996, The Grenville orogenic cycle (c.a. 1350-1000 Ma): an Adirondack perspective: Tectonophysics, v. 265, p. 1-28.

McLelland, J.M., Bickford, M.E., Clechenko, C.C., Valley, J.W., and Hamilton, M.A., 2004, Detrital dating of Adirondack massif anorthosite by U-Pb SHRIMP analysis of igneous zircon: Implications for AMCG complexes: Geological Society of America Bulletin, v. 116, p. 1-19.

Merschat, C.E., and Cattanach, B.L., 2008, Bedrock geologic map of the west half of the Asheville 1:100,000-scale quadrangle, North Carolina and Tennessee, Geologic Map Series 13, North Carolina Geological Survey.

Merschat, C.E., Cattanach, B.L., Carter, M.W., and Wiener, L.S., 2006, Geology of the Mesoproterozoic basement and younger cover rocks in the west half of the Asheville 100,000 quadrangle, North Carolina and Tennessee--An updated look, *in* Labotka, T.C., and Hatcher, R.D., Jr., eds., Southeastern Section Meeting Field Trip Guidebook, Geological Society of America, p. 1-36.

Merschat, C.E., and Wiener, L.S., 1990, Geology of Grenville-age basement and younger cover rocks in the west central Blue Ridge, North Carolina: Carolina Geological Society Field Trip Guidebook, 42 p.

Miller, C.F., Hatcher, R.D., Jr., Ayers, J.C., Coath, C.D., and Harrison, T.M., 2000, Age and zircon inheritance of eastern Blue Ridge plutons, southwestern North Carolina and northeastern Georgia, with implications for magma history and evolution of the southern Appalachian orogen: American Journal of Science, v. 300, p. 142-172.

Moecher, D.P., Hietpas, J., Samson, S.D., and Chakraborty, S., in revision, Insights into southern Appalachian tectonic history from ages of detrital monazite and zircon in modern alluvium and bedrock sources.

Moecher, D.P., and Samson, S.D., 2006, Differential zircon fertility of source terranes and natural bias in the detrital zircon record: Implications for sedimentary provenance analysis: Earth and Planetary Science Letters, v. 247, p. 252-266.

Moecher, D.P., Samson, S.D., and Miller, C.F., 2004, Precise time and conditions of peak Taconian granulite facies metamorphism in the southern Appalachian orogen, USA, with implications for zircon behavior during crustal melting events: Journal of Geology, v. 112, p. 289-304.

Montes, C., 1997, The Greenbrier and Hayesville faults in central-western North Carolina [M.S. thesis], University of Tennessee, Knoxville.

Montes, C., and Hatcher, R.D., Jr., 1999, Documenting Late Proterozoic rifting in the Ocoee Basin, Western Blue Ridge, North Carolina: Southeastern Geology, v. 39, p. 37-50.

Oliver, N.H.S., Bodorkos, S., Nemchin, A.A., Kinny, P.D., and Watt, G.R., 1999, Relationships between zircon U-Pb SHRIMP ages and leucosome type in migmatites of the Halls Creek Orogen, western Australia: Journal of Petrology, v. 40, p. 1553-1575.

Ownby, S.E., Miller, C.F., Berquist, P.J., Carrigan, C.W., Wooden, J.L., and Fullagar, P.D., 2004, U-PB geochronology and geochemistry of a portion of the Mars Hill terrane, North Carolina-Tennessee: Constraints on origin, history, and tectonic assembly, *in* Tollo, R.P., Corriveau, L., McLelland, J., and Bartholomew, M.J., eds., Proterozoic evolution of the Grenville orogen in North America: Boulder, Colorado, Geological Society of America Memoir 197, p. 609-632.

Paces, J.B., and Miller, J., J.D., 1993, Precise U-Pb ages of Duluth Complex and related mafic intrusions, northeastern Minnesota; geochronological insights to physical, petrogenetic, paleomagnetic, and tectonomagnetic processes associated with the 1.1 Ga Midcontinent Rift System.: Journal of Geophysical Research Solid Earth and Planets, v. 98, p. 13,997-14,013.

Quidelleur, X., Grove, M., Lovera, O.M., Harrison, T.M., Yin, A., and Ryerson, F.J., 1997, Thermal evolution and slip history of the Renbu Zedong Thrust, southeastern Tibet: Journal of Geophysical Research, v. 102, p. 2659-2679.

Quinn, M.J., 1991, Two lithotectonic boundaries in western North Carolina: Geologic interpretation of a region surrounding Sylva, Jackson County: Knoxville, University of Tennessee, p. 223.

Rankin, D.W., 1975, The continental margin of eastern North America in the southern Appalachians: The opening and closing of the Proto-Atlantic ocean: American Journal of Science, v. 275A, p. 298-336.

Rankin, D.W., Drake, A.A., and Ratcliffe, N.M., 1990, Geologic map of the U.S. Appalachians showing the Laurentian margin and Taconic orogen: Plate 2, *in* Hatcher, R.D., Jr., Thomas, W.A., and Viele, G.W., eds., The Appalachian-Ouachita Orogen in the United States : The Geology of North America, Volume F-2: Boulder, Colorado, Geological Society of America.

Rast, N., and Kohles, K.M., 1986, The origin of the Ocoee Supergroup: American Journal of Science, v. 286, p. 593-616.

Ratcliffe, N.M., Aleinikoff, J.N., Burton, W.C., and Karabinos, P., 1991, Trondhjemitic, 1.35-1.31 Ga gneisses of the Mount Holly Complex of Vermont: Evidence for an Elzevirian event in the basement of the United States Appalachians: Canadian Journal of Earth Sciences, v. 28, p. 77-93.

Rubatto, D., 2002, Zircon trace element geochemistry: partitioning with garnet and the link between U-Pb ages and metamorphism: Chemical Geology, v. 184, p. 123-138.

Ryan, J.G., Yurkovich, S., Peterson, V., Burr, J., and Kruse, S., 2005, Geology and petrogenesis of mafic and ultramafic rocks of the Willets-Addie area, central Blue Ridge, NC, *in* Hatcher, R.D., Jr., and Merschat, A.J., eds., Blue Ridge Geology Geotraverse East of the Great Smoky Mountain National Park, Western North Carolina: North Carolina Geological Survey, Carolina Geological Society Annual Field Trip Guidebook, p. 91-98.

Southworth, S., Aleinikoff, J.N., Kunk, M.J., Naeser, C.W., and Naeser, N.D., 2005, Geochronology of the Great Smoky Mountains National Park region, TN/NC, with correlation to the rocks and orogenic events of the Appalachian Blue Ridge, *in* Hatcher, R.D., Jr., and Merschat, A.J., eds., Blue Ridge Geology Geotraverse east of the Great Smoky Mountains National Park, western North Carolina: North Carolina Geological Survey, Carolina Geological Society Annual Field Trip Guidebook, p. 45-56.

Streckeisen, A., 1976, To each plutonic rock its proper name: Earth Science Reviews, v. 12, p. 1-33.

Sun, S.S., 1980, Lead isotopic study of young volcanic rocks from mid-ocean ridges, ocean islands, and island arcs: Philosophical Transactions of the Royal Society London, v. A297, p. 409-445.

Taylor, S.R., and McLennan, S.M., 1985, The continental crust: Its composition and evolution: An examination of the geochemical record preserved in sedimentary rocks: Oxford, Blackwell Scientific, 312 p.

Thomas, C.W., 2001, Origin of ultramafic complexes of the eastern Blue Ridge province, southern Appalachians: Geochronological and geochemical constraints [M.S. thesis]: Nashville, Tennessee, Vanderbilt University.

Thomas, W.A., 1991, The Appalachian-Ouachita rifted margin of southeastern North America: Geological Society of America Bulletin, v. 103, p. 415-431.

Tohver, E., Bettencourt, J.S., Tosdal, R., Mezger, K., Leite, W.B., and Payolla, B.L., 2004, Terrane transfer during the Grenville orogeny: tracing the Amazonian ancestry of southern Appalachian basement through Pb and Nd isotopes: Earth and Planetary Science Letters, v. 228, p. 161-176.

Tollo, R.P., Aleinikoff, J.N., Borduas, E.A., Dickin, A.P., McNutt, R.H., and Fanning, M., 2006, Grenvillian magmatism in the northern Virginia Blue Ridge: Petrologic implications of episodic granitic magma production and the significance of postorogenic A-type charnockite: Precambrian Research, v. 151, p. 224-264.

Tollo, R.P., and Hutson, F.E., 1996, 700 Ma rift event in the Blue Ridge province of Virginia: A unique time constraint on pre-Iapetan rifting of Laurentia: Geology, v. 24, p. 59-62.

Walsh, G.J., Aleinikoff, J.N., and Fanning, M., 2004, U-Pb geochronology and evolution of Mesoproterozoic basement rocks, western Connecticut, *in* Tollo, R.P., Corriveau, L., McLelland, J., and Bartholomew, M.J., eds., Proterozoic tectonic evolution of the Grenville orogen in North America: Boulder, Geological Society of America Memoir 197, p. 729-753.

Werner, C.D., 1987, Saxonian granulites--igneous or lithogeneous? A contribution to the chemical diagnosis of the original rocks in high-metamorphic complexes, *in* Gerstenberger, H., ed., Contributions to the geology of the Saxonian granulite massif, Volume 133, Zfl-Mitteilungen Nr, p. 221-250.

Vita

Author's Name – Donald F. Loughry, Jr.

Birthplace – Oakland, Maryland

Birthdate – July 30, 1975

Education

Master of Arts in Secondary Science Education
Georgetown, College
May 2006

Bachelor of Science in Biology Secondary Education
Asbury University
May 1998

Professional Positions Held

Graduate Teaching Assistant
University of Kentucky
2008-present

8th Grade Science Teacher
West Jessamine Middle School
1998-2008

Summer Earth Science Institute Instructor
Appalachian Math and Science Partnership
2005-2006

Expertise, Achievements, and Professional Activities

Member Geological Society of America
Member American Association of Petroleum Geologists
Completed Exxonmobil Reservoir Characterization and Modeling Short Course, La Jolla, CA
UK Pirtle Fellowship Recipient
Field Study: Basement Rocks of the Grenville Orogeny, southern Ontario
West Jessamine Middle School Science Fair Coordinator
West Jessamine Middle School Curriculum Alignment Team

Middle School Teacher of the Year Nominee
Survey of Bahamian Carbonate Platform Geology and Coral Reef Ecology, San Salvador Island, Bahamas

Published Abstracts

Loughry, D.F., Jr., Moecher, D.P., and Anderson, E.D., 2010, Origin of Blue Ridge basement rocks, Dellwood Quad, western NC: New evidence from U-Pb zircon geochronology and whole rock geochemistry: Geological Society of America Abstracts with Programs, v. 42, No. 1, p. 118.